UNIVERSITY OF CALGARY

The author of this thesis has granted the University of Calgary a non-exclusive license to reproduce and distribute copies of this thesis to users of the University of Calgary Archives.

Copyright remains with the author.

Theses and dissertations available in the University of Calgary Institutional Repository are solely for the purpose of private study and research. They may not be copied or reproduced, except as permitted by copyright laws, without written authority of the copyright owner. Any commercial use or publication is strictly prohibited.

The original Partial Copyright License attesting to these terms and signed by the author of this thesis may be found in the original print version of the thesis, held by the University of Calgary Archives.

The thesis approval page signed by the examining committee may also be found in the original print version of the thesis held in the University of Calgary Archives.

Please contact the University of Calgary Archives for further information,
E-mail: uarc@ucalgary.ca
Telephone: (403) 220-7271
Website: http://www.ucalgary.ca/archives/

THE UNIVERSITY OF CALGARY

# Some Investigations on Local Geoid Determination from Airborne Gravity Data

by

Fadi Atef Bayoud

A THESIS

SUBMITTED TO THE FACULTY OF GRADUATE STUDIES

IN PARTIAL FULFILMENT OF THE REQUIREMENTS FOR THE

DEGREE OF MASTER OF SCIENCE
DEPARTMENT OF GEOMATICS ENGINEERING

CALGARY, ALBERTA

DECEMBER, 2001

©Fadi Atef Bayoud 2001

# ABSTRACT

Advances in the Global Positioning System (GPS) and strapdown Inertial Navigation System (INS) have played a significant role in the development of airborne gravimeters. Previous studies have shown that the airborne gravity data obtained from these gravimeters have very good quality. In this thesis some possible procedures to determine the geoid from airborne gravity data are studied. Different practical issues are investigated: the digital terrain model (DTM) resolution needed to quantify the topography at the flight level, the need for terrain effects filtering, and the use of two downward continuation procedures. The results showed that for a geoid of resolution 5' x 5', a DTM of 30 arcsec can be safely used, and in benign topography even a 60 arcsec could be used. Although filtering is essential from the theoretical point of view, practically it is not important. The geoid determined from airborne gravity data, downward continued to the reference sphere using the normal free-air gradient, shows a better agreement with the reference geoid (computed from ground gravity data) than using the inverse Poisson integral. The geoid determined from airborne gravity agreed within the 5 cm RMS from the reference geoid on a 5' x 5' grid.

An additional study performed in this thesis showed that - when ground data is used for geoid determination - the denser the DTM, the better the geoid is determined; also in this case, the normal free-air gradient gave a better-fitting geoid to the GPS/Levelling undulations.

For both data types, airborne and ground, it was also concluded that the 2nd Helmert condensation method is creating a rough field and thus causes problems, along with the problems of high frequency magnification, when it is downward continued by the inverse Poisson integral.

ACKNOWLEDGMENTS

One of the prettiest moments of my graduate studies was when I was completing the cover page of this thesis. It was a wonderful feeling of finishing another important period of my life. A period that was full of happiness and sadness, relaxation and anger, satisfaction and frustration. A period from which I gained so much knowledge; not only scientific knowledge, but that kind of knowledge that is so hard to learn from science; it is the knowledge of how to go on in life and how to share it with those you love, friends, colleagues, and people in general.

Having the opportunity to write what I feel, it is time I wrote my acknowledgments. First, I want to thank God for all the things He has blessed and is still blessing me with, without which I would not be able to pursue knowledge, or even life. I want to thank my parents and my two sisters, whose love and care towards me gave me the push whenever I was sad, angry, or frustrated. It was enough to think of them.

Having a supervisor like Prof. Dr. Michael G. Sideris was one of the best experiences I had. His care, patience, support, encouragement, humour are most appreciated. Despite his busy program his door was always open for my questions and problems and complaints. Is suxapiaxco Mi%aA.r)-

Many thanks go to Prof. Dr. Klaus-Peter Schwarz. Thank you for all the times you have helped me and for the very valuable discussions we had.

Thanks go to Dr. Prof. Larry Lines and Dr. Nico Sneeuw for their suggestion and comments.

I also would like to thank some of my friends and colleagues. Thanks to Michael Kern and Cameron Ellum for the very nice times we had in room 319F-A; it was great getting to know you guys. Also thanks to Michael for providing me with the downward continuation code he had written and the valuable discussions we had. Discussions and help provided Dr. Alex Bruton are most appreciated; thank you Alex for everything, you were a great help. Also thanks go to Dr. Pavel Novak for the many important discussion

we had. Having a Greek friend here was also a very nice thing; I could practice my Greek language and share memories I had in Greece; thank you George Vergos. Thank you Sandy Kennedy for providing few suggestion on the style of writing.

Discussions in the gravity group were so helpful. Thanks to Sujan Bajracharya and Rossen Grebenitcharsky for always having challenging topics to talk about.

Financial support was provided by Teaching and Research assistantships, the Geomatics for Informed Decisions (GEOIDE) Network of Centres of Excellence projects #10 and # 47 and NSERC grants of the supervisor. This is gratefully acknowledged.

Geoid determination code was provided by Ye Cai Li. This is appreciated.

Last but definitely not least, many thanks go to my professors at the Aristotle University of Thessaloniki in Greece, who taught me the first courses of Geomatics.

*Odo the two who were hor>n toyether and wtdh day toyether* uw# *in the etemvah memories of*

*<^o the two who yawe me hove and tauyht me how to hove*

*Clothe ttao who yave me- hife and' tauyhd'me how to hive*

*two who yawe me eajevythiivy have amd taught me thatyt/oiny ha& to he /wow and hwom the inner heawt*

*Q^o the two who hod&o much to atue AO much*

*Cifo my fiawent&j QSZhtefand ^eoryette*

*(^o the other two whme hove waa ahweiyz with me*

*(~$do the other two whoie extreme ha^^toneM WOA whenever they iaw me 'rettwruwy after mont/u*

*ddo the other two that many timet 0$"xntdd not he there with them when they needed me*

*df/o the other two thai my hyewrtand' thwwyhta aw ahwayi with thiem*

*Qdo my two iidem, (Soma/* and (Sdiatha*

***C**^dnd ahwayi*

*<dldo~ the moddowny and camny man who ivom the moment G$'vat horn tooh me a& hiz ion*

*<&o hmfiuve iout'who i& hoverinyjayfuhhy u/i tn the odfeewwi lew ieei/ny me cut&ny my* W *thyrouyh hihe*

*&o~ my behoved' wiche, ^heiMcm*

*Q/flay ^od reat hit aout'in f*ieace*

TABLE OF CONTENTS

**ABSTRACT** ..... **II**

**ACKNOWLEDGMENTS** ..... **III**

**TABLE OF CONTENTS** ..... **VI**

**LIST OF FIGURES** ..... **IX**

**LIST OF TABLES** ..... **XI**

**ACRONYMS AND SYMBOLS** ..... **XIII**

**1. Introduction** ..... **1**

1.1- Background ..... 1

1.2 - Problem statement and objectives ..... 3

1.3 - Thesis Outline ..... 5

**2. Theoretical Background of Geoid Determination from Airborne Gravity Data. 6**

2.1 - Stokes' and Hotine's Boundary Value Problems and Their Solutions ..... 6

2.1.1 - Stokes' integral ..... 9

2.1.2 - Hotine's integral ..... 12

2.2 - Gravity data computation from airborne gravimetry ..... 13

2.2.1 - The concept of airborne gravimetry ..... 13

2.2.2 - Filtering of the airborne gravity data ..... 16

2.2.3 - Cross-over adjustment of the airborne gravity data ..... 19

2.3 - Topographic effects ..... 20

2.4 - Downward continuation ..... 24

2.4.1 - Inverse Poisson integral ..... 25

2.4.2 - Normal free-air gradient ..... 27
2.4.3 - Collocation ..... 28
2.4.4 - Analytical downward continuation ..... 29
2.5 - Geopotential Model contribution ..... 30
2.6 - Noise propagation and filtering ..... 31
2.7 - Combination of airborne with ground gravity data ..... 32
2.8 - Methodologies used for geoid determination from gravity data ..... 34

**3. Gravity Data Processing and Numerical Tests ..... 39**
3.1 - Introduction ..... 39
3.2 - Topographic effects - 2nd Helmert condensation ..... 41
3.2.1 - Topographic effects on ground gravimetry ..... 41
3.2.1.1 - Numerical Test ..... 42
3.2.2 - Topographic effects on airborne gravimetry ..... 52
3.2.2.1 - DTM Resolution ..... 55
3.2.2.2 - Terrain Effect Filtering ..... 58
3.2.2.2.1 - Effect on TC ..... 58
3.2.2.2.2 - Effect on DTE ..... 60
3.3 - Gridding the airborne gravity data ..... 63
3.4 - Downward continuation by inverse Poisson integral ..... 66
3.4.1 - Ground data ..... 67
3.4.2 - Airborne data ..... 67

**4. Geoid determination from ground and airborne gravity data ..... 73**
4.1 - Geoid determined from ground gravity data ..... 73
4.1.1 - Terrain contribution on the geoid ..... 73
4.1.2 - Geoid modelling ..... 77
4.2 - Geoid determined from airborne gravity data ..... 83
4.2.1 - Airborne geoid from the 1st methodology ..... 84
4.2.2 - Airborne geoid from the 2nd methodology ..... 84

4.2.3 - Discussion of geoid results from airborne gravity data.....87

**5. Summary, Conclusions and Recommendations.....90**

5.1 - Summary.....90

5.2 - Conclusions.....91

5.3 - Recommendations.....93

**6. References.....95**

LIST OF FIGURES

Figure 2-1: Geoid and ellipsoid....8
Figure 2-2: Measured and filtered gravity disturbances....17
Figure 2-3: Spectra of the measured and filtered gravity disturbance....18
Figure 2-4: Cumulative spectra of the measured and filtered gravity disturbance....19
Figure 2-5: Methodology # 1 when computing gravity disturbances....37
Figure 2-6: Methodology # 2 when computing gravity disturbances....37
Figure 2-7: Methodology # 1 when computing gravity anomalies....38
Figure 2-8: Methodology # 2 when computing gravity anomalies....38
Figure 3-1: The locations of the ground data and the topography in the region under study, in meters....43
Figure 3-2: Gravity values reduced by the DTE using 15 arcsec DTM and EGM96 (mGal)....46
Figure 3-3: Gravity values reduced to the TC using 15 arcsec DTM and EGM96 (mGal)....47
Figure 3-4: Difference between the TC computed from a 15 and 30 arcsec DTM (mGal)....48
Figure 3-5: Difference between the TC computed from a 15 and 60 arcsec DTM (mGal)....49
Figure 3-6: GIE computed using the 15 arcsec DTM on 5'x 5' grid (m)....51
Figure 3-7: Coverage of the airborne data and the topography of the region, in meters...53
Figure 3-8: TC and DTE computed at the flight level using 15 arcsec DTM (mGal)....54
Figure 3-9: Differences in TC computed at the flight level (mGal)....56
Figure 3-10:Differences in DTE computed at the flight level (mGal)....57
Figure 3-11: Differences between computed and fdtered TC (mGal)....59
Figure 3-12: Difference between computed and fdtered DTEs (mGal)....61
Figure 3-13: Measured and gridded values....63
Figure 3-14: Downward continued gravity anomalies (mGal)....68

Figure 3-15: Airborne and upward continued ground used for padding.....69
Figure 3-16: Downward continued data_30 airborne gravity disturbances (mGal).....70
Figure 3-17: Downward continued data_60 airborne gravity disturbances (mGal).....71
Figure 3-18: Downward continued data_90 airborne gravity disturbances (mGal).....71
Figure 3-19: Downward continued data_dte airborne gravity disturbances (mGal).....72
Figure 4-1: Difference in the geoid contributions of (TC - CTC°) using 15 and 30 arcsec DTMs (m).....74
Figure 4-2: Difference in the geoid contributions of (TC - CTC°) using 15 and 60 arcsec DTMs (m).....75
Figure 4-3 difference in the geoid contributions of the DTE using 15 and 30 arcsec DTMs (m).....76
Figure 4-4:Difference in the geoid contributions of the DTE using 15 and 60 arcsec DTMs (m).....77
Figure 4-5: Residual geoid computed from the 1st methodology (m).....78
Figure 4-6: Residual geoid computed from the 2n methodology (m).....79
Figure 4-7: Difference in geoids between the two methodologies (m).....80
Figure 4-8: Location of the GPS/Levelling points.....82
Figure 4-9: The four residual geoids computed from the four data sets created using the 1st methodology (m).....85
Figure 4-10: Differences between the reference geoid and geoids computed from the 1st methodology (m).....86
Figure 4-11: The four residual geoids computed from the four data sets created using the 2nd methodology (m).....88
Figure 4-12: Differences between the reference geoid and geoids computed from the 2nd methodology (m).....89

LIST OF TABLES

Table 3-1: Statistics of the DTM's used, in meters ..... 42
Table 3-2: Statistics of ground gravity anomalies on 5'x 5' grid (mGal) ..... 44
Table 3-3: Statistics of TC, CTC and DTE computed from 15, 30, and 60 arcsec DTM at the topography on 5'x 5' grid (mGal) ..... 45
Table 3-4: Statistics of the differences in TC, CTC and DTE computed from 15, 30, and 60 arcsec DTM at the topography on 5'x 5' grid (mGal) ..... 45
Table 3-5: Statistics of GIE computed from 15, 30, and 60 arcsec DTM on 5'x 5' grid (m) ..... 50
Table 3-6: Statistics of the differences of GIE compute from the different DTM resolution on 5'x 5' grid (m) ..... 50
Table 3-7: Statistics of TC, CTC and DTE computed from 15, 30, and 60 arcsec DTM at the flight level (mGal) ..... 55
Table 3-8: Statistics of the differences in TC, CTC and DTE computed from 15, 30 and 60 arcsec DTM at the flight level (mGal) ..... 57
Table 3-9: Statistics of the differences between the computed and fdtered TC (mGal) ... 58
Table 3-10: Statistics of the three datasets (refined Bouguer anomalies), reduced using un-filtered TC (mGal) ..... 60
Table 3-11: Statistics of the three datasets (refined Bouguer anomalies) reduced using filtered TC (mGal) ..... 60
Table 3-12: Statistics of the differences between the computed and filtered DTE (mGal) ..... 61
Table 3-13: Statistics of the three datasets reduced by the un-filtered DTE (mGal) ..... 61
Table 3-14: Statistics of the three datasets reduced by the filtered DTE (mGal) ..... 62
Table 3-15: Statistics of the *data_grd* (mGal) ..... 62
Table 3-16: Statistics of the four datasets reduced by the TC (mGal) ..... 64
Table 3-17: Statistics of the four datasets reduced by the DTE (mGal) ..... 65

Table 3-18: Statistics of the differences between data_60 and the other three datasets reduced by the TC (mGal) ..... 65
Table 3-19: Statistics of the differences between data_60 and the other three datasets reduced by the DTE (mGal) ..... 65
Table 3-20: Statistics of the residual Helmert ground anomalies before and after the D.C (mGal) ..... 67
Table 3-21: Statistics of the downward continued airborne gravity data (mGal) ..... 69
Table 3-22: Statistics of the difference between data_60 and the other three datasets (mGal) ..... 70
Table 4-1: Terrain Effects on the geoid using different DTM resolutions (m) ..... 75
Table 4-2: Statistics of the residual geoid from the two methodologies and their difference (m) ..... 81
Table 4-3: Statistics of the differences between the gravimetric and the control geoids at the BM (m) ..... 81
Table 4-4: Statistics of the differences between the gravimetric and the control geoids at the BM after the fit (m) ..... 81
Table 4-5: Statistics of the differences between ground and airborne geoid using the 1st methodology (m) ..... 84
Table 4-6: Statistics of the differences between ground and airborne geoid using the 2nd methodology (m) ..... 87

# ACRONYMS AND SYMBOLS

## Acronyms

| | |
|---|---|
| BM | Benchmark |
| CTC | Condensed Terrain Correction |
| CTC° | Condensed Terrain Correction evaluated at zero level |
| DC | Downward Continuation |
| DGPS | Differential Global Positioning System |
| DTE | Direct Topographic Effect |
| DTM | Digital Terrain Model |
| EGM96 | Earth Geopotential Model 96 |
| ESA | European Space Agency |
| FC | Fast Collocation |
| FFT | Fast Fourier Transform |
| FIR | Finite Impulse Response |
| GIE | Geoid primary Indirect Effect |
| GPS | Global Positioning System |
| GM | Geopotential Model |
| INS | Inertial Navigation System |
| IOST | Input-Output System Theory |
| LSAFD | Least Squares Adjustment in the Frequency Domain |
| RMS | Root Mean Square |
| STD | Standard Deviation |
| TC | Terrain Correction |
| TE | Terrain Effect |

**Super-script**

| | |
|---|---|
| *b* | body frame |
| / | local frame |
| gm | geopotential model contribution |

**Symbols**

| | |
|---|---|
| *a* | ellipsoidal semi-major axis |
| $a^x$ | body acceleration calculated form the GPS measurements in x frame |
| $a_x$ | body acceleration in the x direction |
| $a_0$, a, | constants used in the computation of the normal gravity at the ellipsoid |
| $b_{x\ 2\ 3\ 4\ 5}$ | constants for computation of the normal gravity at the certain height |
| $C_{nn}$ | error covariance function |
| $C_{\&g}o_{8g}i$, | cross-covariance function between 5g° and $8g^h$ |
| C, *, /, *og bg* | auto-covariance function |
| $c_n$ | degree variances of the gravity disturbances (or anomalies) |
| *Cnm' Snm* | harmonic coefficients of the GM |
| *D* | difference between the two datasets |
| *d's* | parameters of the surface computed by the least-squares adjustment |
| / | specific force measured by the accelerometers |
| *g* | gravity value |
| ***G*** | mean gravity value |

| | |
|---|---|
| $H^{topo}$ | height of the topography |
| $J$ | mean curvature of a surface |
| $k$ | gravitational constant |
| $K(r,\backslash\backslash i,R)$ | Poisson integral |
| $L\{r,$ v\|/, $r')$ | distance between the computation and running point |
| $M$ | Earth's mass |
| $N$ | geoid undulation |
| $N^{GIE}$ | geoid indirect effect |
| $P_n(t)$ | Legendre function |
| $r$ | radial distance |
| $R$ | radius of the reference sphere |
| $r',<p',X'$ | are the radial distance $(R + H')$, latitude, and longitude of the running point, |
| $S(\backslash\backslash J)$ | Stokes' kernel |
| $s_i, b_i$ | slope and bias of the flight line $i$ |
| $T$ | disturbing potential |
| v | body velocity measured also by the GPS |
| $W_u$ | partial derivative of the gravity potential along the $i$ - *axis,* |
| y | normal gravity |
| $y^h$ | normal gravity at height $h$ |
| 8g | gravity disturbance |
| $Ag$ | gravity anomaly |

| | |
|---|---|
| SM | difference in mass between the real and normal Earth |
| *bW* | difference in potential between the real and normal Earth |
| A5g | difference in disturbances between flight lines at the crossover points |
| $At_i$ | time difference between start of flight line and crossover point current time |
| p | specific density of the topography |
| a | integration area |
| a((p,^) | condensation density |
| q>, *X* | spherical coordinates |
| v\/ | spherical distance |
| co | rotation rate of the Earth |
| ie | skew-symmetric matrices of the angular velocity ie |
| el | skew-symmetric matrices of the angular velocity el |
| *h* (v\/) | Hotine's kernel |
| *dgI dh* | actual gravity gradi ent |
| *dj/dh* | normal gravity gradient |

# Chapter 1

# Introduction

## 1.1 - Background

For more than a hundred years, gravity measurements have been done mostly on the surface of the earth or in the oceans. In the 1960's, the first attempts were made to indirectly measure gravity by modelling disturbances of the satellite orbits around the Earth. In this case, measurements were not gravity directly, but rather some functionals of the gravity field. Also, in the 1960's, attempts to measure the gravity itself from aeroplanes, using either modified sea gravimeters or Inertial Navigation Systems (INS), were made but were not very successful due to the poor INS system quality at that time and the poor positioning quality with techniques such as the optical methods. In the beginning of the 1990's and with the advent of the Global Positioning System (GPS) attempts at airborne gravity measurements were starting to give acceptable results by using INS and GPS together. Currently, these instruments are considered to be the standard tools for measuring gravity in local and regional scales. The INS/GPS system, which can also be called INS/GPS gravimeter, integrates the two sensors: INS and GPS.

The INS consists of a set of three orthogonal accelerometers that measure the acceleration, and three gyroscopes that define the orientation of the system. According to Einstein's theory of equivalence, it is impossible to distinguish between the effects of inertial acceleration and the gravitational field. In other words, an accelerometer, mounted in a moving body, measures both the acceleration caused by the Earth's gravity field and the

acceleration caused by the actual motion of the body. Hence, an independent determination of the acceleration of the motion of the body is essential in order to separate these two forces.

Although the main measurements of GPS are the position and velocity of a moving body, it can also be used for determining the acceleration, by differentiating the position twice or the velocity once with respect to time. In this context, the difference between INS and GPS measurements yields the gravity.

While this concept seems quite simple, its application is hampered by a wide range of difficulties and challenging problems, such as (in a very general sense) the quality of sensors used, time synchronization, and data processing. The first two problems have been successfully studied in the past 20 years due to the high level of maturity in sensor development. The data processing was extensively studied in the past decade and adequate algorithms were developed. Since most of the challenging problems for obtaining good quality gravity data have been solved (at least those that concern gravity and its applications in geodesy), processing of this data to lead to the desired quantities in geodesy needs to be investigated along with the quality of such quantities.

In applied Earth sciences, the gravity field is used as a tool to determine mathematical and physical parameters needed for a range of applications: mapping, geophysics, exploration, etc. The interested reader can refer to the ESA report (1999). This research concentrates on the mapping part, where geoid determination is the aim. Geoid is the equipotential surface of the Earth's gravity field that best fits the global mean sea level.

Many studies have been published in the past decade on airborne gravity data and its importance in future geoid determination. Different institutes around the globe are conducting research on using airborne gravity data for geoid modelling in the polar gaps and in un-surveyed areas.

At the department of Geomatics Engineering, University of Calgary, many problems related to applications of airborne gravimetry are being studied. Among these problems are the terrain effect on the gravity signal at flight level, downward continuation, and whether

the airborne data can stand alone without the help of other data, like ground measured gravity disturbances/anomalies.

## 1.2 - Problem statement and objectives

The gravity information acquired from the airborne system is filtered to remove the high frequency components due to GPS errors, high aircraft dynamics, and phugoid motion. This filtering forces the gravity signal to be band limited within the frequency of the filtering (Ch. 2), and any processing made to this signal has to take into account this band limitedness. Tziavos et al. (1988) studied the effect of the terrain on airborne gravimetry by investigating the Digital Terrain Model (DTM) resolution and flight height needed to obtain accurate terrain corrections at the flight level. Yet, they did not link the topographic effects to the filtering of the gravity signal. Li (2000) also tried to examine the topographic effect on the filtered gravity signal at the flight level, however he did not study the filtering effect on geoid determination. Other studies, e.g., Forsberg and Solheim (2000), Fernandes et al. (2000), Timmen et al. (2000), among others, do not mention whether they remove the effect of the topography from the measured gravity signal, and most of their measurements are above the sea where there is no need for topographic reduction. Here, therefore, investigation of the effect of the topographic signal on the airborne gravity data taking into account the filtering of the gravity signal, and the effect of the DTM resolution, will be carried out.

Downward continuation is well studied in the geodetic literature. Rigorously, it is evaluated by the inverse Poisson integral; other methods to downward continue the gravity data are collocation, analytical downward continuation, and free-air gradient, etc. When the inverse Poisson integral is used, problems are created due to the magnification of the high frequency part of the signal, and mainly the errors; thus, regularization of this inverse problem is applied using different methods (Bouman, 1998), i.e., Tikhonov-Philips, Collocation (either in space or frequency domain), iterative solutions, etc. Forsberg and Solheim (2000), Fernandes et al. (2000), Timmen et al. (2000) did not apply downward continuation, because measurements were either done at low altitudes or above the sea or

both. Forsberg and Kenyon (1995), on the other hand, studied the use of collocation and FFT for the downward continuation without dealing with the cumbersome rigorous inverse Poisson integral. Novak et al. (2001) studied the downward continuation by evaluating the inverse Poisson integral on a synthetic field and on actual data at low altitude. Neither study assessed the effect of the downward continuation and/or its absence on geoid modelling. As for the regularization, many studies dealt with this topic in the geodetic literature; among the many, we mention Schwarz (1979), Bouman (1998), Sun and Vanicek (1996), Rauhut (1992), Kern and Schwarz (2001). Since this topic needs, by itself, an in-depth investigation, this thesis deals with it passively by applying the iterative method.

The main objective of this thesis is to compare two methods of geoid determination from airborne gravity, considering two downward continuation methods (inverse Poisson integral and normal free-air gradient), topographic effects, filtering of topographic effects, and terrain resolution. The two solutions will be compared to a reference geoid obtained form ground data and recommendations will be made, based on the accuracy, resolution, and efficiency of each method.

Specifically, the first set of objectives of this thesis is to answer the following points:

1. What D T M resolution is needed in airborne gravimetry?
2. Is filtering of the topographic effects essential from the practical point of view?
3. Which downward continuation method gives the best fit to the reference geoid?
4. How different is the geoid when determined from data filtered to different frequencies?
5. How good is the geoid determined from airborne gravimetry?

Ground gravity data are used in this thesis mainly as a reference gravity field and the geoid determined from them as the reference geoid. In an attempt to make this study more complete, some investigation will be done on the geoid determined from ground gravity data in order to answer these two questions:

1. How do the terrain effects computed from different digital elevation model resolutions affect the geoid, and

2. Which downward continuation method gives a best-fitting geoid to the GPS/levelling benchmarks when using ground gravity data?

The airborne gravity data set that is used in this study was measured by a Honeywell LRFIII strapdown system over the Rocky Mountains; this data and missions are described in Bruton (2000). As for the ground data, the databases in the Geodetic Survey Division, NRCan, were used, with the addition of 176 values measured by the GEOIDE project group 47 with the assistance of Mr. Philip Salib of NRCan during the summers of 1999 and 2000.

## 1.3 - Thesis Outline

The main objective of this research is the geoid computation from airborne gravity data. To accomplish this, different tasks are studied. This thesis is divided as follows.

The second chapter covers the theoretical background of geoid determination: Stokes' and Hotine's Boundary Value Problems are stated and their solutions are discussed; the concept of airborne gravimetry is outlined; terrain effects are examined; downward continuation is studied; and the methodologies followed in this thesis are stated.

The third and fourth chapters contain the numerical tests conducted. The third chapter deals with the DTM resolution needed for geoid determination and whether the topographic effects, used in airborne gravimetry, need filtering so that they are consistent with the gravity signal. This chapter also discusses the DTM resolutions needed for the geoid computed using ground gravity data. The use of the rigorous Poisson integral for downward continuation is also studied in this chapter. The fourth chapter examines geoid determination using ground and airborne gravity data. This chapter answers almost all the questions of the thesis, since the final product is the geoid. The fifth chapter summarizes the research, with recommendations for future research topics.

# Chapter 2

# Theoretical Background of Geoid Determination from Airborne Gravity Data

## 2.1 - Stokes' and Hotine's Boundary Value Problems and Their Solutions

For the geodetic modelling of the gravity field, gravity values have to be given either on the topography and solved by Molodensky's theory (Moritz, 1980; Sideris, 1987) or on the geoid - approximated by a reference sphere - and solved by the classical Stokes/Hotine formulation (Stokes, 1849; Hotine, 1969). In this research, the Stokes/Hotine formulation will be used for geoid determination. The processing of the airborne data is very similar to that of the ground data with the difference that the points are not at the topography, neither are they close to the reference sphere, but rather at some altitude above the topography. The impact of this is the attenuation of the gravity signal and the problem of bringing the measurements to the reference sphere to be used either for geodetic or geophysical purposes.

Geoid determination has been the centre of study in geodesy during the previous century. It is based on the third boundary value problem, developed by Neumann, that determines the disturbing potential, $T$, exterior to or on a surface, on which values functionally related to this disturbing potential exist. Stokes (1949) formulated this problem and developed the well-known Stokes' integral for determining the disturbing potential using gravity anomalies, $\Delta g$, at the surface of the geoid. Using Bruns's formula, one can obtain the geoid undulations from the computed disturbing potential. Hotine (1969) used gravity

disturbances, *8g,* to compute the disturbing potential, and in turn geoid undulations, using Neumann's problem, thus leading to Hotine's integral. To resolve these two formulations, the following differential equation needs to be solved:

A ² r = 0 (2.1)

with the boundary conditions

A g ~ § - | r (2.2)
*or* *R*

or

^g = ~ (2.3)
*or*

*dr* is the radial derivative.

So, the gravity values used to compute the geoid are gravity anomalies, *Ag*, or disturbances, 5g. From the theoretical point of view, there is no difference between using Stokes' and Hotine's integrals; actually in planar approximation, the two integrals are identical. The two quantities, gravity disturbance and gravity anomaly, are related to each other by the *fundamental equation of physical geodesy* (Eq. 2.2). If we consider the planar approximation, *R* —» oo , we achieve the following expression,

Ag = - ^ = 5g. (2.4)
*or*

Numerically, these two quantities can be related to each other as follows,

$$\left.\begin{aligned}\Delta g &= g_p - \gamma_q \\ \delta g &= g_p - \gamma_p\end{aligned}\right\} \quad <=> \quad 8g = Ag + y \ -y \qquad 8g = Ag- \ \ {}_{dh}^{N} \qquad (2.5)$$

where $g$ is the gravity measured at point P, y, is the normal gravity computed at point $i = \{p,q\}$, $N$ is the geoid undulation at point $i$, and $dy/dh$ is the normal free-air gravity gradient; see Fig. 2-1.

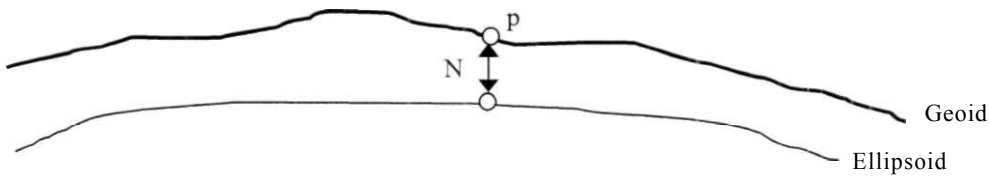


**Figure 2-1: Geoid and ellipsoid**

Since /V is usually not known, we usually use a high degree and order geopotential model (GM) to approximate it and use it in this transformation.

As mentioned above, the gravity information has to be on the boundary surface - the geoid approximated by a reference sphere in our case- so that it can be used in Stokes' or Hotine's integral to give the geoid. The gravity is measured at an altitude above the geoid and a way to downward continue it has to be followed. The harmonicity of the field is achieved by removing all masses above the geoid. This is done by removing the topographic and atmospheric effects from the measured gravity signal.

So, the first step in geoid determination from airborne gravity data is the terrain effects computation. The atmospheric effects are added as a constant number depending on the height at which the measurements take place; see Moritz (1984) for more details. The terrain effects are computed by evaluating the potential of the topographic masses around the measuring location; then, they are low-pass filtered so that they are consistent with the

airborne gravity data before being added. To account for the global gravity field effect, a high degree and order geopotential model (GM) is subtracted from the data. The downward continuation of the residual gravity data brings the data to the reference sphere. Having residual gravity values on the reference sphere, Stokes/Hotine formulation is applied to determine the co-geoid. To obtain the geoid, the topographic indirect effect is added to the co-geoid. When the GM contribution is added again in terms of geoid values, the final geoid is achieved.

In this chapter, the theoretical formulation of the geoid computation will be made following Helmert's 2nd condensation method. The classical remove-restore technique will be followed. There are many studies that compute the geoid differently; for example, some studies use the measured gravity at the surface of the topography without any kind of reduction, where the effect of these reductions are taken care of independently (e.g., Sjoberg and Nahavandchi, 1999; Sjoberg, 2000; Sjoberg, 2001). Here, the classical remove-restore technique will be followed.

### 2.1.1 - Stokes' integral

As was mentioned previously, the geoid can be determined by either one of two integrals: Stokes' integral if **gravity anomalies** are available; and, Hotine's integral if **gravity disturbances** are available. First, we will present Stokes' approach and after that Hotine's. Since the derivation of both equations is similar and can be found in physical geodesy textbooks (e.g., Heiskanen and Moritz, 1967; Hotine, 1969; Dragomir et al., 1982), the equations will only be shown with a short discussion.

Stokes' integral can be derived from Equations 2.1 and 2.2. The most general form of Stokes' integral is (Heiskanen and Moritz, 1967),

(2.6)

where

$k$ is the gravitational constant,

$8M$ is the difference in mass between the real earth and the normal earth,

$8W$ is the difference in potential between the real earth and the normal earth,

$R$ is the radius of the reference sphere that approximate the geoid,

y is the mean value of gravity,

Ag are gravity anomalies reduced to the topography and to the G M, and downward continued to the geoid,

$S(\backslash\backslash i)$ is Stokes' function or kernel and it is expressed either as:

*a function ofLesendre polynomials:*

$$\hat{(m)} = X \frac{\hat{}}{n=2 \quad n-1} P_{,,} (\cos vj/), \text{ where } P_{n}\, it) \text{ is the Legendre function}$$

*or a closed formula:*

$$b\{\backslash y) = \backslash + \frac{ct \backslash \quad , \quad 1}{\sin(W2)} \hat{} \bullet W \quad r \quad v\text{-}6\sin — \text{-}5\cos\backslash\backslash i\text{-}3\cos\backslash\backslash J\log \quad \sin — + \sin'' \quad \hat{} . \quad \backslash 1/ \quad . \; \backslash \; Vf \quad \backslash \quad \cdot J \tag{2.7}$$

Assuming that the mass of the real earth is equal to the mass of the normal earth and that the potentials generated from the two masses are equal, the first two terms of Eq. 2.6

become zero. In terms of the latitude cp and longitude *X,* the final form of Stokes' integral is,

$$N(<?,X) \quad \frac{R}{4\%y} \int_{v=o}^{2\pi} \int_{<p'=v2}^{\pi/2} \backslash Ag(y',),')s(\backslash\backslash r)cos<p'd<p'dk'. \tag{2.8}$$

For the practical implementation of the above equation (Eq. 2.8), the integral turns into summation. This equation can be implemented in different ways, depending on the approximation used: planar or spherical. It can be evaluated by one-dimensional Fast Fourier Transform (FFT) or two-dimensional FFT (e.g., Hagmaans et al., 1993; Sideris and She, 1992; Li, 1993). The 1-D FFT is applied in this thesis.

Since the contribution of a GM is subtracted from the gravity anomalies this contribution is added back in terms of geoid undulation after computing the residual geoid from Eq. 2.8. Also, the indirect topographical effect is to be added. So, the final geoid is obtained as follows:

$$N(<p, X) = N^{S}(cp, X) + N^{GM}(<p, X) + N^{GIE}(cp, X) \tag{2.9}$$

where the superscripts 'S', and 'GM' stand for the geoid computed from Stokes' integral (Eq. 2.8) and the GM (Eq. 2.10), respectively, and $N^{GIE}$ is the indirect topographic effect and its computation is discussed in Section 2.3.

$$N^{GM} \quad \frac{}{r} \sum_{n=2}^{\infty} \sum_{m=0}^{} E\,l^{c} \ll m^{\cos} \wedge + \wedge m^{\sin} \wedge r \wedge (^{\cos \&}) \tag{2.10}$$

### 2.1.2 - Hotine's integral

Instead of using gravity anomalies, the gravity disturbances are used here. A11 the derivations, implementations, and modifications are similar to Stokes' integral (Hotine, 1969; Novak et a1, 2001).

Hotine's integral is derived from Equations 2.1 and 2.3 and written as follows,

$$N(\varphi,\lambda)=\frac{R}{4\pi\gamma}\iint_{\sigma}\delta g(\varphi,\lambda)\hbar(\psi)d\sigma \tag{2.11}$$

where $h(\backslash\backslash i)$ is Hotine's function or kernel and it can be described either as:

*a function of Legendre polynomials:*

$$(2\mathbf{k}+1)$$

$$n=2$$

*a closed formula:*

$$hM= \quad \text{sm}'(v/2) \quad -\log 1+ \quad \sin(W2)J' \tag{2.12}$$

Both kernels, Stokes' and Hotine's, can also be described spatially, where the kernel relates data on the reference sphere to data outside the reference sphere at some given height.

The equation used in this thesis takes the form,

$$iV\sim(q>A) = \frac{n}{4IZ\,Y} \int_{V=0<p'=-7r/2}^{271\quad 7t/2} J8g((p',X')h(^)cos(p'd^'dX'. \qquad (2.13)$$

The contributions of the GM and the topography are added in the same way as in Eq. 2.10.

## 2.2 - Gravity data computation from airborne gravimetry

### 2.2.1 - The concept of airborne gravimetry

The main equation of airborne gravimetry is based on the Newton's equation of motion, and in the local-level frame is (Schwarz and L i , 1996a)

$$a^{l}=f-(2ri_{ie}+Q^{l}_{el}y+g^{l}, \qquad (2.14)$$

where $a^{l}$ is the body acceleration calculated form the GPS measurements, /' is the specific force measured by the accelerometers, $v^{l}$ is the body velocity measured also by the GPS, $Q.\backslash_{e}$ and $Q.'_{el}$ are skew-symmetric matrices of the angular velocities $co_{ie}$ and $\&^{1}_{e1}$ due to the earth rate and body rate over the ellipsoid, and $g^{l}$ is the gravity vector that we are seeking.

Introducing the normal gravity vector $y'$ referenced to an ellipsoid, the gravity disturbance vector $8g^{l}$ can be computed for the stable platform form

8 g' =a'-f' +(2Q'_{ie}+Q'_{e}y -y' (2.15)

Considering a strapdown system, a rotation matrix should be introduced to transform the specific force measured in the body frame *(b)* to the local-level frame (/), and the equation becomes

8g' =a'-R'_{b}f'_{+}(2Q'_{ie+}Q'_{el}\'  y' (2.16)

In detail, this equation has the following form,

| | | | | | | | | |
|---|---|---|---|---|---|---|---|---|
| ny | = | $a_E$ | – | cos y cos $r$ - sin $y$ sin $p$ sin $r$ | - sin y cos $p$ | cos y sin r + sin y sin /? cos $r$ | /e |
| | | $a_N$ | | sin $y$ cos $r$ + cos y sin $p$ sin $r$ | cosy cos $p$ | sin y sin $r$ - cos y sin $p$ cos r | $f_N$ |
| | | $a_u$ | | - cosy sin $r$ | sin $p$ | cos /? cos $r$ | fu |

$$+ \begin{vmatrix} f \\ 2 \\ \\ \end{vmatrix} \begin{vmatrix} 0 & -co(_e & 0 \\ & 0 & 0 \\ 0 & 0 & 0 \end{vmatrix} + \begin{vmatrix} 0 & -X\sin\varphi & I\cos\varphi \\ l\sin(p & 0 & \\ X\cos\varphi & -\langle P & 0 \end{vmatrix} \begin{vmatrix} \\ \\ \end{vmatrix} - \begin{vmatrix} \text{"o"} \\ 0 \\ .y. \end{vmatrix}$$

where

(p = (r^ + /z)cos(p

and y, p, and r are the yaw, pitch and roll angles of the body that carries the apparatus. Other notations are the same as above, with the E, N, and U superscripts denoting the east, north, and up directions, respectively.

Before applying equation (2.16), processing of raw INS and GPS collected data has to be done separately. This processing currently takes place in three distinct steps (Glennie, 1999). In the first step, the attitude, position, and velocity of the airborne gravity system is calculated by integrating the inertial measurements with the DGPS carrier phase and phase rate measurements. This is done by applying Kalman filtering techniques using the decentralized filter concept. In the second step, GPS position and velocity information are used to estimate the body's accelerations. The GPS system outputs are also used to determine the Coriolis acceleration correction.

The centres of the INS and GPS are not coincident, so a relation between both references has to be established. This is done by the use of a theodolite and it is called the lever-arm offset connection. Then, double differentiation of the offset orientation is applied to add it to the derived accelerations of both systems.

The third step is to estimate the gravity disturbance vector by differencing the INS specific force measurements and the GPS accelerations, and applying the corrections due to Coriolis and the lever-arm offset acceleration.

To reduce the measurement noise the gravity disturbances are then low-pass filtered to a desired cut-off frequency using a finite impulse response (FIR) filter. The best FIR period is found to be 90 seconds for the acceleration computation.

The output is still suffering from some systematic effects due to the tilt of the flight lines and accelerometer biases. This was investigated by Glennie (1999) where he applied some polynomial fit for the accelerometer bias, and a least-squares adjustment for the computation of the cross over points. This is not the case when there is only one flight line, but such surveys are avoided.

The final output of this system is the disturbance vector, which consists of the magnitude of the disturbance and the two components of the deflection of the vertical multiplied by the normal gravity vector that refers to the point of measurement.

Every value in equations (2.15) or (2.16) is affected by its measuring errors; specific force errors come from the accelerometer imperfections; yaw, pitch and roll errors come from the gyros, drift errors for example; acceleration, velocity, and position errors come from GPS.

By linearization of equation (2.16), one can derive an error model as follows (Schwarz and Li, 1996a):

$$ddgi=da^{i}+f'e\ '-R[df^{n}\ +\ (2Q^{i}_{ie}\ +\ Q.^{i}_{el}\ ]dv'\ -\ v^{i}\ (ldw^{i}_{ie}\ +\ dw^{i}_{el})$$

$$-dy\qquad {}^{i}_{+}(R^{i}J^{n}_{+}R'^{n}_{b}f^{n})dt \qquad (2.17)$$

All the notations are considered known, except for the *dt*, which is the synchronization error between the GPS and INS timing, and s ', which is the attitude errors due to the initial misalignment and gyro measurement noise. Because of the good estimates of velocity and position derived form GPS, there terms can be neglected without introducing much effect on the overall error model (ibid), so the final error model becomes

$$dbg^{i}-da^{i}\qquad +f^{i}e^{i}-R^{i}_{b}df^{n}_{+}(R^{i}_{b}f^{n}_{+}R'^{n}_{b}f^{n})dt \qquad (2.18)$$

### 2.2.2 - Filtering of the airborne gravity data

The output of equation (2.16) is low pass fdtered to remove the high frequency errors that come from the high dynamics of the moving body, GPS errors, and phugoid motion. The reader can refer to Schwarz et al. (1994), Hammada (1996), Schwarz and Li (1996b) Glennie (1999), Bruton (2000), for spectral characteristics and low-pass filtering procedures.

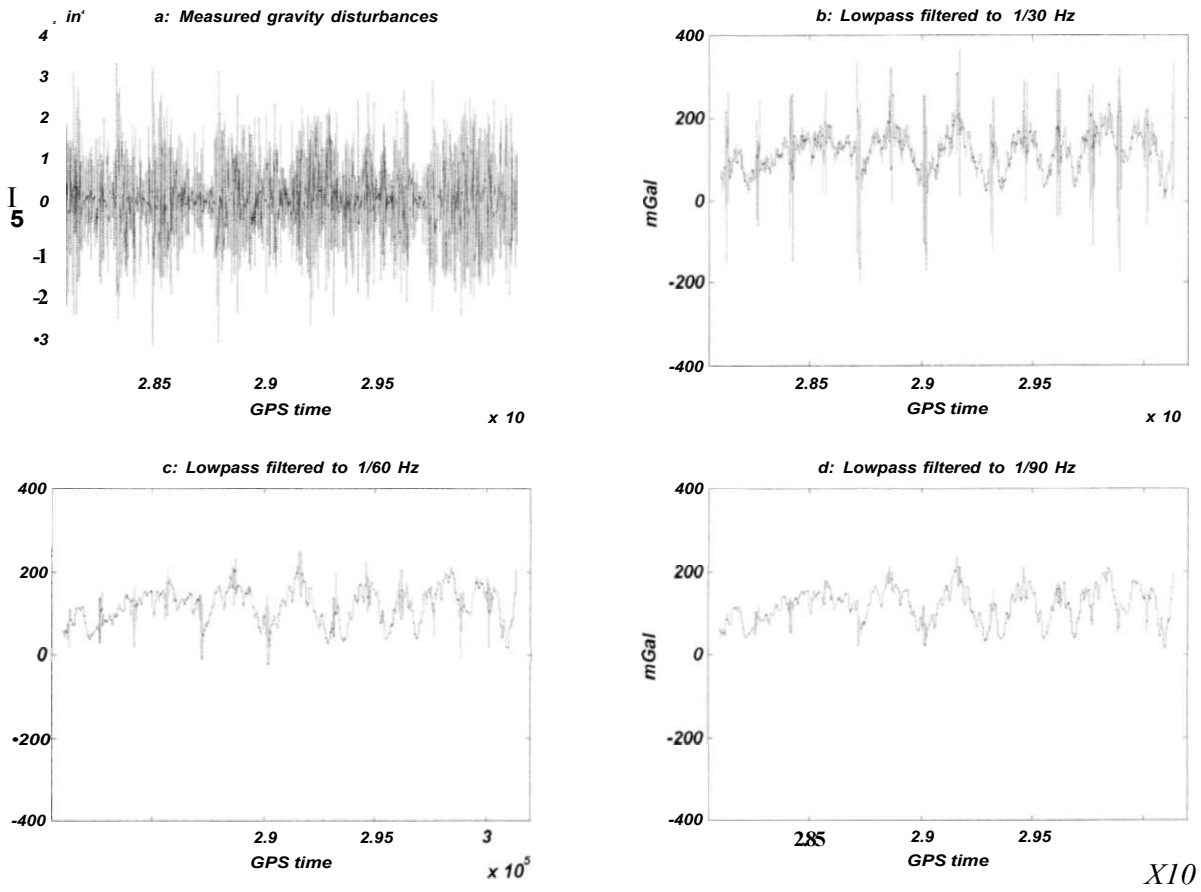


**Figure 2-2: Measured and filtered gravity disturbances**

Here we will show an example of filtering on one dataset from the survey that took place in the Rocky Mountains in 1996. This campaign is well documented in Bruton (2000).

Figure 2-2 shows the measured and the filtered gravity disturbances to 1/30, 1/60, and 1/90 Hz cut-off frequency plotted versus the GPS time (in seconds). Fig. 2-3 shows the spectra of this data, and Fig. 2-4 shows the cumulative spectra. These plots demonstrate clearly why filtering is required. The raw measurements are so noisy that the real gravity signal is completely covered by noise (Fig 2-2.a). After applying the lowpass filter, the gravity signal becomes visible. Comparing the filtered data to upward continued ground data taken as reference, it was shown that the filtering frequency of 1/90 Hz gave the best fit. This is demonstrated in Glennie (1999) and Bruton (2000).

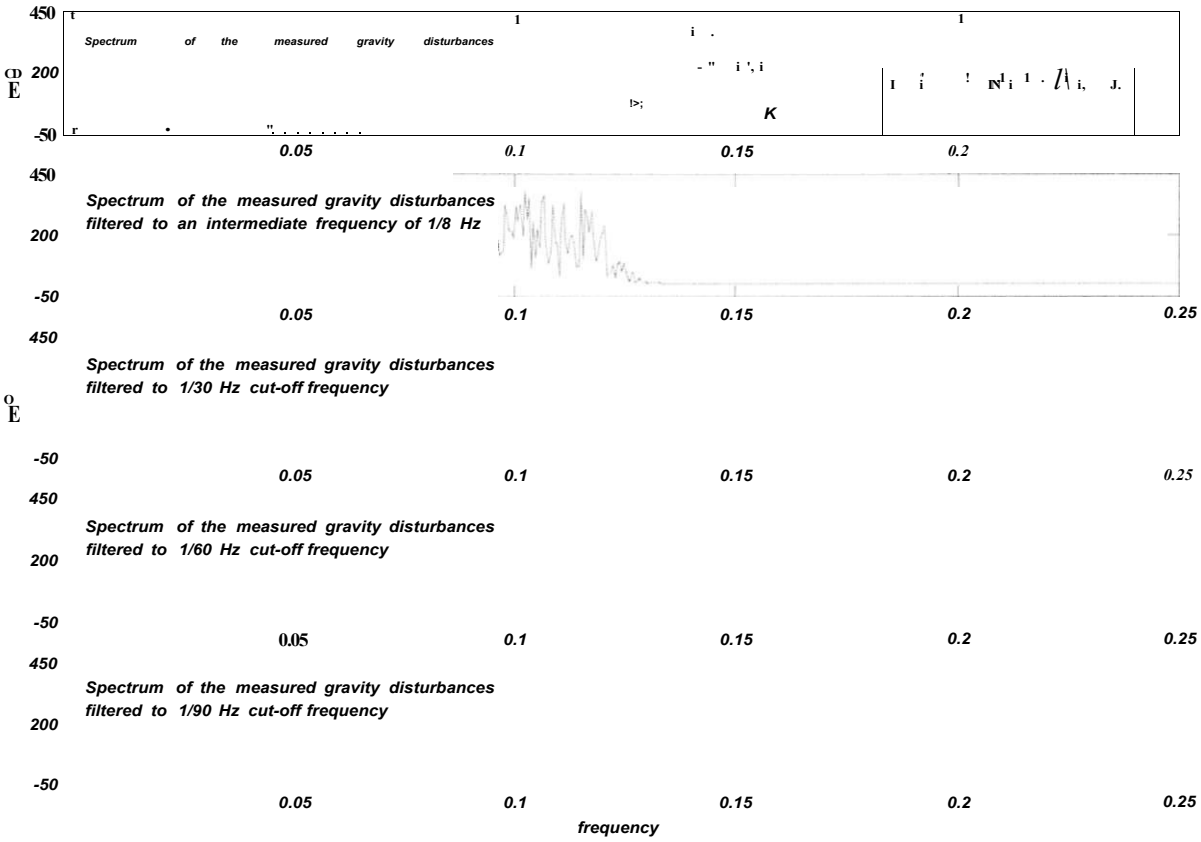


**Figure 2-3: Spectra of the measured and filtered gravity disturbance**

Figures 2-3 and 2-4 reveal the spectral contents of the signals plotted in Fig. 2-2. It is clearly shown how filtering gets rid of the high frequencies from the signal. These high frequencies are not only the errors embedded in the signal, but also the high frequency signature of the gravity field itself; hence, the high frequency parts of the gravity spectrum, beyond the cut-off frequency, are also smoothed by the filtering. This analysis leads us to the belief that any post-processing of this gravity signal has to take into account this smoothing; this applies mainly to the reduction of the gravity data.

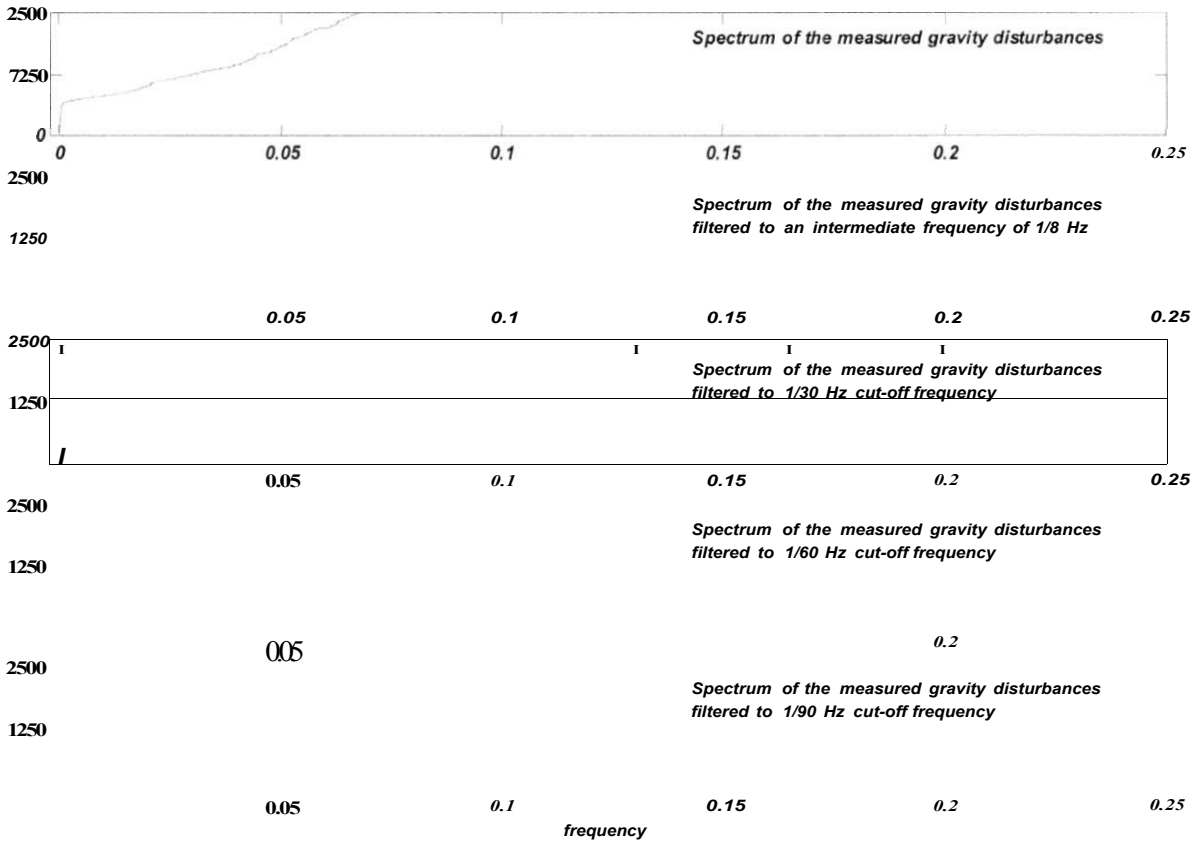


**Figure 2-4: Cumulative spectra of the measured and filtered gravity disturbance**

### 2.2.3 - Cross-over adjustment of the airborne gravity data

Near the origin of the spectra in Fig. 2-3, one notices a sharp decay. This is due to the low frequency contents in the data, which come from the low frequency of the gravity signal as well as the un-modelled biases in the accelerometers. Glennie (1999) tried different procedures to subtract or remove this bias and he concluded that the crossover adjustment is the best way. Bruton (2000), on the other hand, tried to combine a lowpass filtered geopotential model (GM) with the airborne gravity data after high-passing them to the frequency that corresponds to the extent of the surveyed region. He concluded that this couldn't be done due to the bad quality of the current GMs in the specific band of the spectra. He also stated that the best procedure for the time being is the crossover

adjustment. The output of this adjustment is a dataset of gravity disturbance with very good relative accuracy but with poor absolute orientation. To link this arbitrary dataset to the global gravity space, at least three gravity values from an independent instrument have to be available in the region. It should be noted that not all airborne gravimeters suffer from the long wavelength errors.

The crossover adjustment takes into consideration that the value of the gravity signal does not change during the survey. So, if the same location is occupied twice at different times, the time dependent accelerometer bias and the slope in the gravity signal along the flight line can be modelled and removed from the data by a least-squares adjustment. The measurement model of this adjustment is given as (Glennie, 1999):

$$A5g = s_i At_i + S_j Atj + b_i + bj \qquad (2.20)$$

where $Adg$ is the difference in disturbances between flight lines at the crossover points, $Sj, Sj, bi, bj$ are the slopes and biases of the flight lines rand $j$, respectively, and $At^{\wedge}Atj$ are the time difference between the start of the flight line and the time of the current crossover point.

For more details, one can refer to Glennie and Schwarz (1999) and Glennie (1999).

## 2.3 - Topographic effects

There are different methods for the treatment of the topographic effects, which can be classified as approximation methods and as reduction methods. For the former, there is the ***planar approximation*** (e.g., Nagy, 1966; Sideris, 1984; Sideris, 1990; Li, 1993; Peng, 1994; Li and Sideris, 1997; Omang and Forsberg, 2000; Nagy et al., 2000; Smith et al., 2001) and the ***spherical approximation*** (e.g., Martinec and Vanicek, 1994a; Martinec and Vanicek, 1994b; Martinec, 1998; Novak, 2000; Smith et al., 2001). Concerning the reduction methods, there are many procedures available: ***Bouguer*** (Heiskanen and Moritz,

1967), ***Isostatic*** (Heiskanen and Moritz, 1967; Sjoberg, 1998; Tsoulis, 2001), ***Helmert*** (Heiskanen and Moritz, 1967; Sideris, 1990; Martinec, 1998), and others like ***Rudzki*** and ***Poincare and Prey*** (Heiskanen and Moritz, 1967, Dragomir et al., 1982). As mentioned in the introduction, the 2nd Helmert condensation method in the spherical approximation is used in this research due to the small indirect effect it creates and to its wide use for geoid determination.

The potential of the topographical masses can be quantified by the Newtonian theory of attraction. In spherical approximation, the equation takes the form (Martinec, 1998)

$$V(r,qU)= k \; \backslash \; \backslash \; f^{HW\,r\,K\,p\,9}\wedge\wedge\wedge\}r^{P}dr'co\wedge'd\wedge dX' \qquad (2.21)$$

where

£ = 6.672x10-" $m^3/kg/\sec^2$ is the gravitational constant,

p *(kg I* $^3$) is the specific density of the topography,

*r,* cp, *X* are the radial distance ***(R + H***$^{TOPO}$), latitude, and longitude of the computation point,

*r',* cp', *X'* are the radial distance ***(R + H'),*** latitude, and longitude of the running point,

*L(r,\\j,r')* = *$Jr^2$ + $r'^2$ - 2rr'cosv|/ is the distance between the computation and running points,

cos\|/ = sincpsincp' + cosAxosVcosfV-X) is the angular distance between the computation and running points, and

***R*** = 6371 *km* is the mean radius of the Earth.

The above equation (2.21) is handled by splitting the topography into a regular part, the Bouguer shell, and irregular part, the actual topography. For a thorough analysis of the above equation, the reader is referred to Martinec (1998). The final equation used for the terrain correction (TC) in Helmert's 2nd condensation method, takes the form

$$TC(r,(p,k) = Gil \int_{r'=R}^{r'=R+H((p'X)} dr \cdot p(<pA) \int_{r'=R}^{r'=R+H(ip,X)} \frac{dL^{-1}(r,y,r')}{dr} cosq'dy'dX' \quad (2.22)$$

and the Condensed Terrain Corrections (CTC), on the other hand, is

$$CTC(r,(p,\backslash)=GR^2 \mathbf{1J}[a((p\backslash A,')-a(q>,X)\} \int_{=R+H\{y,\backslash)}^{5Z''(r,_M/,i?)} (7/- coscp'dcpW \quad (2.23)$$

where

a(cp, X) is the condensation density and it takes two forms:

$$<s = pH\left(1+\frac{H}{R}+\frac{H^2}{3R^2}\right)$$

applied to the first methodology considering that the potential of the Bouguer shell is equal to the potential of the condensed Bouguer shell ***both*** evaluated at the measuring location (Martinec, 1998);

or

applied to the second methodology considering that the potential of the Bouguer shell evaluated ***at the measuring*** location is equal to the potential of the condensed Bouguer shell **evaluated *at the geoid.***

This investigation showed that the difference between the two condensation-density equations listed above is negligible when evaluated on a 5'x 5' grid for it does not exceed 20 uGal for the CTC and 5 mm for the GIE.

The partial derivative

$$fe^{\wedge} = [(r'^2 + 3r^2)\cos_v + (1 - 6\cos^2\psi)rr']L^{-1}(r,\psi,r') + \\ + r(3\cos^2\psi)\log|r' - r\cos\psi + L(r,\psi,r')|$$

is used for the TC and is the radial derivative of the kernel

$$L'(r, V|/, R) = —(r' + 3r\cos \backslash\backslash i)L(r, \quad r) + + —(3\cos^2 \; y \; -1 \; \text{llog}\, r' - r\cos \backslash ]) + L(r, \backslash\backslash), r'J + C$$

where C is a constant, and

$$\frac{dL^{-1}(r,y,r')}{dr} \qquad \frac{r - r'\cos i|/}{\left(r^2 - r'^2 - 2rr'\cos\psi\right)^{3/2}},$$

which is used for the CTC and is the radial derivative of the Newton kernel 1/Z(r, *r')*.

As it is well know, the Direct Topographic Effect (DTE) is the difference between the TC (Eq. 2.22) and CTC (Eq. 2.23).

Finally, the topographic indirect effect of both the actual and condensed topography is expressed as follows:

$$G \quad 2np(<p,X)H^{2}(<p,X)(l_{+}*^{\wedge\wedge} \quad 3 \quad R$$

$$-p\{(p,XpL \quad [R,\backslash\backslash i,r \quad 1$$

$$q(<p',A/)-(r((pA) \quad L\{R,y,R) \quad \cos q>'dq>'dX'$$

(2.24)

with y(cp, A,) being the normal gravity computed from an approximation to Somigliana's formula:

$$y(cp, X) = y_0 (1 + a_0 \sin^2 cp + a_x \sin^4 cp) \qquad (2.25)$$

where $y_0$ is the normal gravity value at the equator of the best-fit ellipsoid of revolution, and $a_0$ and $a_x$ are constants that depend on the reference ellipsoid. The WGS84 reference ellipsoid was used here.

## 2.4 - Downward continuation

The downward continuation (D.C.) can be evaluated in different ways: inverse Poisson integral (e.g., Heiskanen and Moritz, 1967; Sun and Vanicek, 1996, among others), analytical downward continuation, collocation (Moritz, 1980), actual gravity gradient approximated by the normal free-air gradient, etc. Each of these methods gives a different

procedure to compute the gravity anomalies or disturbances on the reference sphere. From these, the inverse Poisson integral and the free-air gradient are used here.

### 2.4.1 - Inverse Poisson integral

The Poisson integral is usually used to compute gravity field functionals at a height above the Earth when the same (or other) gravity field functionals exist at the reference sphere. For example, if the gravity anomalies need to be known at some altitude above the reference sphere, the Poisson integral can make use of gravity field functionals, such as gravity anomalies or deflections of the vertical, located at the reference sphere to predict the wanted values at the desired altitude.

The problem of downward continuation is the opposite. Gravity anomalies or disturbances are located at some altitude and need to be known at the reference sphere. This is evaluated by the inverse of the Poisson integral.

Since it is an inverse problem, its regularization is a must (Schwarz, 1979; Bouman, 1998; Novak et al., 2000; Kern and Schwarz, 2001). Some of the regularization methods that are used in Geodesy are (Bouman, 1998):

- Tikhonov-Phillips regularization: this regularization removes the numerical instability by adding a stabilizer to the functional minimized (Tikhonov, 1963). This stabilizer is a parameter added to the normal matrix of the solution and it acts as a weighting factor between the relative importance of the prediction error and minimizing the solution norm (Rauhut, 1992).
- Collocation (can be either in the space or frequency domain and can be a built-in filter in the convolution; see, e.g., Li (2000)): it is based on the minimization of the norm of the observation error; this restricts the errors from being magnified. The use of an error covariance matrix also strengthens the diagonal elements of the covariance matrix to make its inversion stable,

- Iteration: the idea here is to make as many iterations to the system to extract the low order components and to stop before the solution becomes oscillatory due to the magnification of data errors (Bouman, 1998).

The Poisson equation, to upward continue the gravity disturbances (or anomalies), is written as:

$$rhg(r, (p, X) = \frac{}{4n} \iint dg(R, \varphi, f) K(r, R) d<5 \qquad (2.26)$$

where 8g(r,cp,A.) is the upward continued gravity disturbance to the radial distance r, $8g(R,(p,X)$ is the gravity disturbance at an equipotential sphere of radius $R$ , and

<u>a function of Legendre polynomials</u>:

$$K(r, \psi, R) = Y, (\sum_{n=2}^{\infty} + U- \left(\frac{R}{r}\right)^{n} (\cos v)/)$$

<u>a closed formula</u>:

$$K\{r,y,R) = R \frac{R'}{(R^2 + r^2 - 2rR\cos\psi)^{3/2}} (\cos v)/ \qquad (2.27)$$

with $\psi$ being the spherical distance and $P_n(\cos \psi)$ the Legendre function of degree $n$ .

The gravity disturbance (or anomaly) itself is not a harmonic function, so its multiplication with its radial distance creates a harmonic function that can be used in the Poisson integral (Heiskanen and Moritz, 1967).

In an inverse problem, the possibility of the ill posedness of the solution is present. Sun and Vanicek (1996) showed that the D.C. of gravity disturbances (or anomalies) is a well-posed problem when gridded to a 5'x 5' grid using the iterative scheme. The procedure of the iterative scheme will be used in this study, which is well documented in the geodetic literature, e.g. Sun and Vanicek, (1998); Martinec, (1998).

### 2.4.2 - Normal free-air gradient

Gravity changes with altitude. This change is called the vertical gravity gradient and it is computed from (Heiskanen and Moritz, 1969):

$$\frac{\wedge}{3H} = -2gJ + 4nkp - 2ay^2 \qquad (2.28)$$

where $\frac{dg}{dH}$ is the gravity gradient sought,

$g$ is the gravity value,

$J$ is the mean curvature of a surface and is equal to:

$j \frac{W_{xx} + W}{x \quad y} JL_s$ with $W_u$ is the second partial derivative of the gravity potential along the

$i$ — *axis,*

p is the density of the topography and the crust, and

co is the rotation rate of the earth.

This equation (2.28) cannot be evaluated directly because it is difficult to compute the mean curvature and because of lack of density information. Instead of using the gradient of the real gravity field, the normal gravity gradient is used as an approximation.

The normal gravity y at altitude $h$ can be expanded into a series in terms of $h$ :

$$\frac{\partial \gamma}{\partial h} h + \frac{1}{2} \frac{\partial^2 \gamma}{\partial h^2} h^2 + \cdots \tag{2.29}$$

From this series, only the first two terms are worth using due to the small effects of the other terms. The first term is approximately equal to $0.3086\, mGal\, I\, m$ and the second can reach approximately the value of 1 mGal for heights of 3500 meters and is approximated as:

$$\frac{\partial^2 \gamma}{dh^2} \quad \frac{6\gamma}{a^2} \tag{2.30}$$

where $a$ is the semi-major axis of the ellipsoid, and y is the normal gravity.

The normal free-air gradient series up to $2^{nd}$ order term is used in this thesis as approximation of the real gravity gradient to move the measured gravity value at certain height to the reference sphere at height zero.

### 2.4.3 - Collocation

Collocation is used to stochastically link the observed gravity signal at a certain altitude above the geoid to values on the geoid by their auto- and cross-covairiance functions. The principal equation of collocation is based on the minimization of the norm of the observation error; thus, collocation is by itself a regularization procedure. The collocation equation is

$$\delta g(R) = C_{\delta g^0 \delta g^h} \left( C_{\delta g^h \delta g^h} + C_{nn} \right)^{-1} \delta g(r) \tag{2.31}$$

where $C_{nn}$ is the error covariance matrix of the data, $C_{bg\,Hg}$ is the cross-covariance matrix of the data, and $C$, *. » is the auto-covariance function at flight level.

Collocation also provides errors estimates for the results expressed by the prediction error covariance matrix (Moritz, 1980).

### 2.4.4 - Analytical downward continuation

In the analytical downward continuation, the gravity disturbances (or anomalies) at the reference sphere are linked to the gravity disturbances (or anomalies) at some height by Taylor power series, as:

$$Zg(r) = bg(R) \pm\pm \frac{h''}{n!} \quad dr'' \tag{2.32}$$

The solution in Equation (2.32) can be simplified by using the first term of the series only (Moritz, 1980) and it can be written as:

$$h(R) = ?>g(r)-^h \quad or \tag{2.33}$$

with the vertical gradient equal to:

$$\frac{dbg}{dr} = \frac{8_g(qa)}{R} \quad R^2 \; \frac{5_g((p'A0-8_g(q),X.)}{2tz\,J \quad L^3(r,y,r')} \tag{2.34}$$

All terms have been defined previously. This equation allows for the evaluation of the vertical gradient by the use of data on the reference sphere.

## 2.5 - Geopotential Model contribution

The contribution of the geopotential model (GM) is evaluated by a spherical harmonic expansion series. In the spherical approximation, the gravity anomaly is:

$$Ag^{GM} = \sum_{n=2}^{n_{max}} \sum_{m=0}^{n} (C_{nm} \cos mX + S_{nm} \sin mX) P_{nm}(\cos \theta) \qquad (2.35)$$

whereas the gravity disturbance is:

$$\delta g^{GM} = \frac{kM}{r^2} \sum_{n=2}^{n_{max}} \left(\frac{a}{r}\right)^{n+1} (n+1) \sum_{m=0}^{n} (C_{nm} \cos mX + S_{nm} \sin mX) P_{nm}(\cos \theta) \qquad (2.36)$$

where M is the mass of the Earth,

$n$, m and $n_{max}$ are the degree, order, and the maximum degree of the GM used, respectively,

$C_{nm}$ and $S_{nm}$ are the normalized spherical harmonic coefficients of the disturbing potential,

$r$ is the radial distance to the computation point,

$P_{nm}(\cos \theta)$ is the normalized associated Legendre function evaluated at the co-latitude $\theta$, and $X$ is the longitude.

The super-script "GM" refers to the values evaluated using the GM.

The GM contribution is not studied explicitly in this thesis. Previous studies have shown that, for the region under study, the optimal contribution of the EGM96 geopotential model is obtained by using a maximum degree and order 200 with an integration cap size of not less than ten degrees (Esan, 2000).

## 2.6 - Noise propagation and filtering

Noise exists in every type of measurement. When these measurements are used in mathematical models to determine certain functionals, the noise is propagated through the model parameters into the estimated functionals. Noise propagation is used to determine the noise in the final results, provided that statistical information - variances and covariances - on the initial measurement noise is known. In airborne gravimetry, this is done through equations 2.17 and 2.18. Noise propagation can be applied to all physical geodesy mathematical equations: terrain effects, downward continuation (when inverse Poisson integral, collocation, and analytical downward continuation are used), Stokes/Hotine formulations, GM contributions, etc.

Noise propagation requires the existence or knowledge of the noise variance and covariance of the initial data. DTM variances and covariance have to be known to estimate the noise in the terrain effects. As for the downward continuation, the noise in the data, plus the noise propagated after the terrain reduction, can be used to estimate the noise of the downward continued gravity values at the reference sphere. In addition to this, noise information can also be used for regularizing the ill-posed problem when the inverse Poisson integral is used, e.g. using Tikhonov-Phillips regularization or collocation. Stokes'/Hotine's integrals can also be used to propagate the gravity noise into noise in the determined geoid. The variances and covariances in the GM coefficients are used to estimate the error introduced into the final geoid from the uncertainty of the GM coefficients.

Error propagation is a very good tool when the errors of the initial data are known, but unfortunately this is not the case here. For example, error propagation in geoid determination from airborne gravimetry (Eq. 2.17) has not been implemented explicitly; however, a spectral study of the errors of the subsystems revealed that the airborne gravity

data have a white noise of approximately 2 mGal; for more details see, Bruton (2000) and Schwarz et al. (1994). Moreover, the differences between the airborne and the ground gravity data do not yield the right error knowledge to use in the propagation, due to the fact that the ground gravity data are also polluted with errors whose neither the real value nor the distribution is known.

Noise filtering, on the other hand, can be applied to measurements when predicting functionals obtained from the measurements. The requirement for filtering is the knowledge of the behaviour and the type of the noise, i.e., stationarity, non-stationarity, white, coloured, etc. Also, filtering can be built into the mathematical model; for example, Wiener filtering (Sideris, 1996) can be built into the convolution integrals used in physical geodesy, i.e., Stokes'/Hotine's, Poisson's integral, inverse Poisson's integral (Li, 2000), etc.

Theoretically speaking, filtering is possible but, unfortunately, the errors in the data do not match our desire of being randomly distributed and with known variances. In the real geodetic world, errors are non-stationary and are not normally distributed. Errors that accompanied the data - in databases - can be used, but we have to realize that if they do not represent the real situation, no improvements should be expected in the solution (Bayoud and Sideris, 2001).

For the reasons mentioned above, error propagation and stochastic noise filtering have not been applied here. An independent study has to take place on this topic.

## 2.7 - Combination of airborne with ground gravity data

Airborne gravity data suffer from high and low frequency errors. Combination of different ground gravity data with the airborne data is a good tool to minimize these errors.

It is the author's opinion that the combination between airborne and ground gravity data is useful only for the long wavelength errors. This is because the high frequency errors, of both data types, are filtered out when they are input into Stokes'/Hotine's integral. Stochastic combination (Bendat and Piersol, 1996; Sideris, 1996)) of data sets can improve

the solution immensely as long as the right error model is chosen; otherwise, the solution is not improved (Bayoud and Sideris, 2001).

As mentioned before, the imperfections in the accelerometers cause long wavelength errors in the airborne gravity data. The crossover adjustment has proven to be the best way to minimize these errors (Glennie, 1999), but the outcome is a dataset that does not fit the long wavelengths of the gravity field on the region. This means that the crossover adjusted airborne gravity data refer to an arbitrary plane in space. A way to correct this is to link the airborne data to ground data by removing the systematic differences between them.

In theory, only three points are sufficient to define a plane, so three ground gravity measurements are sufficient to orient the airborne gravity data. Due to the possibility of outliers in the ground gravity data, several ground gravity points are recommended, the number of which depends on their accuracy and coverage, and on the extent of the area of airborne gravity data. One has to recognize that ground measurements in old databases are mostly gravity anomalies, while the airborne system outputs gravity disturbances; a systematic transformation between the two quantities (described in Sec. 2.1) has to take place before the combination.

When a stochastic combination is required - and it is only recommended when we have a sound knowledge of the data errors - different methods can be employed: *Input-Output System Theory* ***(IOST)*** (Andritsanos, 2000; Andritsanos et. al, 2000; Sideris, 1996; Bendat and Piersol, 1986), *Least-Squares Collocation* ***(LSC)*** (Moritz, 1980; Tscherning, 1974), *Fast Collocation* ***(FC)*** (Bottoni and Barzaghi, 1993; and Eren, 1980), and *Least Squares Adjustment in the Frequency Domain* ***(LSAFD)*** (Li and Sideris, 1997; Bouman and Koop, 1998). A very brief comment on each method is given below.

- ***IOST:*** Among these methods, the IOST proved to be slightly superior (Li and Sideris, 1997; Tziavos et al., 1996, Tziavos et al., 1998, among others) for the reason that it uses a detailed (anisotropic) signal Power Spectral Density (PSD), and is computationally efficient. But gridded data and coverage of all datasets on the same grid are required.

- ***LSC:*** Collocation overcomes the disadvantage of the previous method, but its inefficiency is well known. The use of an isotropic covariance function introduces an approximation, yet this is not a problem for local geoid modelling.
- ***FC:*** The FC, on the other hand, proved to be efficient in computational speed compared to the LSC but has the same requirements as the IOST.
- ***LSAFD:*** The LSAFD uses the least-squares technique in the frequency domain. This method assumes that the observations and their noise PSD's are known. Studies in (Barzaghi et al, 1993; and Li and Sideris, 1997) showed that this method gives worse results than the other methods listed above, because it is more sensitive to the input noise.

As for the systematic errors, a surface between the datasets is removed after modelling it. This model has to be of low order and describes also the differences in datum between the two datasets. The model often used in geodetic literature is the four-parameter model (Heiskanen and Moritz, 1967):

$$D = d_x \cos q > \cos A. + < i_2 \cos(p \sin X + d_3 \sin cp + d_4 , \qquad (2.37)$$

where $D$ is the difference between the two datasets, cp and $X$ are the spherical coordinates, and the $d_i$'s are the parameters of the surface computed by the least-squares adjustment.

This model was used to make the airborne and ground datasets consistent in Chapter 3 and also to combine the gravimetric and geometric geoids in Chapter 4.

## 2.8 - Methodologies used for geoid determination from gravity data

The two methodologies that are used in this research are generated from the procedure for computing the gravity disturbances (or anomalies) at the reference sphere; this depends on

the downward continuation method. They apply to the use of either ground or airborne gravity data for geoid determination.

***1st methodology:*** (Fig. 2.5 and 2.7)

When the inverse Poisson integral is used, the procedure for computing gravity disturbances (or anomalies) on the reference sphere is described in the following scheme:

1. Compute the normal gravity at the same location as the measured gravity values when $\delta g$ is sought (or at the telluroid when $\Delta g$ is sought) and subtract them,

   $$\gamma^h = b_0\left(1 + b_1 \sin^2 \varphi + b_2 \sin^4 \varphi\right) + \left(b_3 + b_4 \sin^2 \varphi\right)h + b_5 h^2 \qquad (2.38)$$

   The '6' coefficients depend on the reference ellipsoid; see Fleiskanen and Moritz (1967) for more details. The WGS84 reference ellipsoid was used here.

2. Compute the direct topographic effects (DTE) at the computation point (filter them in case of airborne data), and add them to the values of step 1
3. Subtract the Geopotential Model contribution from the values of step 2
4. Downward continue the values of step 3 to the reference sphere using the inverse Poisson integral
5. Determine the co-geoid by Stokes/Hotine formulation
6. Compute the geoid by adding the Geoid Indirect Effect (GIE) and the GM contribution.

The interested reader can refer to Vanicek and Martinec, (1994), Martinec and Vanicek (1994a), and Martinec and Vanicek (1994b) for a thorough analysis of this methodology.

***2nd methodology:*** (Fig. 2.6 and 2.8)

On the other hand, when the normal free-air gradient is used, the computation of gravity anomalies or disturbances on the reference sphere is described in the following scheme:

1. Compute the normal gravity at the geoid when $5g$ is sought (or at the reference sphere when $Ag$ is sought) and subtract it from the measured gravity values,
2. Compute the Terrain Corrections (roughness of the topography, TC) at the computation point (filter them in case of airborne data), and add them to the values from step 1
3. Compute the Condensed Terrain Corrections (CTC) at the reference sphere (filter them in case of airborne data), and subtract them from the values from step 2
4. Subtract the Geopotential Model contribution from the values of step 3
5. Use the normal free-air gradient up to the second order (the $2^{nd}$ order term can reach a value of approximately 1 mGal for heights of 3500 metres) to downward continue the measured gravity values to the reference sphere
6. Determine the co-geoid by Stokes/Hotine formulation
7. Compute the geoid by adding the Geoid Indirect Effect (GIE) and the GM contribution.

The interested reader can refer to Sideris (1990) for thorough analysis of this methodology. Although the planar approximation was used in (ibid), the main methodology is the same.

These two methodologies are applied when either ground or airborne gravity data is used. The only difference is with the computation of the topographic effects, where the computation point in the case of the airborne data is not at the topography but at the flight height. Also, when the airborne gravity data is used, the topographic effects - whether they are the DTE, TC, or CTC - have to be filtered first before used in the gravity disturbances (or anomalies) computations. The effect of filtering will be discussed in the next chapters.

Based on these methodologies, the main objective of this thesis is studied, along with the tasks that are stated in the first chapter.

$$Zg_{Po}=g_p-y_p+TC_p-CTC_p+DC-GM$$

$$N = S(bg_{Po}) + N^{GM} + N^{GIE}$$

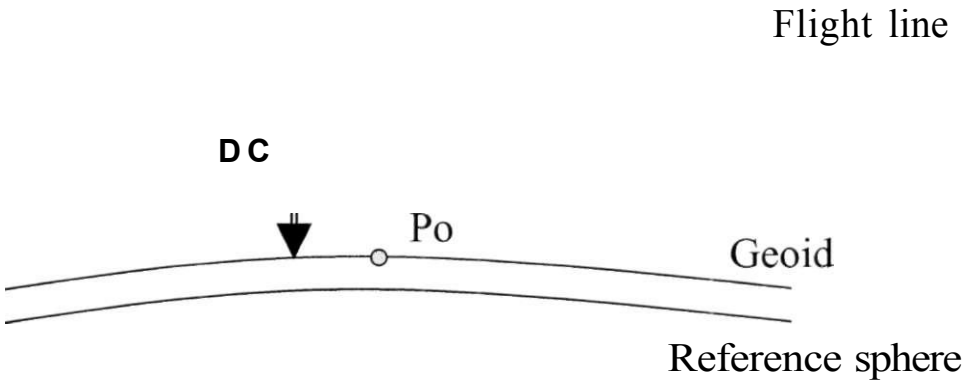


**Figure 2-5: Methodology # 1 when computing gravity disturbances**

$$H_{Po} = g_p - \frac{\partial H}{dH} - \frac{\partial H}{2\, dH^2} - l_{po} + TC_p - CTC_{DO} - GM$$

$$dH \sim dh \qquad \frac{d^2g}{dH^2} \sim \frac{d^2y}{dh^2}$$

$$N = S(5g_{Po}) + N^{GM} + N^{GIE}$$

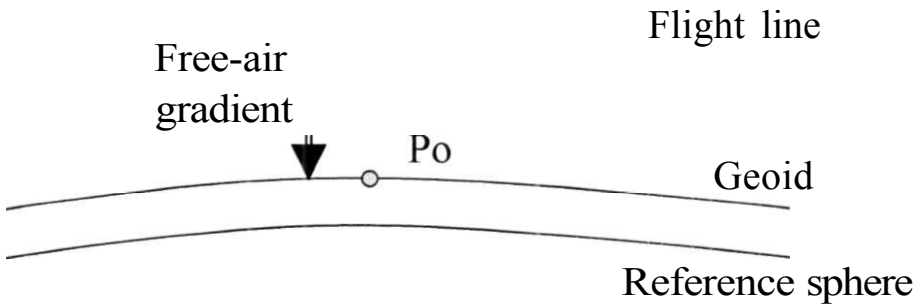


**Figure 2-6: Methodology # 2 when computing gravity disturbances**

^rr -CTC + DC - GM
\ - a - Y +1C, ^'^p

N

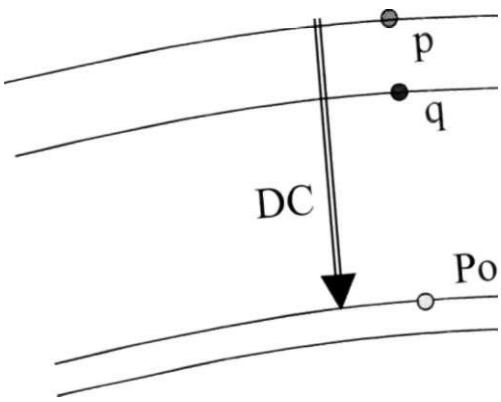


Flight line

" Telluroid

Geoid

Reference sphere

! when computing gravity anomalies

**Figure 2-7: Methodology #**

A g P o = g p - m n 2 d H

a n 2 s / j 2

IE

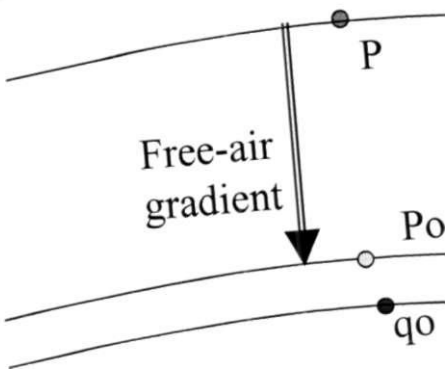


Flight line

Geoid

Reference sphere

omputing gravity anomalies

**F i g u r e 2-8: Methodology* 2 w h e n c**

# Chapter 3

# Gravity Data Processing and Numerical Tests

In this chapter, the pre-processing of gravity data will be analysed. Two data types will be used: ground and airborne gravity data. These analyses start after the initial processing (Kalman and low-pass filtering in case of airborne data) of the gravity data, and they include: terrain effects, gridding, and downward continuation. After the introduction, the reduction of the topographic masses follows, for both the ground and airborne gravity data. Then the gridding follows for the airborne data, where different datasets will be examined. Downward continuation is the last item studied in this chapter, when the inverse Poisson integral is used. The use of the ground gravity data illustrates the differences in processing methodologies, and is used to investigate the two objectives listed in the introduction. Also, as mentioned before, the ground data is used as a reference for the airborne gravity data.

## 3.1 - Introduction

Due to the lowpass filtering of the airborne data in the frequency domain (Ch. 2), the part of the topographic gravity signal that exists beyond the filtering frequency is also filtered out. This leads to the idea that to have consistent datasets when reducing the filtered gravity signal, the contribution of the topography has to be filtered first and then be used for reduction purposes. It is the author's opinion that although this is theoretically correct, investigation should be done to study the effect of not filtering the terrain effects on the geoid. In this chapter, analysis of the contributions of the terrain effects on ground and airborne gravity data computed from different DTM resolutions will be made by evaluating these effects DTM resolutions of 15, 30, and 60 arc seconds (averaged from a 3 arcsec

DTM). The second task will be to investigate if the filtering of the topographic effects is essential from a practical point of view.

After the topographic reductions, using the 2nd Helmert condensation, the data have to be brought to the reference sphere for the geoid determination. This downward continuation is done either rigorously by applying the inverse Poisson integral or by simply applying the gravity gradient. Since the true vertical gradient is not known, the normal free-air gradient is used as an approximation.

The downward continuation will be the second step of the processing. First, the inverse Poisson integral will be applied on the ground and then on the airborne gravity data. The normal free-air gradient solution is applied to the data in the process of computing the gravity anomalies or disturbances (as shown in the equations in Fig. 2-6 and 2-8). This leads to the two methodologies discussed in the previous chapter.

Due to the imperfections of the accelerometers (Allied Signal Q-Flex model QA 2000-010) in the INS system used (Honeywell system), it is highly recommended that ground data be used for linking the crossover adjusted airborne data to the gravity space by removing systematic differences between the ground and airborne data (as discussed in Ch. 2). Note that other systems might not have the same problem in the accelerometers and a link to the gravity space using ground data might not be needed.

In the above procedure, the geopotential model contribution - i.e., the EGM96 (Lemoine et al., 1996) to degree and order 360, and the GPMar, br, or cr (Wenzel, 1998) to degree and order of 720 - is removed from the data before the downward continuation. This contribution is added back either after downward continuation as gravity information when gravity is the final product, or as geoid information after Stokes/Hotine formulation is applied when the geoid is the final product.

In the following, we will implement the previously discussed methodologies on the airborne as well as on the ground gravity data, using the latter as the reference. The ground data will also be upward continued to the flight level to be used for the consistency check of the two data sets, as well as for padding the edges of the airborne data before downward continuing them when the first methodology is employed.

## 3.2 - Topographic effects - 2 Helmert condensation

In this section, the evaluation of the terrain effects is studied for the ground and airborne gravity data. First, the terrain effect on ground data using different DTM resolutions is studied; then, the terrain effects evaluated at the flight level are examined using different DTM resolutions along with the study of the filtering effects. A code in C++ was written by the author to carry out the computation of the terrain effects in this thesis.

### 3.2.1 - Topographic effects on ground gravimetry

For the practical implementation of the equations discussed in Section 2.3 and assuming constant topographic density, they can be written as follows,

***Terrain Correction (TC)***

$$7\,r\,(\,r\,,\,q\,a\,) = G\,p\,X\,I \left.\frac{dL\text{-}^{l}(R \quad + \quad H^{topo},\backslash y,r')}{dr}\right|_{r'=R+H((p,\backslash)}^{r'=R+H(ip'X)} \quad \text{coscp'AcpAA.} \qquad (3.1)$$

***Condensed Terrain Correction (CTC)***

$$CTC\{r,\ q>,A.) = GR^{2}\ XI\ H<p\backslash\ A.')\text{-}o(q>,\ *)\Big]\left.\frac{dL\text{-}^{x}(R \quad + \quad H^{topo},\backslash y,R)}{dr}\right|_{r=R+H(<p,X)} \quad \text{cos cp'AcpAA.} \qquad (3.2)$$

***Geoid Indirect Topographic Effect (GIE)***

$$iV^{G/\pounds}(9A) = \frac{Gp}{y(<p,X)} \quad 3 \quad 7?$$

$$7? \quad \frac{(j(<p',X')-cj(q>,X)}{L(R,y,R)} \cos(p'A9AX$$

(3.3)

### 3.2.1.1 - Numerical Test

In the numerical test with ground data, the same region where we have airborne data was chosen. There are 2110 gravity values, 176 out of which were measured in the summer 1999 and 2000, located between 49.3° < cp < 52.4° and 241.5° < $X$ < 246.5°. The geographical coverage and the topography in that region are shown in Fig. 3-1.

For the quantification of the topographic gravity signal, three Digital Elevation Model (DTM) resolutions were used: 15, 30, and 60 arcsec, averaged from a 3 arcsec DTM (Table 3-1). The integration radius was chosen to be 1 degree. Table 3-2 shows the statistics of the free-air gravity anomalies (the first and second terms of the Taylor series were used), complete Bouguer anomalies, and refined Bouguer anomalies.

**Table 3-1: Statistics of the DTM's used, in meters**

| | Max | Min | Mean | ~5td~ | RMS |
|---|---|---|---|---|---|
| 15 arcsec | ***3851*** | ***186*** | ***1306*** | ***521*** | ***1406*** |
| 30 arcsec | ***3670*** | ***216*** | ***1306*** | ***519*** | ***1405*** |
| 60 arcsec | ***3405*** | ***233*** | ***1306*** | ***513*** | ***1403*** |

The refined Bouguer anomalies, computed from the 15 arcsec DTM, were used to form a 5'x5' grid between the boundaries: 49.4333° < (p < 52.35° and 241.875° < $X$ < 246.45833° generating 2016 values. This grid was chosen because of the

availability of airborne data at its nodes between the boundaries: $50.4333° < cp < 51.35°$ and $243.5167° < X < 245.0417°$.

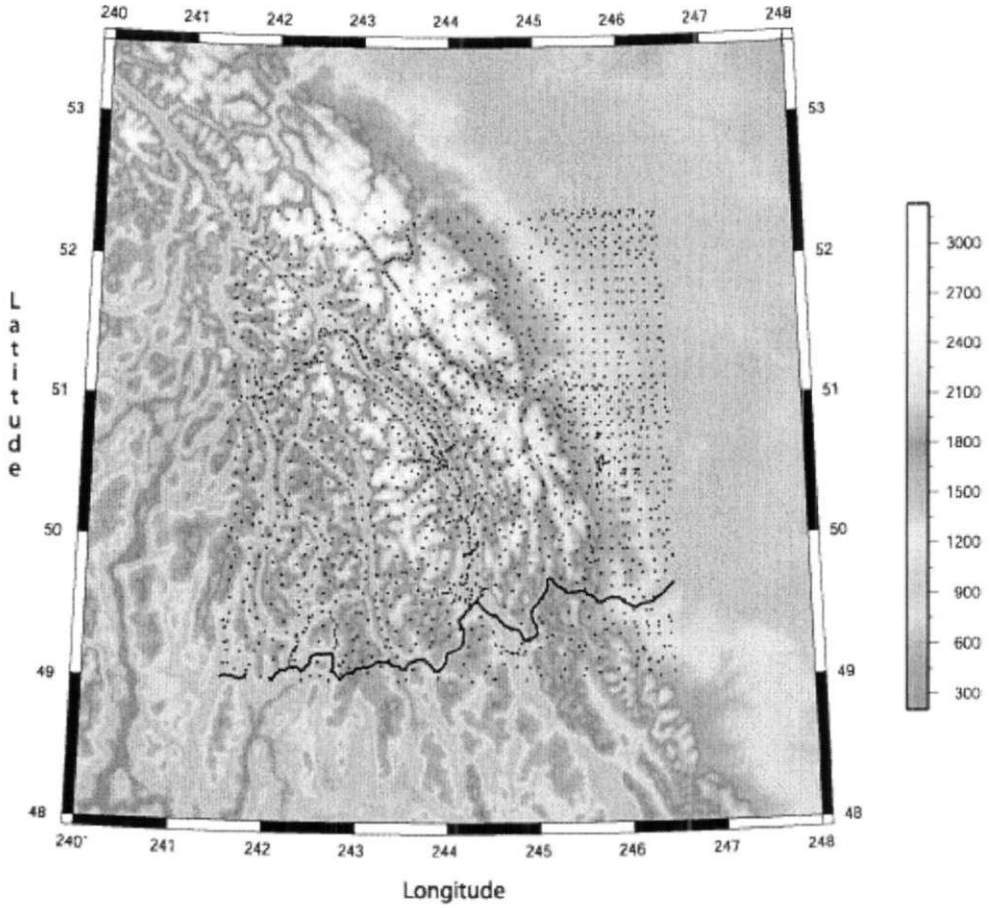


**Figure 3-1: The locations of the ground data and the topography in the region under study, in meters**

A larger region was chosen to perform the integration in geoid determination. The gridded gravity anomalies reduced to the topography and to EGM96 to degree and order 360 are also listed in Table 3-2. These are the (free-air + DTE - $Ag^{GM}$) values and (free-air + $TC^{h}$ - $CTC^{0}$ - $Ag^{GM}$) values; the first will be used in the inverse Poisson integral for downward continuation and the second will be used in the $2^{nd}$ methodology for the geoid determination as described in (Sideris, 1990). Figures 3-2 and 3-3 show these datasets computed using the 15 arcsec DTM. In the $2^{nd}$ methodology, $TC^{h}$ is computed at the topography and $CTC^{0}$ is computed at the reference sphere. $CTC^{0}$ has small values whose

effect on the geoid does not exceed 2 cm in the region under study with a grid spacing of 5'x5'.

**Table 3-2: Statistics of ground gravity anomalies on 5'x 5' grid (mGal)**

| Reduced anomalies | DTM resolution | Max | Min | Mean | Std | RMS |
|---|---|---|---|---|---|---|
| Free-air | | 484.1 | -497.4 | -14.4 | 62.7 | 64.3 |
| Complete Bouguer | | 189.3 | -596.5 | -167.2 | 40.1 | 172.0 |
| Refined Bouguer | 15 | 102.0 | -347.6 | -162.5 | 31.2 | 165.5 |
| | 30 | 101.8 | -352.7 | -162.5 | 31.2 | 165.5 |
| | 60 | 102.3 | -348.2 | -161.6 | 31.6 | 164.7 |
| Free-air + DTE - $Ag^{GM}$ | 15 | 123.4 | -144.6 | -7.1 | 29.4 | 30.3 |
| | 30 | 121.6 | -144.5 | -8.0 | 29.2 | 30.3 |
| | 60 | 119.7 | -144.4 | -9.3 | 28.9 | 30.4 |
| Free-air + $TC^h$ - $CTC^0$ - $Ag^{GM}$ | 15 | 158.6 | -161.0 | -4.9 | 44.1 | 44.3 |
| | 30 | 156.8 | -161.1 | -5.8 | 43.8 | 44.2 |
| | 60 | 155.0 | -161.3 | -7.2 | 43.5 | 44.1 |

Table 3-3 shows the statistics of TC, CTC, and DTE computed at the nodes of the grid. Table 3-4 shows the statistics of the differences in TC, CTC, and DTE computed from 15, 30, and 60 arcsec DTM. The differences in TC (15 minus 30, and 15 minus 60 arcsec) computed from the different DTM resolutions are shown in Fig. 3-4 and 3-5. Their correlation with the topography is well displayed. Studying Fig. 3-4 and the first row of Table 3-4, it is observed that the effect of DTM resolution on the TC is immense. Although in rough topography the differences are much larger than those in smooth topography, as is expected, a shift of around 1 mGal is distributed all over the region, indicating that the 15 arcsec data set contains more information and a larger signal is detected. A regional bias of around 1 mGal causes major problems in the geoid computation; the denser the DTM is, the better the geoid is modelled. As for the 60 arcsec data set, the shift of around 2.3 mGal clearly indicates a problem if used in the geoid modelling. In the next chapter, the geoid differences are shown when these DTM resolutions are used. The DTM resolution has no

significance on the computation of $CTC^{0}$ due to its small values and thus they are not shown here. The difference in DTE, on the other hand, has a similar behaviour as that of the TC, from which similar conclusions can be drawn. Here these differences in terms of gravity signal are not shown, but they will be re-visited in terms of their effect on geoid modelling in the next chapter (4).

**Table 3-3: Statistics of TC, CTC and DTE computed from 15, 30, and 60 arcsec DTM at the topography on 5'x 5' grid (mGal)**

| Terrain reduction | DTM resolution | Max | Min | Mean | Std | RMS |
|---|---|---|---|---|---|---|
| TC | 15 | ***78.8*** | ***0.0*** | ***9.3*** | ***8.3*** | ***12.4*** |
| | 30 | ***78.6*** | ***0.0*** | ***8.4*** | ***7.6*** | ***11.3*** |
| | 60 | ***74.0*** | ***0.0*** | ***7.0*** | ***6.7*** | ***9.7*** |
| CTC | 15 | ***132.0*** | ***-69.7*** | ***2.2*** | ***23.7*** | ***23.8*** |
| | 30 | ***132.1*** | ***-71.1*** | ***2.2*** | ***23.8*** | ***23.9*** |
| | 60 | ***132.3*** | ***-75.7*** | ***2.1*** | ***24.1*** | ***24.1*** |
| DTE | 15 | ***112.8*** | ***-59.1*** | ***7.0*** | ***23.3*** | ***24.4*** |
| | 30 | ***115.7*** | ***-59.4*** | ***6.1*** | ***23.4*** | ***24.2*** |
| | 60 | ***121.1*** | ***-63.2*** | ***4.8*** | ***23.8*** | ***24.2*** |

**Table 3-4: Statistics of the differences in TC, CTC and DTE computed from 15, 30, and 60 arcsec DTM at the topography on 5'x 5' grid (mGal)**

| Terrain reduction | DTM resolution | Max | Min | Mean | Std | RMS |
|---|---|---|---|---|---|---|
| TC | 15-30 | ***6.3*** | ***-1.4*** | ***0.9*** | ***1.1*** | ***1.4*** |
| | 15-60 | ***14.7*** | ***-2.3*** | ***2.2*** | ***2.4*** | ***3.3*** |
| CTC | 15-30 | ***1.5*** | ***-2.8*** | ***0.0*** | ***0.1*** | ***0.1*** |
| | 15-60 | ***5.9*** | ***-7.7*** | ***0.0*** | ***0.7*** | ***0.7*** |
| DTE | 15-30 | ***6.4*** | ***-2.9*** | ***0.9*** | ***1.1*** | ***1.4*** |
| | 15-60 | ***16.3*** | ***-8.3*** | ***2.1*** | ***2.6*** | ***3.4*** |

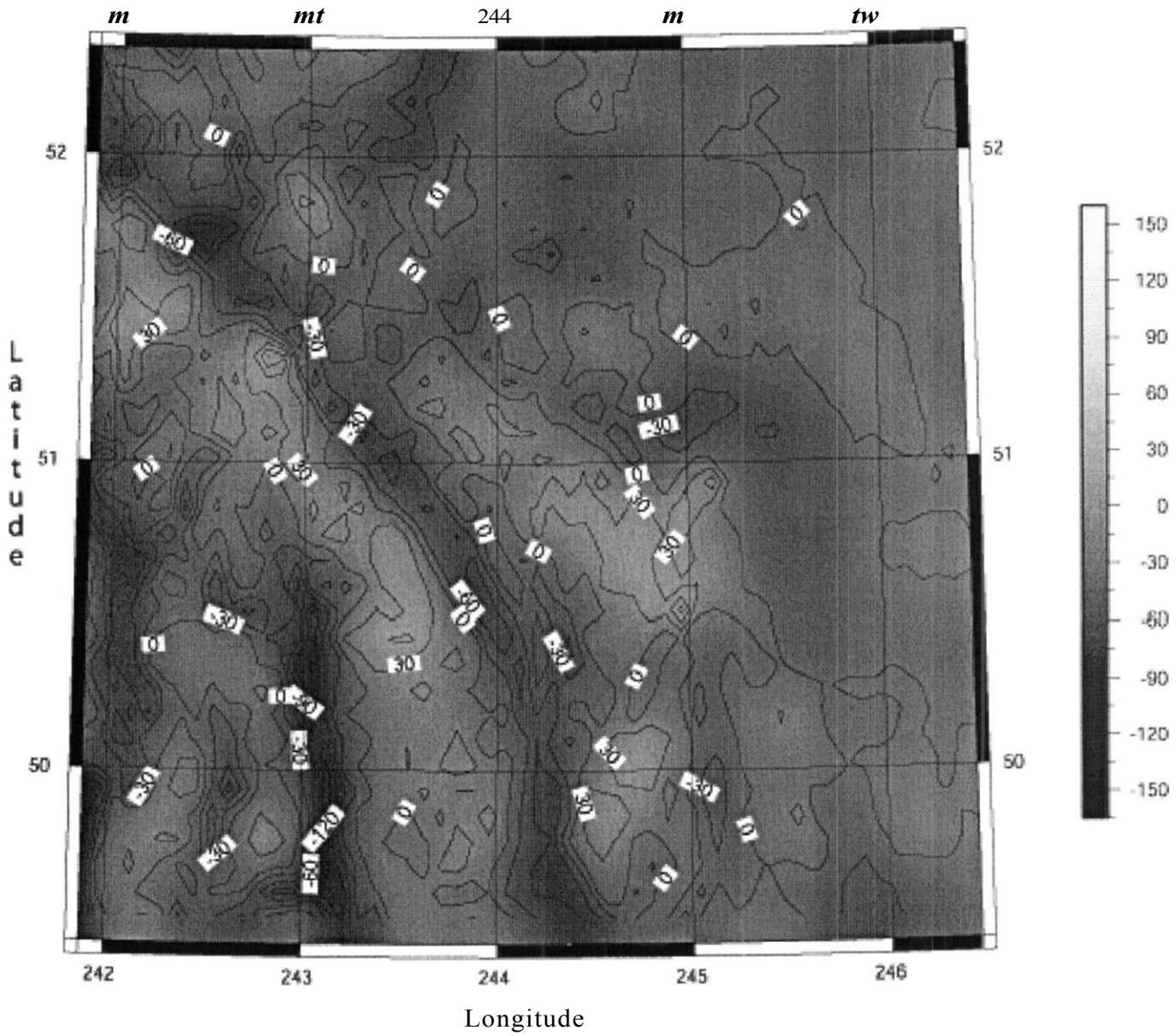


**Figure 3-2: Gravity values reduced by the DTE using 15 arcsec DTM and EGM96 (mGal)**

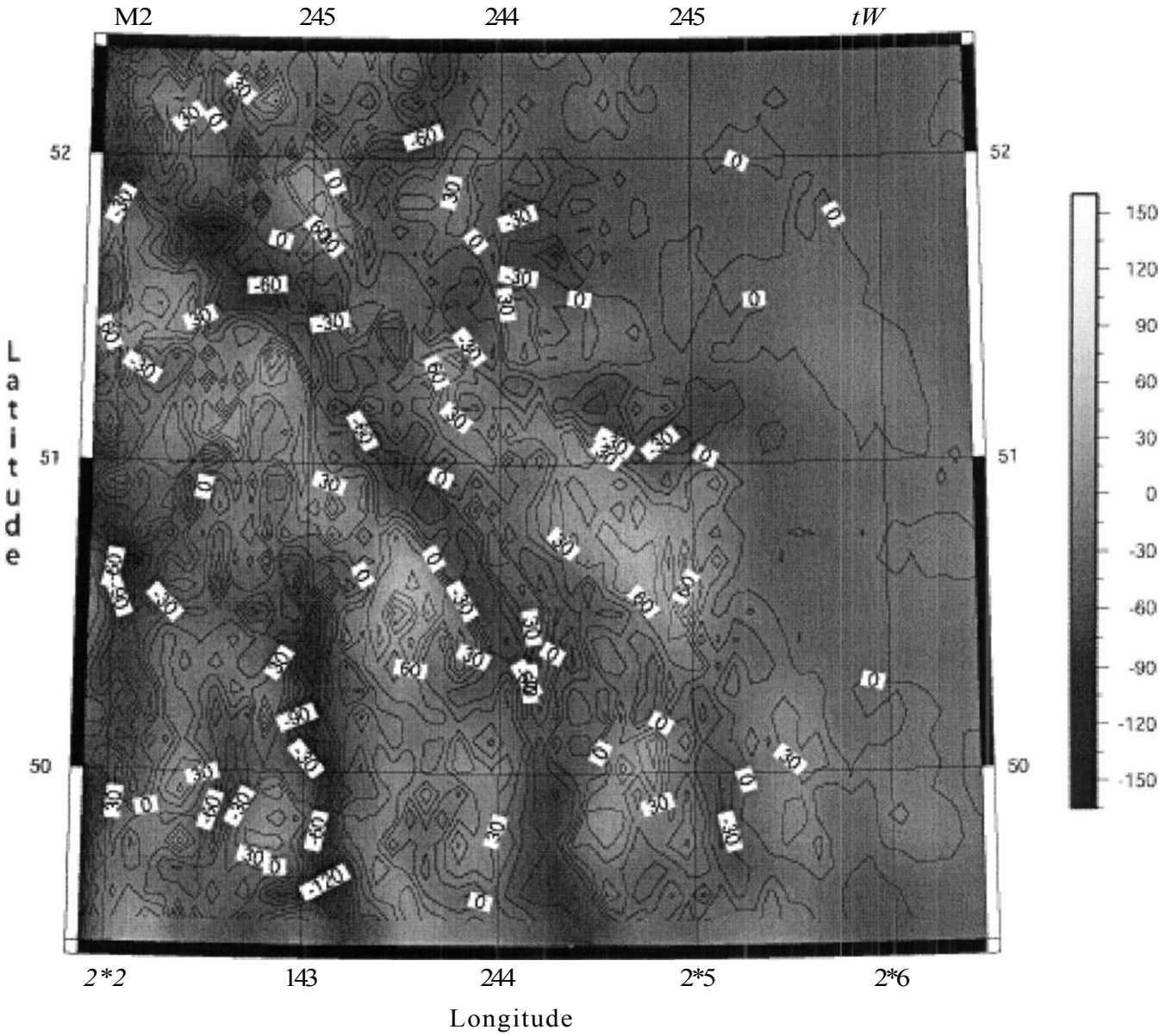


**Figure 3-3: Gravity values reduced to the TC using 15 arcsec DTM and EGM96 (mGal)**

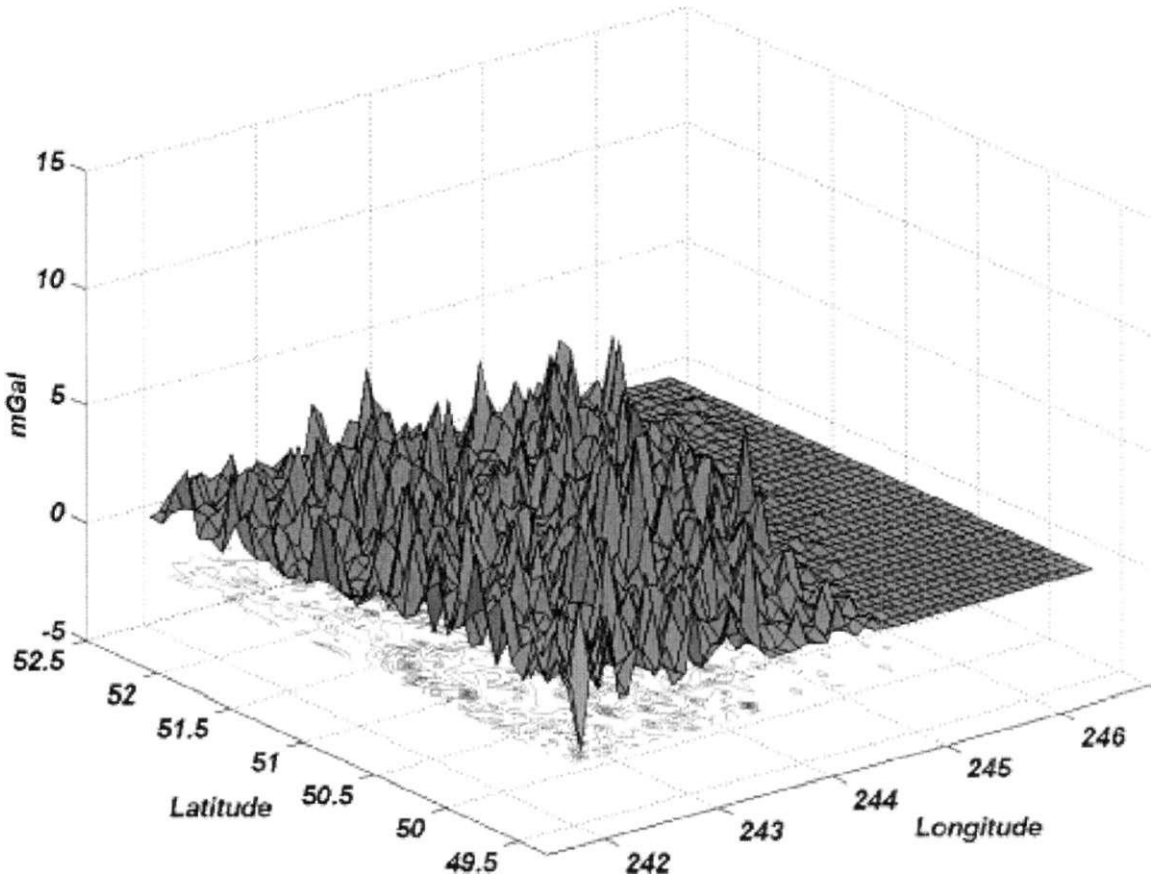


**Figure 3-4: Difference between the TC computed from a 15 and 30 arcsec D T M (mGal)**

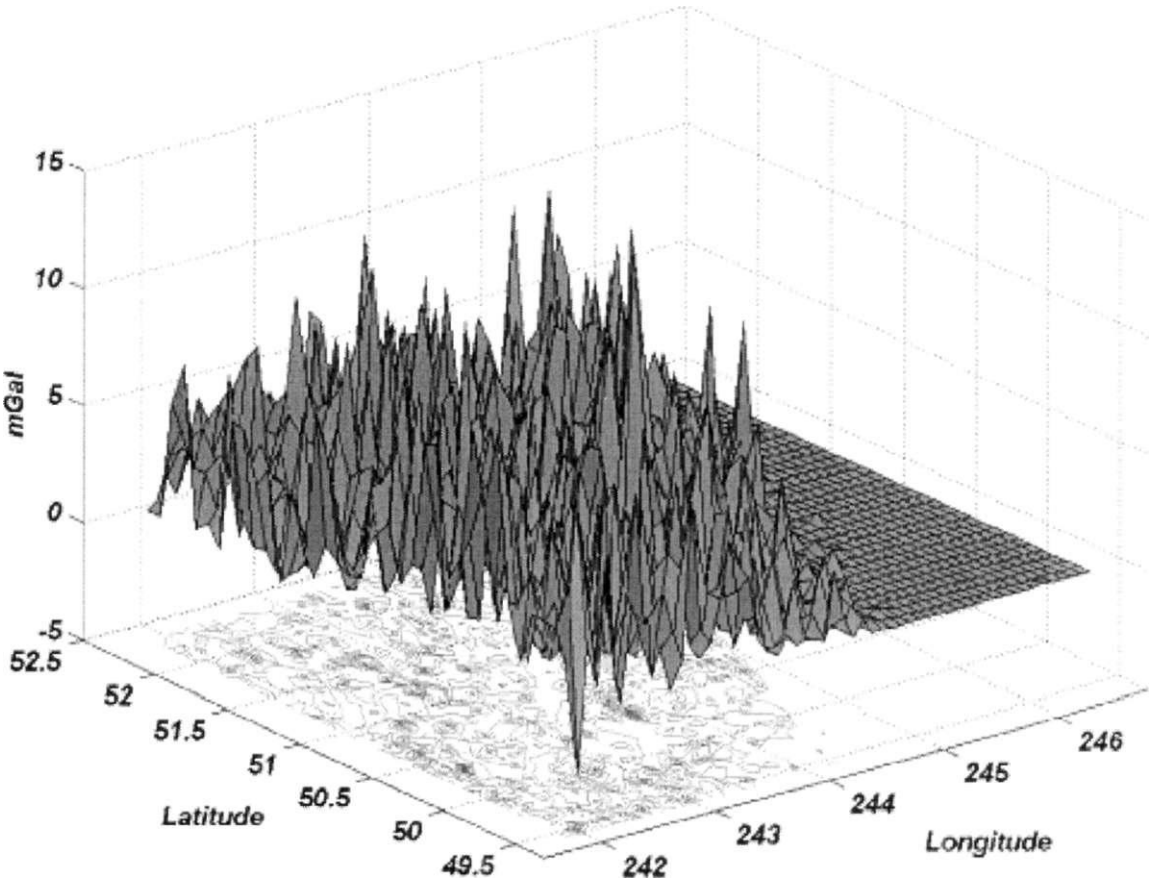


**Figure 3-5: Difference between the TC computed from a 15 and 60 arcsec D T M (mGal)**

The GIE is computed using Eq. (3.3). This quantity is in meters and is added to the co-geoid computed by Stokes'/Hotine's integral to obtain the geoid. Its values can range from zero to a couple of meters in very rough topography and are always negative. In Table 3-5, the GIE computed from the different DTM resolutions are listed, and Table 3-6 shows the statistics of these differences.

**Table 3-5: Statistics of GIE computed from 15, 30, and 60 arcsec DTM on 5'x 5' grid (m)**

| Indirect effect | DTM resolution | Max | Min | Mean | Std | RMS |
|---|---|---|---|---|---|---|
| GIE | 15 | ***-0.023*** | ***-1.067*** | ***-0.325*** | ***0.191*** | ***0.377*** |
| | 30 | ***-0.023*** | ***-1.067*** | ***-0.325*** | ***0.191*** | ***0.377*** |
| | 60 | ***-0.023*** | ***-1.066*** | ***-0.324*** | ***0.191*** | ***0.376*** |

**Table 3-6: Statistics of the differences of GIE compute from the different DTM resolution on 5'x 5' grid (m)**

| Indirect effect | DTM resolution | Max | Min | Mean | Std | RMS |
|---|---|---|---|---|---|---|
| GIE | 15-30 | 0.004 | -0.004 | -0.000 | 0.001 | 0.001 |
| | 15-60 | 0.009 | -0.013 | -0.001 | 0.003 | 0.003 |

As it is clearly seen, the GIE is less affected by the DTM resolution due to the fact that it is of low frequency nature and thus is hardly influenced by the high frequencies coming from the topographic masses. For completeness, Fig 3-6 shows the GIE computed from the 15 arcsec DTM.

In this section, the terrain reductions were processed for ground data using two different reduction methods and three DTM resolutions: 15, 30, and 60 arcsec all, averaged from a 3 arcsec DTM. The integration cap chosen was one degree. An integration cap of half a degree would result in an omission signal of up to a few centimetres in terms of the geoid (RMS = 5 cm).

5* J \ . . . . . , ; ., . •
51 ' ^ 2 4 5
50.5 * \ - • •* " .244
Latitude e t t ^ - . r- • '
SO ^ 24$ Longitude
49,5 242

**Figure 3-6: GIE computed using the 15 arcsec DTM on 5'x 5' grid (m)**

### 3.2.2 - Topographic effects on airborne gravimetry

For the estimation of the terrain effects at flight level, the same equations as in the previous section are used with a slight change in the radial distance of the computation point. Equations (3.1), (3.2), and (3.3) are written as follows:

***Terrain Correction (TC)***

$$71C(r,9A)=C?pI£ \quad dL-'[R + H^{flsht},\backslash y,r') \quad \text{or} \quad r'=R+H(<\$',\backslash') \quad r'=R+H(<p,X) \quad \cos(p'A9AA, \qquad (3.4)$$

***Condensed Terrain Correction (CTC)***

$$CTC(r,<\$>,X) = GR'ZZHV'^)-^)\} \quad dL-^{x}(R + H^{flsh>},\backslash y,R) \quad \text{or} \quad =R+H((p,X) \quad \cos y'AyA'k \qquad (3.5)$$

***Geoid Indirect Topographic Effect (GIE)***

$$Gp \quad y(<pA) \quad R \quad a((p',X')-a((p,X) \quad L(R,y,R) \quad \cos 9'A9A?I \quad J \quad =/?+//(<p',V) \quad =«+//(<p,X) \qquad (3.6)$$

Note that the only change in the above equations is the radial distance of the computation points, where now we have it at the flight level: $R + H^{\wedge\backslash ghl}$. The computation of the GIE is the same for it is evaluated at the reference sphere since we are after the geoid and not the

quasi-geoid. The height of the flight is nearly constant throughout the survey, and thus all the points have the same height.

As mentioned before, the terrain effects - TC, CTC, and DTE - have to be fdtered first and then used in the processing. To do so, the terrain effects were computed at the locations of the airborne measurements. Figure 3-7 shows the flight lines and the topography in the region, which is the same as the region in Figure 3-1.

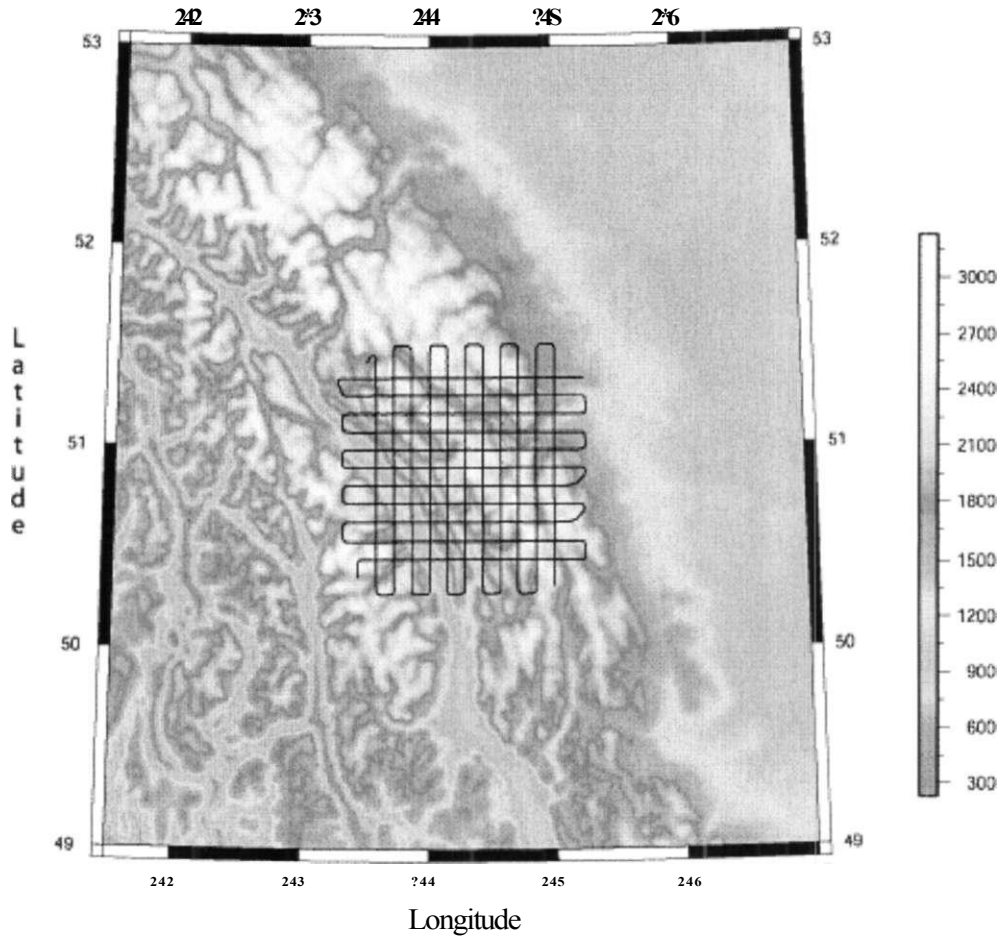


**Figure 3-7: Coverage of the airborne data and the topography of the region, in meters**

The data that is used in the following were collected two days, and merged into one dataset. The terrain effect computations took place at an approximate altitude of 4325 meters above the reference sphere and with an integration cap of one degree. Three DTM resolutions (as

in the ground case) were used: 15, 30, and 60 arcsec. The effect of the DTM resolution on the terrain effect computed at the flight level is studied first. These values will be shown in a profile along the flight lines due to the way the airborne gravity data is measured. Then, the impact of terrain effect filtering will be studied by computing the differences between the computed and filtered terrain effects to see if their values are significant. Figure 3-8 shows the TC and DTE computed using the 15 arcsec DTM.

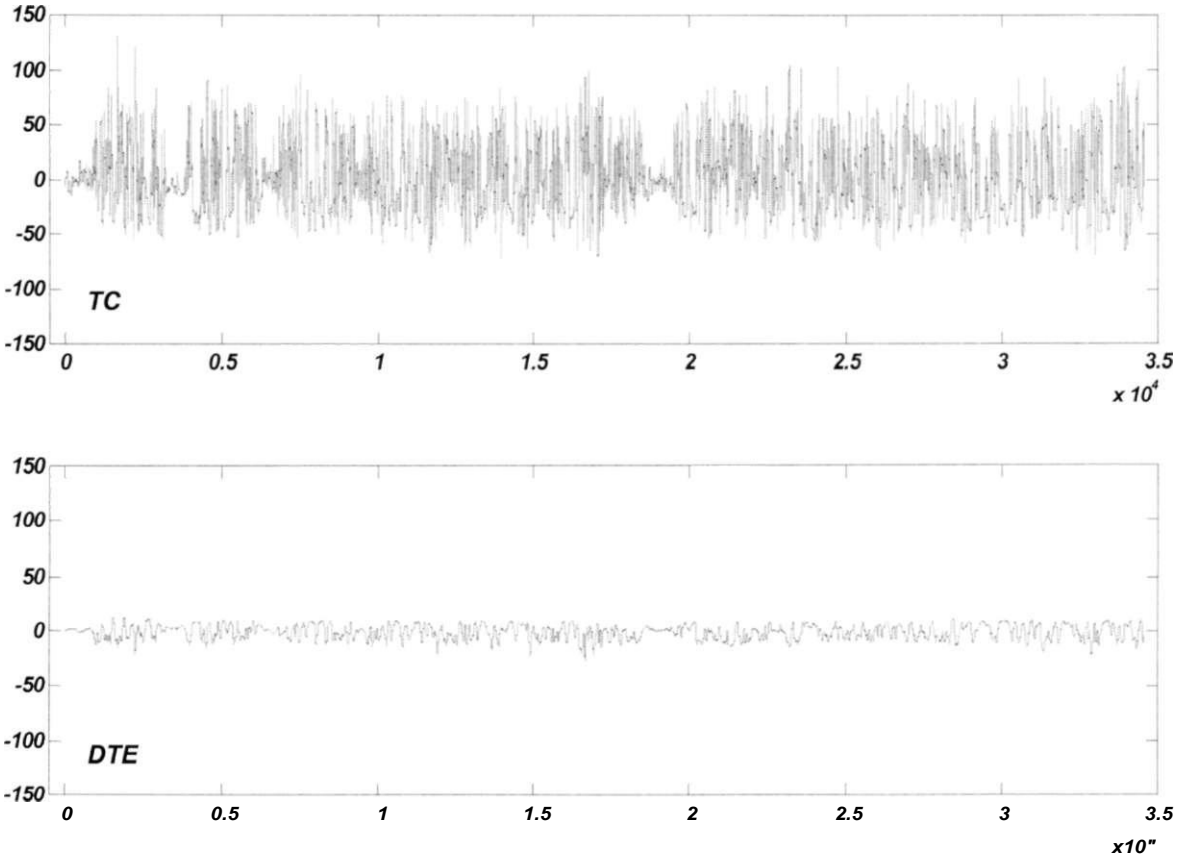


**Figure 3-8: TC and DTE computed at the flight level using 15 arcsec DTM (mGal)**

Comparing the values in Fig. 3-8 with those computed at the topography (although they are different datasets, some general conclusions can be drawn) it can be seen that the values of TC at the flight level become larger, whereas the DTE happens to be smaller. Concerning the TC, the large values are because the topography is right below the computation point and the radial attraction due to the radial derivative of the potential becomes larger. Also,

the TC can have large negative values, which can be expected because the topography is below the computation point and the Bouguer plate/shell passes through the corresponding location of the computation point at the topography. The larger negative values are not surprising and also occur in terrain correction for bathymetry used in the reduction of gravity data for applied geophysics. Concerning the DTE, it becomes smaller and it can be assumed that at larger altitudes the DTE becomes.

#### 3.2.2.1 - DTM Resolution

The TC and DTE were computed for the airborne dataset (34,560 values) using the same 15, 30, and 60 arcsec DTM used on the ground case; see the statistics in Table 3-7. The 15 arcsec DTM was used as reference in the comparisons. Figure 3-9 shows the difference in TC and Fig. 3-10 shows the difference in DTE. The statistics of these differences are listed in Table 3-8.

**Table 3-7: Statistics of TC, CTC and DTE computed from 15, 30, and 60 arcsec DTM at the flight level (mGal)**

| Terrain reduction | DTM resolution | Max | Min | Mean | Std | RMS |
|---|---|---|---|---|---|---|
| TC | 15 | ***131.2*** | ***-73.1*** | ***1.0*** | ***30.0*** | ***30.0*** |
| | 30 | ***132.8*** | ***-73.2*** | ***1.0*** | ***30.1*** | ***30.1*** |
| | 60 | ***133.1*** | ***-73.3*** | ***1.0*** | ***30.3*** | ***30.3*** |
| CTC | 15 | ***143.5*** | ***-77.8*** | ***1.5*** | ***34.9*** | ***34.9*** |
| | 30 | ***143.5*** | ***-77.8*** | ***1.5*** | ***34.9*** | ***34.9*** |
| | 60 | ***143.6*** | ***-78.0*** | ***1.5*** | ***34.9*** | ***35.0*** |
| DTE | 15 | ***13.2*** | ***-25.4*** | ***-0.4*** | ***6.5*** | ***6.5*** |
| | 30 | ***13.1*** | ***-25.2*** | ***-0.4*** | ***6.4*** | ***6.5*** |
| | 60 | ***12.9*** | ***-24.5*** | ***-0.4*** | ***6.3*** | ***6.3*** |

Contrary to the ground data, the airborne data are less sensitive to the D T M resolution. As we see from Fig. 3-9 and 3-10 and Table 3-8, a 30 arcsec D T M can be used safely without losing much information (a =0.1 mGal and max = 2 mGal). In some cases, even the 60 arcsec can be used, since a a of 0.4 mGal and a maximum of 6.9 mGal does not cause major problems in the geoid modelling. From here further on, only data reduced using the 15 arcsec D T M will be used.

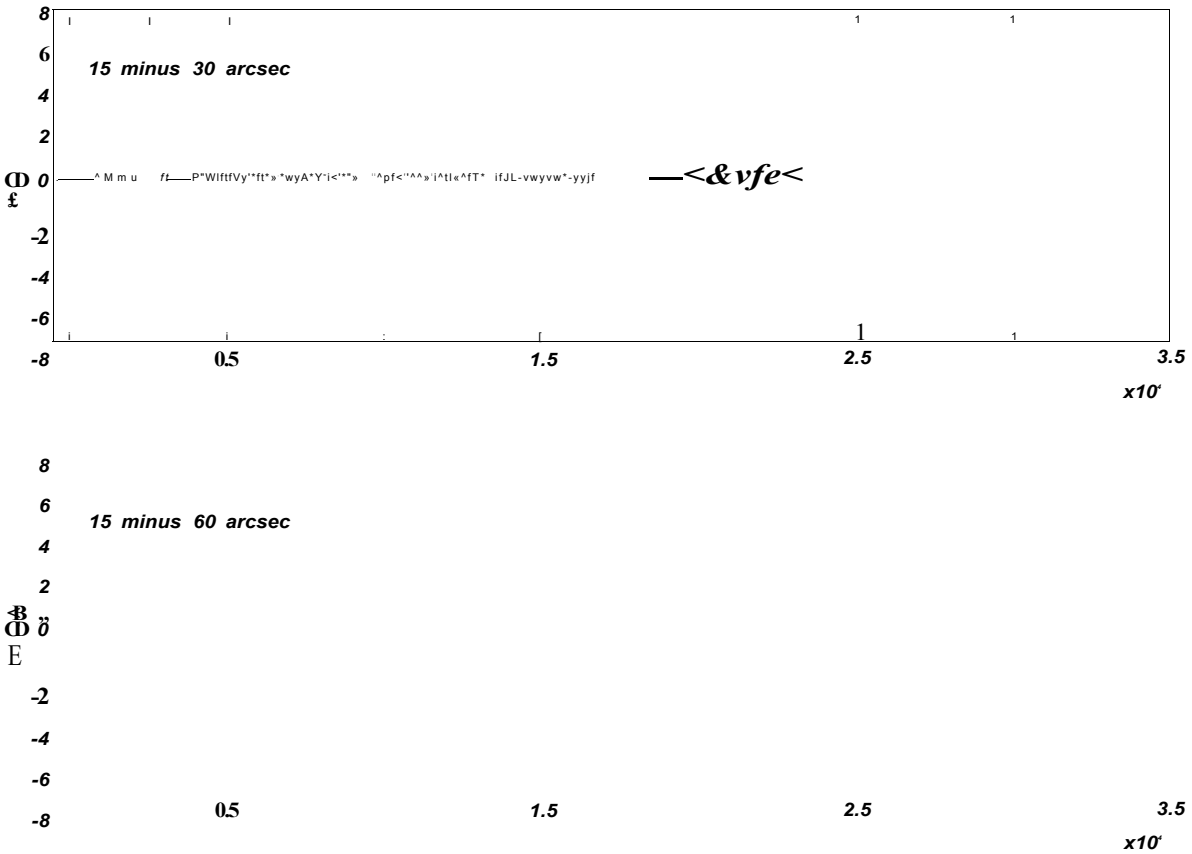


**Figure 3-9: Differences in TC computed at the flight level (mGal)**

**Table 3-8: Statistics of the differences in T C , C T C and D T E computed from 15,30 and 60 arcsec D T M at the flight level (mGal)**

| Terrain reduction | DTM resolution | Max | Min | Mean | Std | RMS |
|---|---|---|---|---|---|---|
| TC | *15- 30* | *1.3* | *-2.1* | *-0.0* | *0.0* | *0.0* |
| | *15- 60* | *6.9* | *-3.7* | *-0.0* | *0.4* | *0.4* |
| CTC | *15- 30* | *0.1* | *-0.1* | *-0.0* | *0.0* | *0.0* |
| | *15- 60* | *0.8* | *-0.7* | *-0.0* | *0.0* | *0.0* |
| DTE | *15- 30* | *1.2* | *-1.9* | *-0.0* | *0.0* | *0.0* |
| | *15- 60* | *6.1* | *-3.6* | *-0.0* | *0.3* | *0.3* |

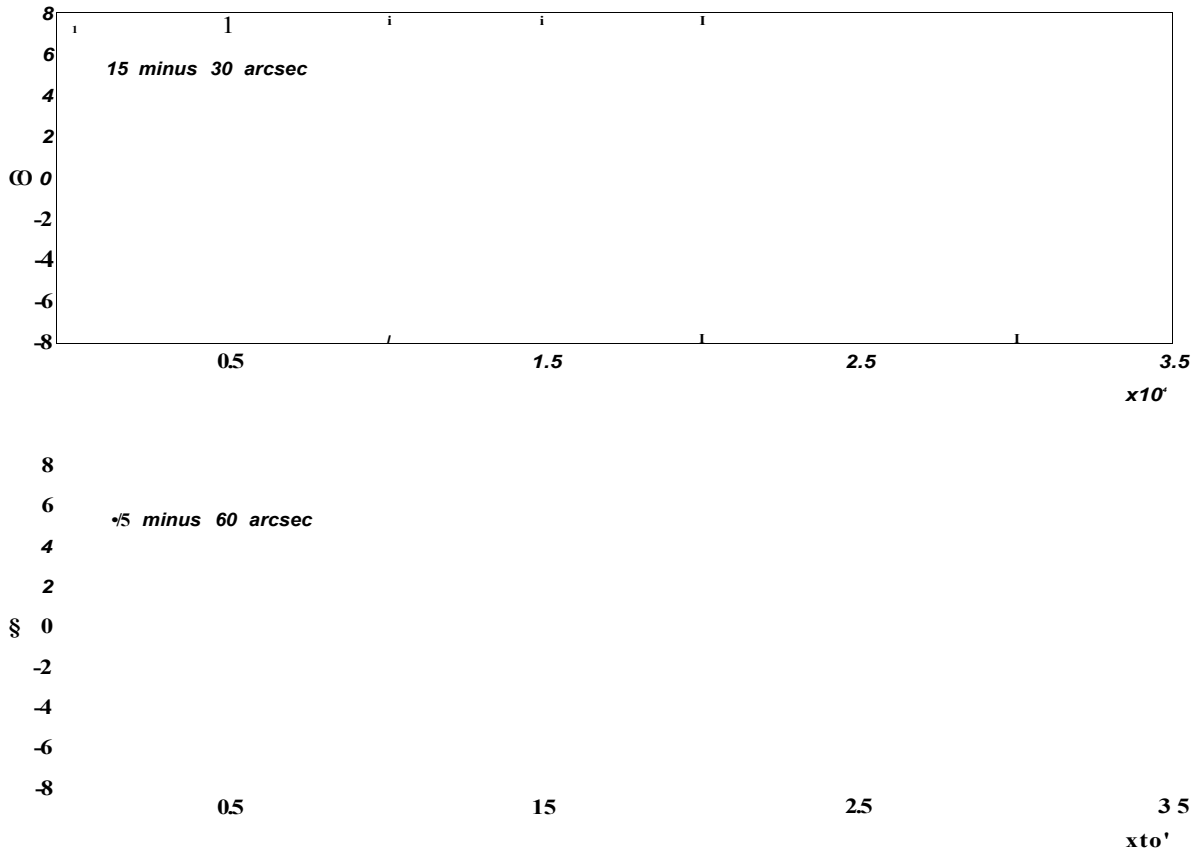


**Figure 3-10:Differences in D T E computed at the flight level (mGal)**

### 3.2.2.2 - Terrain Effect Filtering

The TC and DTE computed from the 15 arcsec DTM (Fig. 3-8) were filtered to 1/30, 1/60, and 1/90 Hz cut-off frequency. These filtered values were compared with the corresponding values before filtering and were plotted in profiles. Figures 3-11 and 3-12 show the differences between the computed and filtered TC and DTE, respectively. Tables 3-9 and 3-12 list the statistics of these differences.

#### *3.2.2.2.1 - Effect on TC*

The effect of TC filtering is very well illustrated in the plots of Fig. 3-11, where a large part of the signal is removed. A thorough investigation of the effect of filtering on the geoid is not possible at this point and is left to the next chapter. Yet, it is interesting to study the effect of filtered TCs after adding them to the data and using them for gridding when forming the refined Bouguer gravity disturbances.

**Table 3-9: Statistics of the differences between the computed and filtered TC (mGal)**

| Filtering frequencies | Max | Min | Mean | Std | RMS |
|---|---|---|---|---|---|
| 1/30 Hz | ***44.4*** | ***-37.2*** | ***-0.0*** | ***7.2*** | ***7.2*** |
| 1/60 Hz | ***59.2*** | ***-50.0*** | ***-0.0*** | ***12.7*** | ***12.7*** |
| 1/90 Hz | ***92.5*** | ***-66.5*** | ***-0.0*** | ***17.2*** | ***17.2*** |

Three terrain-reduced disturbances data sets are formed, each with TCs filtered to one of the three frequencies, and are labelled ***data_30, data_60,*** and ***data_90.*** Note again that all three datasets are based on a 15 arcsec DTM. Tables 3-10 and 3-11 have the statistics of these datasets before gridding, using filtered and unfiltered TCs, respectively. Although the differences between filtered and un-filtered TCs are well pronounced in Fig 3-11 and Table 3-9, they are less distinct when added to the gravity data. These values reflect a very interesting fact about the smoothing the TC does when added to the Bouguer disturbances. In Table 3-10, the c's are smaller that the a's in Table 3-11 because, for the latter, filtered, smoother TC was used. ***Data 90*** is the smoothest dataset before reduction because it is

more filtered, but when reduced by the terrain effects, depending on whether the terrain effects are filtered or not, it changes its behaviour. For example, when un-fdtered TC (rough) was added, ***Data_90*** becomes smoother (RMS = ***12.8*** mGal) than the other two datasets ***(data_30*** RMS = ***19.6*** and ***data_60*** RMS = 76.9); when fdtered TC (smooth) was added, ***Data_90*** becomes rougher (RMS = ***22.2*** mGal) than the other two datasets ***(data_30*** RMS = ***20.9*** and ***data_60*** RMS = ***21.3)***

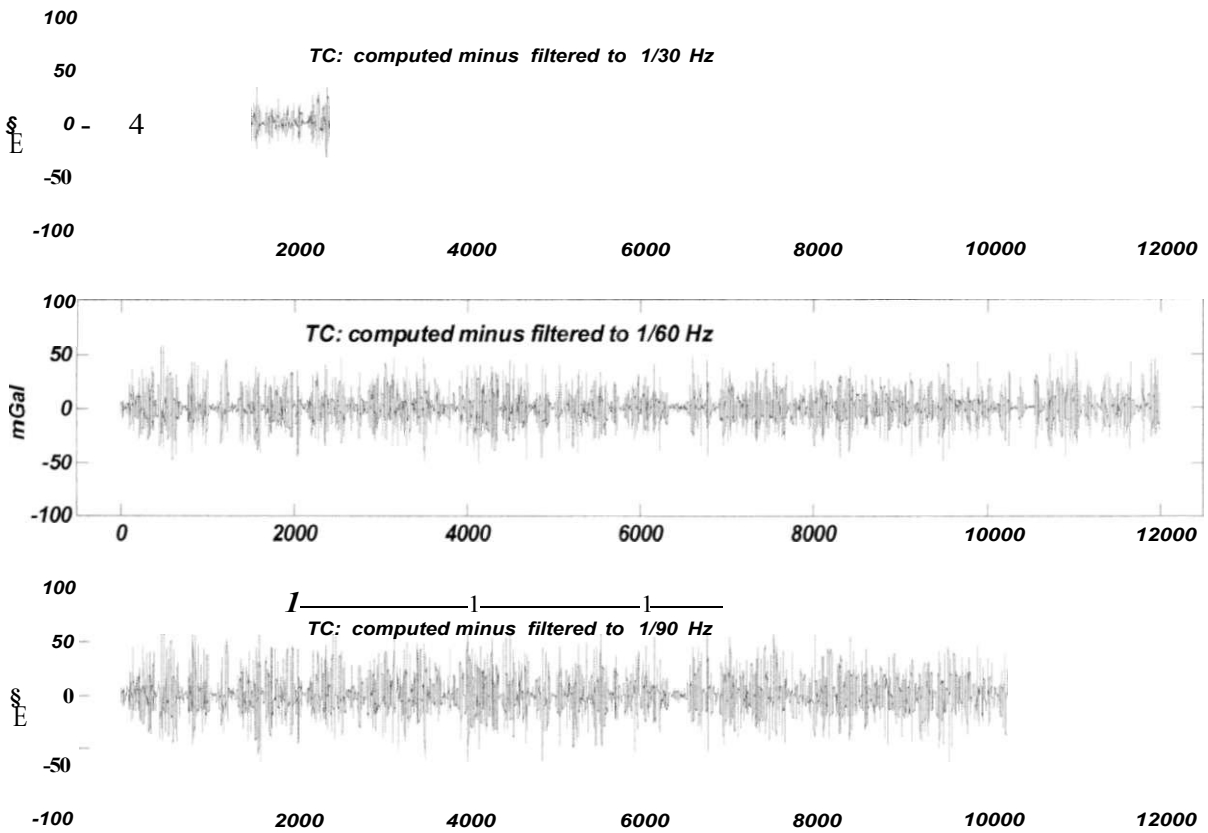


**Figure 3-11: Differences between computed and fdtered TC (mGal)**

**Table 3-10: Statistics of the three datasets (refined Bouguer anomalies), reduced using un-filtered TC (mGal)**

| Data set | Max | Min | Mean | Std | RMS |
|---|---|---|---|---|---|
| ***data_30*** | ***-123.3*** | ***-291.3*** | ***-207.8*** | ***19.6*** | ***208.7*** |
| ***data_60*** | ***-142.5*** | ***-257.2*** | ***-210.6*** | ***16.9*** | ***211.3*** |
| ***data_90*** | ***-159.6*** | ***-253.9*** | ***-210.8*** | ***12.8*** | ***211.2*** |

**Table 3-11: Statistics of the three datasets (refined Bouguer anomalies) reduced using filtered TC (mGal)**

| Data set | Max | Min | Mean | Std | RMS |
|---|---|---|---|---|---|
| ***data_30*** | ***-118.1*** | ***-297.7*** | ***-207.7*** | ***20.9*** | ***208.8*** |
| ***data_60*** | ***-123.6*** | ***-290.0*** | ***-210.6*** | ***21.3*** | ***211.7*** |
| ***data_90*** | ***-120.3*** | ***-313.1*** | ***-210.8*** | ***22.2*** | ***211.9*** |

After gridding (Sec. 3.3), the Bouguer plate is added back leaving the gravity anomalies reduced only to the TC. Note that these datasets will be used in the second methodology.

#### *3.2.2.2.2 - Effect on DTE*

The effect of filtering on DTE is certainly small as seen in Fig 3-12 and Table 3-12. The statistics and the plots show the high frequency nature of these differences. These are filtered out when Stokes'/Hotine's integral are used due to the low-pass nature of the integrals. If the second methodology is to be used, it might be recommended that the DTE be added to the data; then, form the grid without filtering the DTE. This argument is also strongly supported by the statistics of the three datasets reduced by the DTE without and with filtering listed in Table 3-13 and Table 3-14, respectively.

**Table 3-12: Statistics of the differences between the computed and filtered DTE (mGal)**

| Filtering frequencies | Max | Min | Mean | Std | RMS |
|---|---|---|---|---|---|
| 1/30 Hz | *1.0* | *-0.6* | *0.0* | *0.1* | *0.1* |
| 1/60 Hz | *1.6* | *-1.5* | *0.0* | *0.2* | *0.2* |
| 1/90 Hz | *4.4* | *-4.3* | *0.0* | *0.8* | *0.8* |

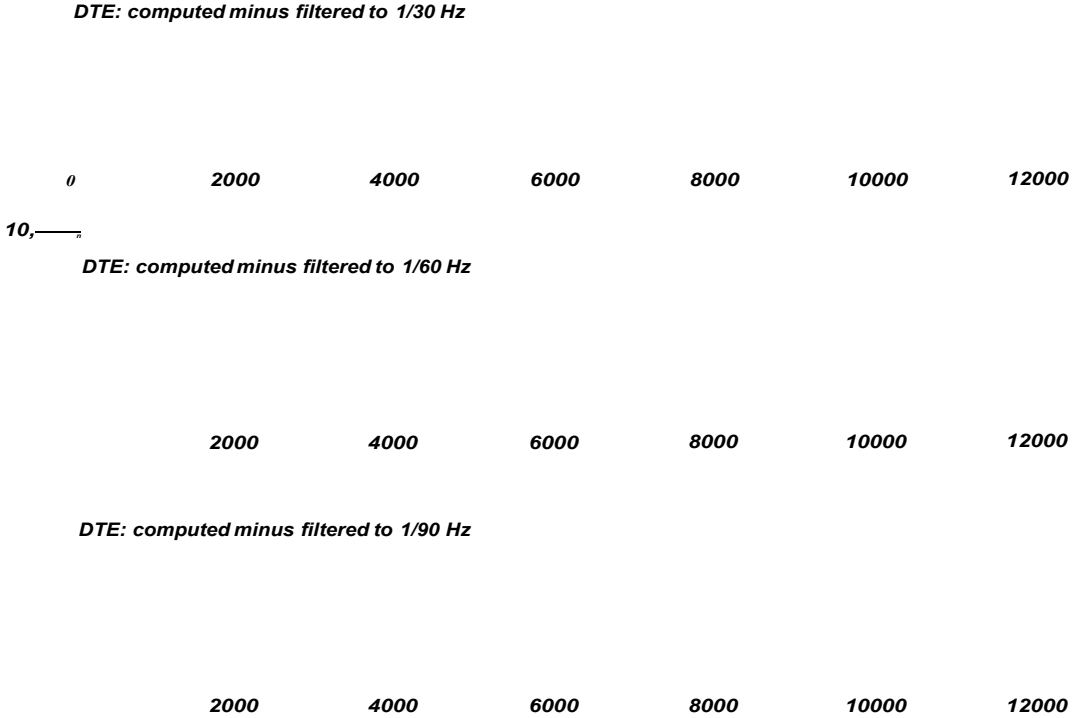


**Figure 3-12: Difference between computed and filtered DTEs (mGal)**

**Table 3-13: Statistics of the three datasets reduced by the un-filtered DTE (mGal)**

| Data set | Max | Min | Mean | Std | RMS |
|---|---|---|---|---|---|
| *Data_30* | *118.7* | *-91.4* | *2.6* | *28.6* | *28.7* |
| *Data_60* | *92.8* | *-86.8* | *-2.2* | *28.0* | *28.0* |
| *Data_90* | *74.2* | *-84.9* | *-2.4* | *28.2* | *28.2* |

**Table 3-14: Statistics of the three datasets reduced by the filtered DTE (mGal)**

| Data set | Max | Min | Mean | Std | RMS |
|---|---|---|---|---|---|
| ***Data_30*** | ***118.6*** | ***-91.4*** | ***2.6*** | ***28.6*** | ***28.7*** |
| ***Data_60*** | ***92.5*** | ***-86.8*** | ***-0.2*** | ***28.0*** | ***28.0*** |
| ***Data_90*** | ***76.5*** | ***-84.9*** | ***-0.4*** | ***28.2*** | ***28.2*** |

***Fourth data set:*** Another dataset was formed without any filtering of the terrain; this dataset was created as follows: grid the measured values and then add the terrain effects on the grid nodes. For this dataset, we will use the one filtered to 1/60 Hz. The aim of the fourth dataset is to see if we can simplify our computation procedures by not computing the terrain effects at all the points along the flight lines and not filtering them thus saving a lot of computation time (e.g., computation of 35000 terrain effect values takes more than 70 hours using a personal Pentium III computer with a 500 MHz processor!) The fourth dataset is labelled ***data_grd;*** see Table 3-15 for the statistics. These values are less smooth when compared to those reduced by the terrain effects as is well expected. The fourth dataset can be reduced after gridding to either TC-CTC° or DTE, and after that used in the corresponding methodology.

**Table 3-15: Statistics of the *datagrd* (mGal)**

| Data set | Max | Min | Mean | Std | RMS |
|---|---|---|---|---|---|
| ***Datagrd*** | ***111.8*** | ***-89.4*** | ***2.0*** | ***32.3*** | ***32.3*** |

***Geoid Indirect Effect:*** The GIE is computed as in the case of ground data using Eq. (3.3). Since it is added to the residual geoid computed from the Stokes/Hotine formulation, there is no need for filtering. Tables 3-5 and 3-6 and Fig 3-6 can be consulted.

## 3.3 - Gridding the airborne gravity data

After forming the seven datasets - three reduced by the complete Bouguer reduction, three reduced by the DTE, and one not reduced at all — they were gridded onto a 5' x 5' grid between the boundaries $50.4333° < cp < 51.35°$ and $243.5167° < X < 245.0417°$, generating 228 values. Figure 3-13 shows the measured data of the two days and the grid formed from them. Due to the high dynamics of the aircraft during the turns, data acquired at those locations were not used. Due to edge effects, out of these 228 points only 170 will be used for geoid determination by removing the perimeter points.

The statistics of the datasets before gridding (Tables 3-10, 3-11, 3-13, 3-14, and 3-15) show that the smoothest ones are those reduced by the complete Bouguer reduction.

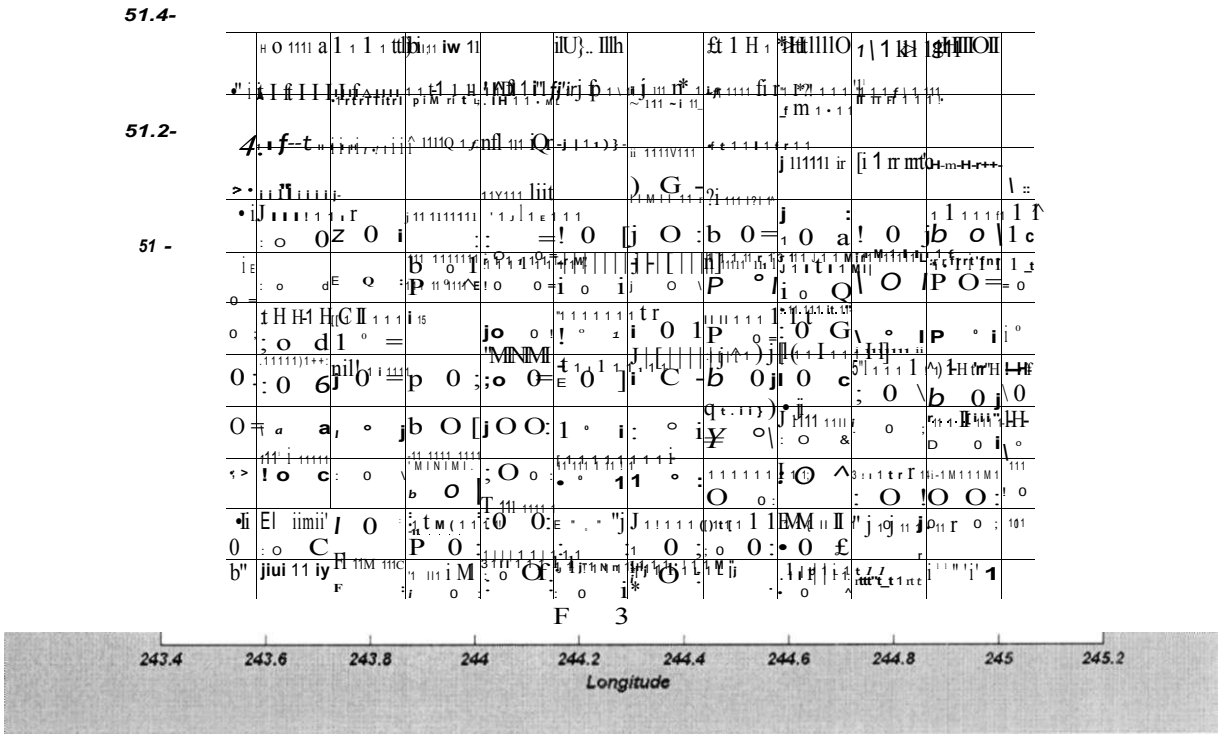


**Figure 3-13: Measured and gridded values**

The first three datasets, used in the second methodology, will be used directly in the geoid modelling after subtracting the $CTC^{o}$ and adding the Bouguer shell at the nodes of the grid. So they will be re-visited in the next chapter when the geoid is modelled. The other three datasets, used in the first methodology, will be passed through the inverse Poisson integral to downward continue them to the geoid, approximated by a reference sphere with mean radius of 6371 km. The last dataset on the other hand can be used in either method as long as it is correctly reduced for the topography, i.e., for the DTE for the first methodology and for the TC minus $CTC^{o}$ for the second methodology.

Since data is acquired using the Honeywell RFIII INS system, owned by Intermap® and operated by Intermap® and the U of C, a problem of data pollution with biases coming from the imperfections of the accelerometers occurs here. For this, we have first to remove the bias by linking this data to upward continued gravity data. The data used in Section 3.2.1.1 were upward continued to the height of the airborne data and used for this task. The link was made after gridding the airborne data. Using other measuring systems with temperature control over the accelerometers, e.g. AIRGrav built by Sander Geophysics Limited, it was observed that the bias is less than 1 mGal; hence, a link to ground data might not be necessary.

The statistics of the gridded datasets, reduced by the TC, are listed in Table 3-16, and those reduced by the DTE are listed in Table 3-17. Recall that the fourth dataset in each Table was reduced after forming the grid and without any filtering of the terrain effects. Taking the ***data_60*** as reference, in both cases, we subtracted the other three datasets from it; Tables 3-18 and 3-19 show the statistics of the differences.

**Table 3-16: Statistics of the four datasets reduced by the TC (mGal)**

| Data set | Max | Min | Mean | Std | RMS |
|---|---|---|---|---|---|
| ***Data_30*** | ***145.5*** | ***-125.3*** | ***7.2*** | ***58.9*** | ***59.2*** |
| ***Data_60*** | ***166.5*** | ***-129.6*** | ***7.2*** | ***58.7*** | ***59.0*** |
| ***Data_90*** | ***158.7*** | ***-123.7*** | ***7.2*** | ***58.9*** | ***59.2*** |
| ***Data tc*** | ***142.9*** | ***-120.1*** | ***7.2*** | ***56.6*** | ***57.0*** |

**Table 3-17: Statistics of the four datasets reduced by the DTE (mGal)**

| Data set | Max | Min | Mean | Std | RMS |
|---|---|---|---|---|---|
| ***Data_30*** | ***74.5*** | ***-72.3*** | ***2.8*** | ***32.5*** | ***32.6*** |
| ***Data_60*** | ***65.1*** | ***-72.2*** | ***2.8*** | ***32.6*** | ***32.6*** |
| ***Data 90*** | ***63.9*** | ***-75.1*** | ***2.8*** | ***33.2*** | ***33.2*** |
| ***Datadte*** | ***67.9*** | ***-74.0*** | ***2.8*** | ***32.7*** | ***32.8*** |

**Table 3-18: Statistics of the differences between data 60 and the other three datasets reduced by the TC (mGal)**

| Differences | Max | Min | Mean | Std | RMS |
|---|---|---|---|---|---|
| ***Data_60 - Data_30*** | ***28.7*** | ***-39.4*** | ***0.0*** | ***10.1*** | ***10.1*** |
| ***Data 60-Data_90*** | ***21.5*** | ***-22.8*** | ***0.0*** | ***7.6*** | ***7.6*** |
| ***Data 60 - Datajc*** | ***39.6*** | ***-22.7*** | ***0.0*** | ***8.9*** | ***8.9*** |

**Table 3-19: Statistics of the differences between data_60 and the other three datasets reduced by the DTE (mGal)**

| Difference | Max | Min | Mean | Std | RMS |
|---|---|---|---|---|---|
| ***Data 60 - Data_30*** | ***27.1*** | ***-31.9*** | ***0.0*** | ***9.100*** | ***9.0*** |
| ***Data 60 - DataJO*** | ***7.0*** | ***-9.6*** | ***0.0*** | ***2.293*** | ***2.2*** |
| ***Data_60 - Datadte*** | ***10.0*** | ***-11.6*** | ***0.0*** | ***3.347*** | ***3.3*** |

From the values in Table 3-19 (when the DTE is used for reduction), it can be noticed that ***Data_60, Data_90,*** and ***Datadte*** are close to each other, with an RMS of ***2.2*** mGal and ***3.3*** mGal, respectively.

Although the differences between ***Data_60, Data_90*** and ***Datadte*** in Table 3-18 (when the TC is used for reduction) are much larger, than RMS of ***7.6*** mGal and ***8.9*** mGal, respectively, it is still expected that, when used on a 5'x 5' grid, these values will not affect the geoid computation due to their high frequency nature.

In this section, it has been shown that for airborne gravimetry, the DTM resolution does not play such a significant role as in the case of ground gravimetry. A DTM resolution of 30 arcsec can be safely used without loss of information; a 60 arcsec DTM can also be used in

an area with a smoother topography. While filtering of the terrain effects is essential from the theoretical side, its practical implication is minor and can be omitted as a process for the geoid determination. If gravity values are needed, then it is essential to filter the terrain effects.

To summarize, eight datasets were created, four for each methodology, as follows:

1. Data set filtered to 1/30 Hz, reduced for filtered topographic effects to the same frequency ***(data_30).***
2. Data set filtered to 1/60 Hz, reduced for filtered topographic effects to the same frequency ***(data_60).***
3. Data set filtered to 1/90 Hz, reduced for filtered topographic effects to the same frequency ***(data_90).***
4. Data set filtered to 1/60 Hz, gridded, and then reduced for the topographic effects without filtering ***(datatc, datadte).***

The first three data sets are used to investigate whether we can use the 1/30 and 1/60 Hz filtered data to achieve a high-resolution geoid. The fourth data set is to study the effect of TE filtering on the whole procedure. It is clear that if we do not have to filter the TE, the processing becomes very easy and straightforward.

For the 1st methodology, these data sets will first be downward continued to the reference sphere and then be used to compute the geoid. In the 2nd methodology, they are used for geoid determination right after the gridding.

## 3.4 - Downward continuation by inverse Poisson integral

The downward continuation with inverse Poisson integral formula is discussed in Chapter 2. In this section, the evaluation of the equation is done using ground and airborne gravity data. First, the ground gravity data will be downward continued; then, the four sets of airborne gravity data are downward continued.

### 3.4.1 - Ground data

The data described in the section (3.2.1.1) was used for the D.C. Specifically, we used the gridded gravity anomalies reduced by the DTE computed using the 15-arcsec DTM (Fig 3-2). The number of iterations was 25 with a threshold of less than 1 pGal. The statistics of the downward continued gravity anomalies are listed in Table 3-20 and shown in Fig. 3-14. These values will be passed through the Stokes'/Hotine's integral in the next chapter to give the residual geoid.

**Table 3-20: Statistics of the residual Helmert ground anomalies before and after the D.C. (mGal)**

| Data set | Max | Min | Mean | Std | RMS |
|---|---|---|---|---|---|
| Free-air + DTE - $\Delta g^{UM}$ | ***123.4*** | ***-144.6*** | ***-7.1*** | ***29.4*** | ***30.3*** |
| Downward continued | ***375.5*** | ***-180.2*** | ***-0.3*** | ***66.9*** | ***66.9*** |

Comparing these values with the values of the gravity anomalies that will be used for the second methodology (statistics in Table 3-2, row 10), it is seen that these values are larger and rougher. This is attributed to the magnification of the high frequency signal in the gravity data because of their use in an inverse problem. According to Heck (2001), the 2nd Helmert condensation method creates a rough gravity field that is not suitable to use in the inverse Poisson integral. The smoother the gravity field, the better it fits the requirements for stable downward continuation.

### 3.4.2 - Airborne data

In this section, four datasets are downward continued: the three datasets that were reduced by the filtered DTE before gridding and the fourth with the measured, filtered to 1/60 Hz, with the unfiltered DTE added after gridding (Table 3-17). These datasets are labelled ***data_30, data_60, data_90,*** and ***datadte.*** For an integration area of 1 degree, upward continued ground gravity data was padded around the airborne gravity data as shown in Figure 3-15. As in the case of the ground data, the iterative method was used for the Poisson inversion.

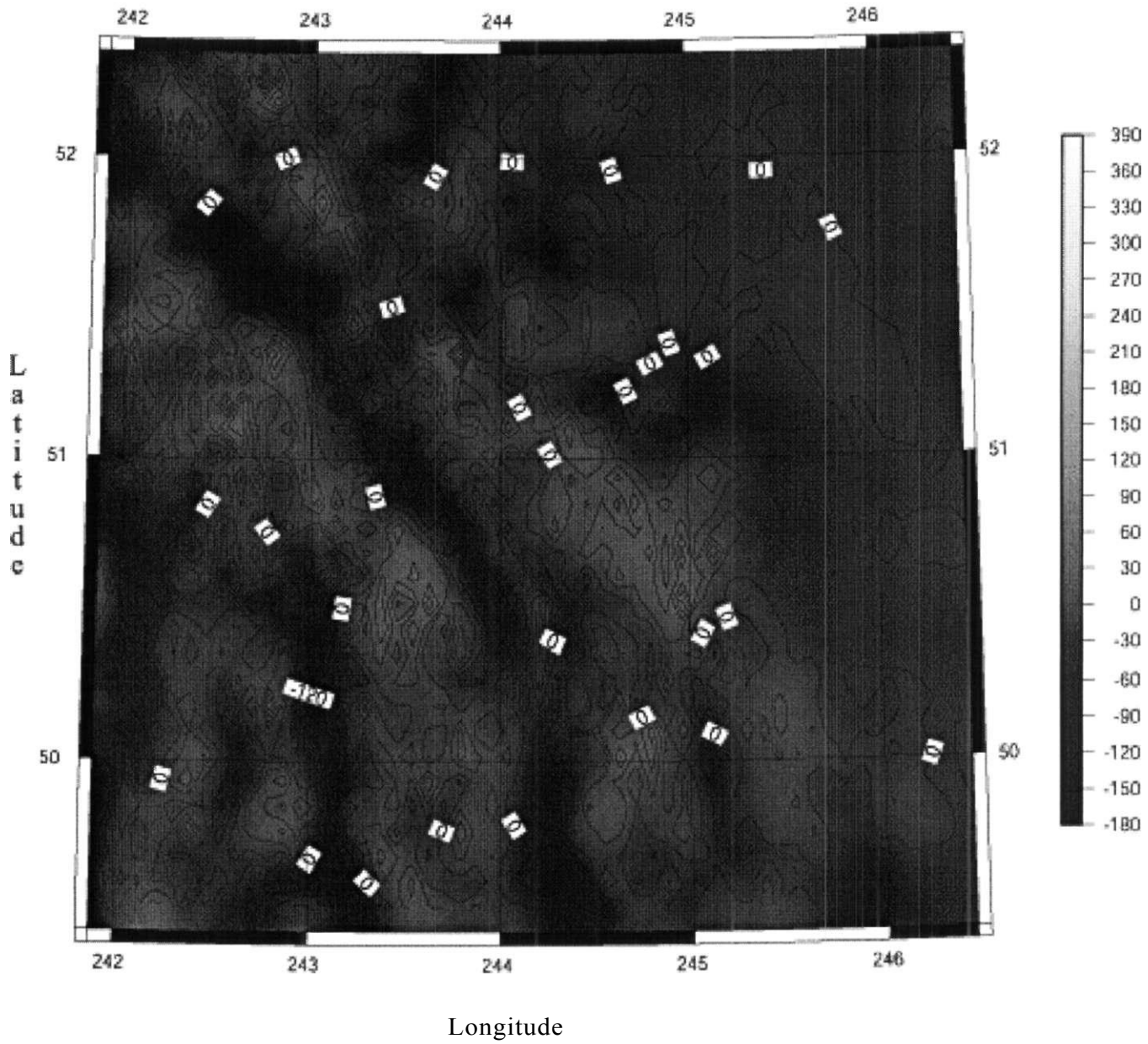


**Figure 3-14: Downward continued gravity anomalies (mGal)**

Figures 3-16 to 3-19 show the downward continued airborne gravity data. The data used in these figures are the 170 values that correspond to the 170 airborne data. The statistics are listed in Table 3-21.

**Table 3-21: Statistics of the downward continued airborne gravity data (mGal)**

| Data set | Max | Min | Mean | Std | RMS |
|---|---|---|---|---|---|
| ***Data_30*** | ***160.0*** | ***-156.7*** | ***4.3*** | ***56.2*** | ***56.2*** |
| ***Data_60*** | ***115.6*** | ***-129.9*** | ***3.1*** | ***51.8*** | ***51.8*** |
| ***Data_90*** | ***105.5*** | ***-137.8*** | ***2.9*** | ***52.4*** | ***52.4*** |
| ***Datadte*** | ***129.3*** | ***-141.4*** | ***3.2*** | ***55.2*** | ***55.2*** |

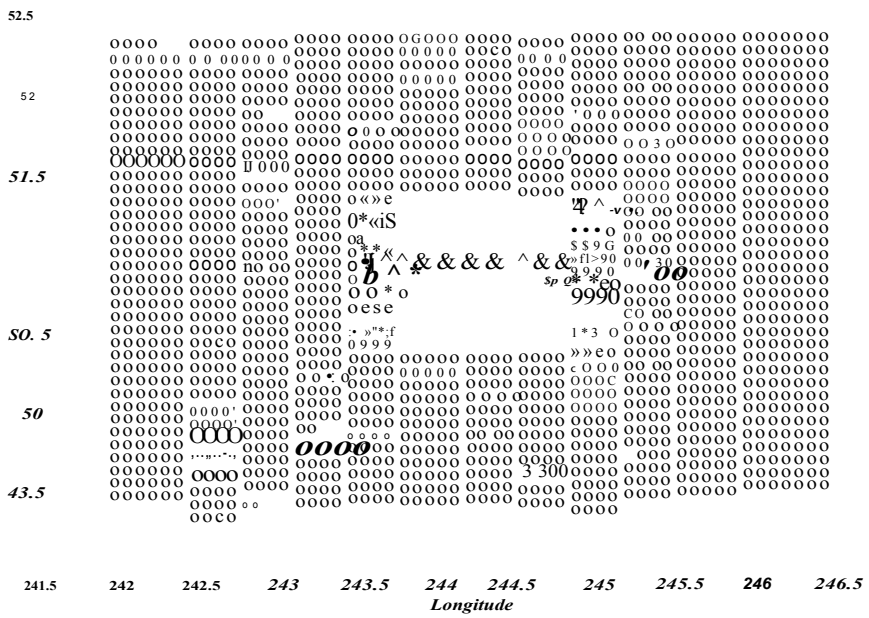


**Figure 3-15: Airborne and upward continued ground used for padding**

Taking the ***data_60*** as reference, comparisons were made with the other three datasets. Table 3-22 has the statistics. As it is seen, there are significant differences between ***data_60***

and ***data_30*** with a mean of -1.1 mGal and an RMS of 26.7 mGal. this is expected since the noise in ***data_30*** is more magnified than the noise found in ***data_60.*** Concerning the other two datasets, ***data_90*** (mean of 0.1 mGal and RMS of 7.0 mGal) and ***datadte*** (mean of -0.0 mGal and RMS of 14.9 mGal), their differences, although not as large, are still significant. While these differences can be considered noteworthy in terms of gravity information, their effect is minimized when they are input to the Hotine's integration, because of the low-pass filtering nature of this integral.

**Table 3-22: Statistics of the difference between data_60 and the other three datasets (mGal)**

| Data set | Max | Min | Mean | Std | RMS |
|---|---|---|---|---|---|
| ***Data 60 - Data 30*** | ***91.4*** | ***-100.9*** | ***-1.1*** | ***26.4*** | ***26.4*** |
| ***Data_60 - Data_90*** | ***27.9*** | ***-37.4*** | ***0.1*** | ***7.0*** | ***7.0*** |
| ***Data_60 - Data_dte*** | ***43.9*** | ***-50.9*** | ***-0.0*** | ***14.9*** | ***14.9*** |

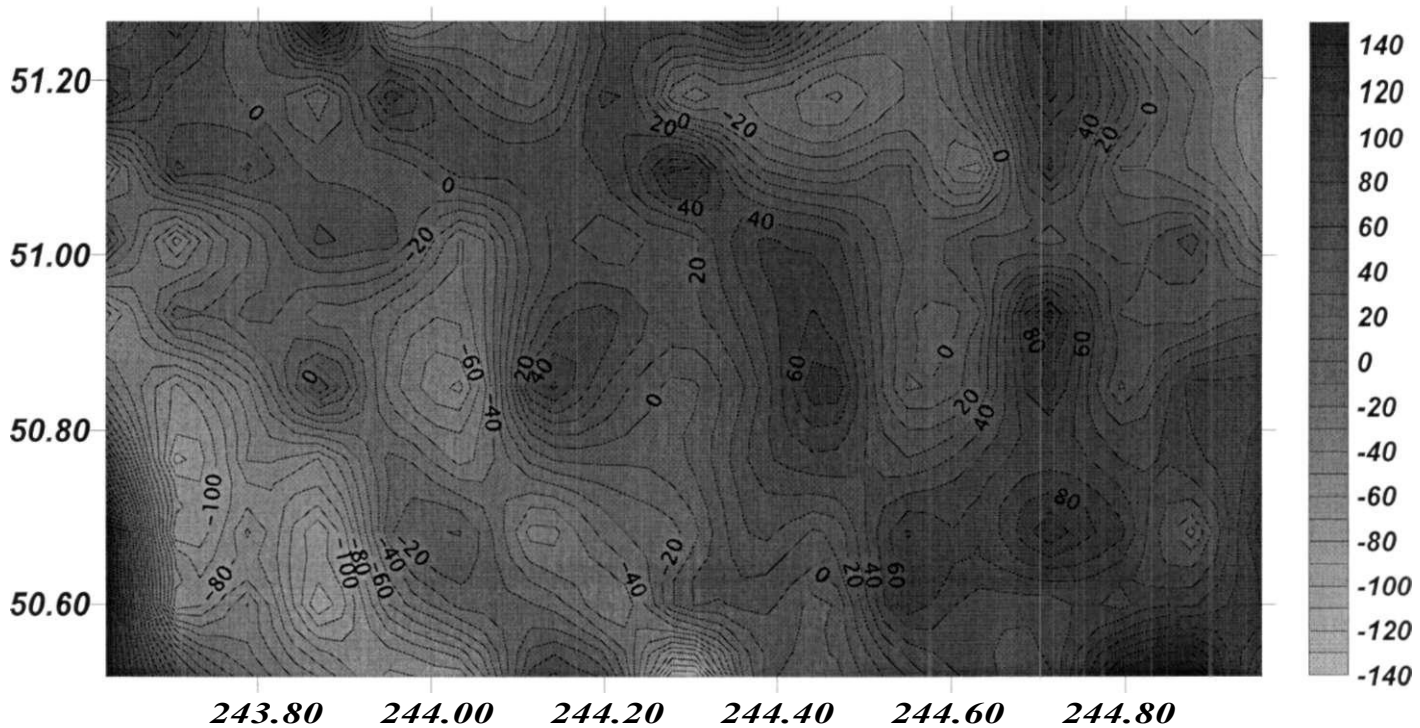


**Figure 3-16: Downward continued data_30 airborne gravity disturbances (mGal)**

243.80 244.00 244.20 244.40 244.60 244.80

**Figure 3-17: Downward continued data_60 airborne gravity disturbances (mGal)**

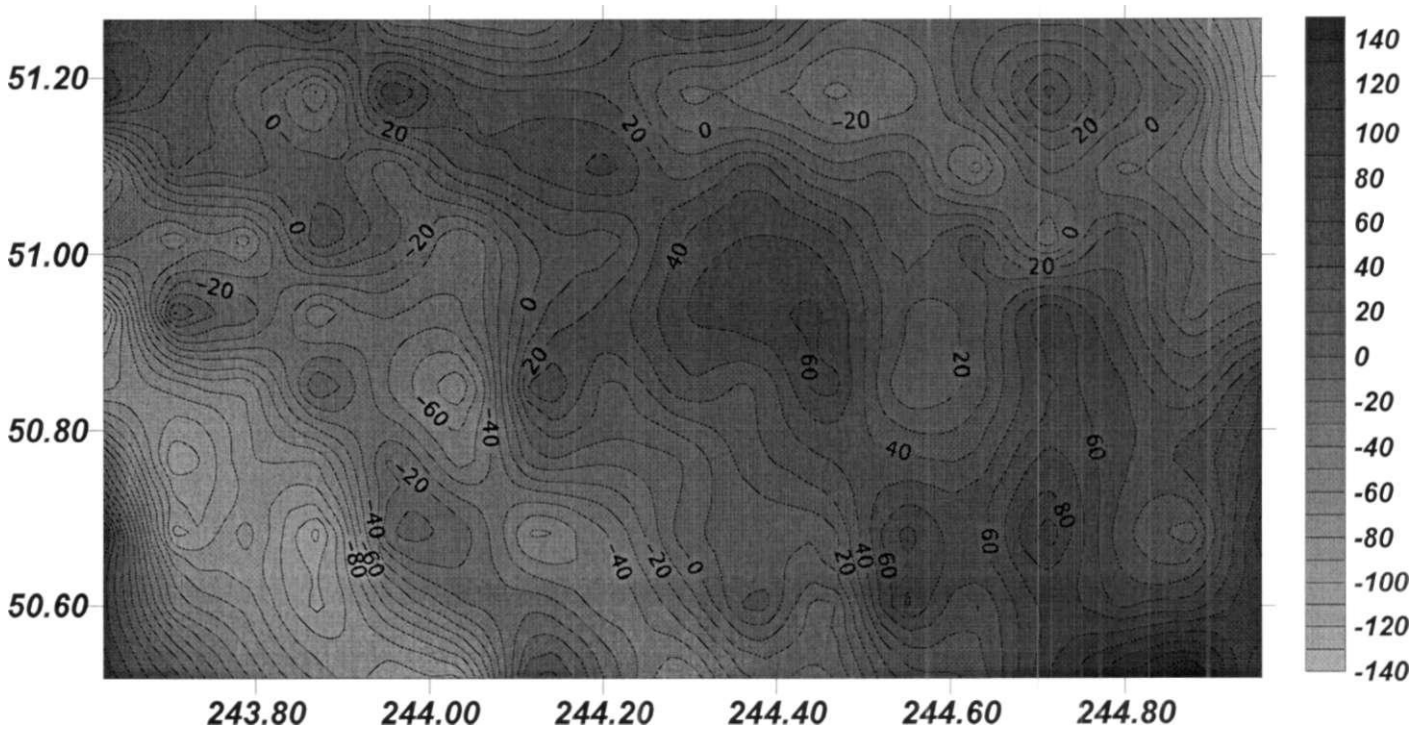


**Figure 3-18: Downward continued data_90 airborne gravity disturbances (mGal)**

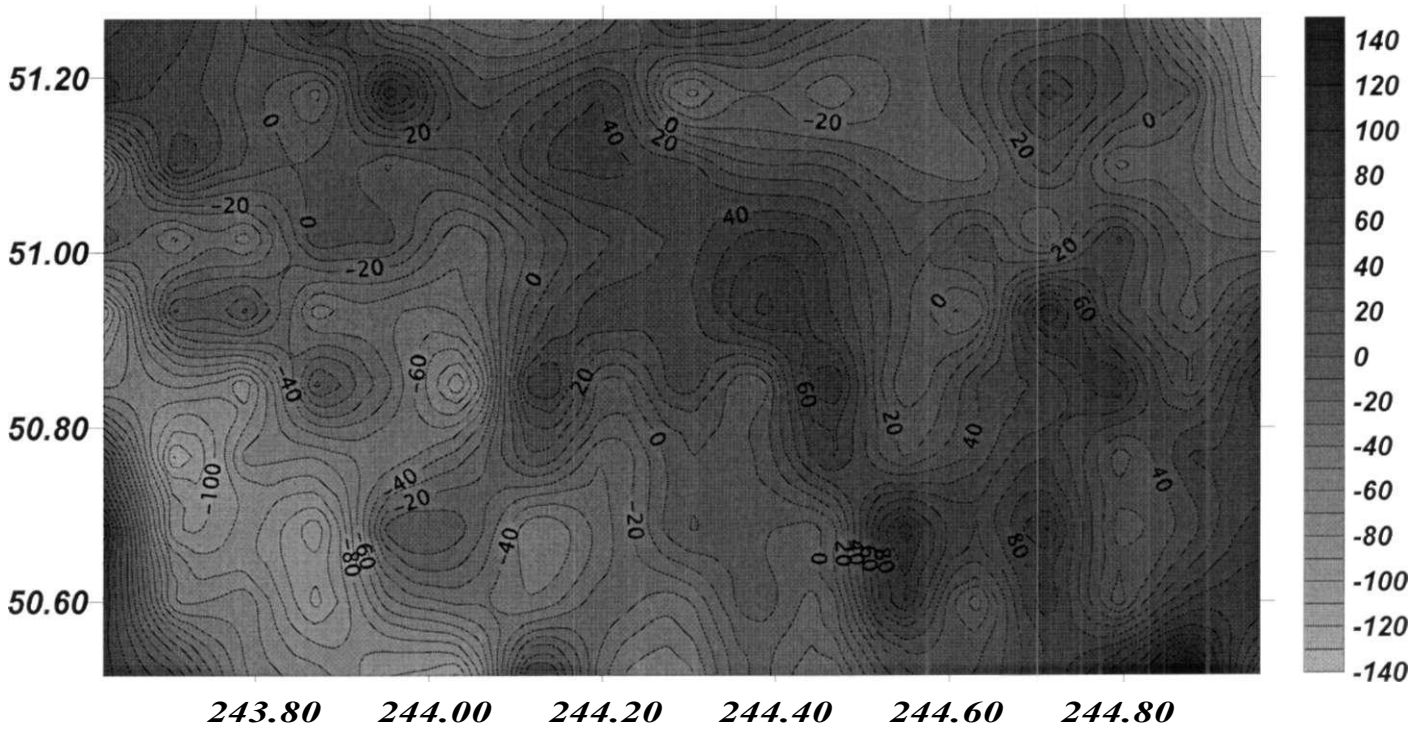


**Figure 3-19: Downward continued datadte airborne gravity disturbances (mGal)**

# Chapter 4

# Geoid determination from ground and airborne gravity data

In the fourth chapter, the geoid determination from ground and airborne gravity data is discussed. Geoid determination using ground data will be discussed first; the DTM resolution effect will also be studied. The eight airborne data sets generated in the previous section will also be processed to determine the geoid. Decisions on the methodology and DTM resolution will be the outcome of this chapter, along with the judgment on whether the filtering of the TE for airborne gravity data is needed or not.

## 4.1 - Geoid determined from ground gravity data

Firstly, a study of the effect on the geoid of different DTM resolutions will be made by evaluating the TC and DTE contributions by Stokes' integral. After that, the final geoid (Eq. 2.7) will be computed using the gravity data using the two datasets that emerged from the two methodologies described in Ch. 2.

### 4.1.1 - Terrain contribution on the geoid

To study the effect of the DTM resolution on the geoid, we used the differences in TC computed from DTMs with 15, 30, and 60 resolutions (Fig. 3-4 and 3-5, Table 3-4) as input

into Stokes' integral. The differences in DTE (Table 3-4) will also be used as input in Stokes' for the same purpose.

The contribution of the differences in terms of TC is seen in Fig. 4-1 and Fig 4-2 and in terms of DTE in Fig 4-3 and 4-4. The statistics are tabulated in Table 4-1. As it is seen, moving from a 15 arcsec to a 30 and 60 arcsec DTM resolution, gives a lower geoid by around 17 cm and 40 cm, respectively, in the case of the second methodology. This difference does not change much in the case of the 1st methodology (16 cm and 40 cm, respectively). As can be seen from the statistics and the graphs, they are both sensitive with respect to the DTM resolution, with a negligible difference of 1 to 2 cm between them.

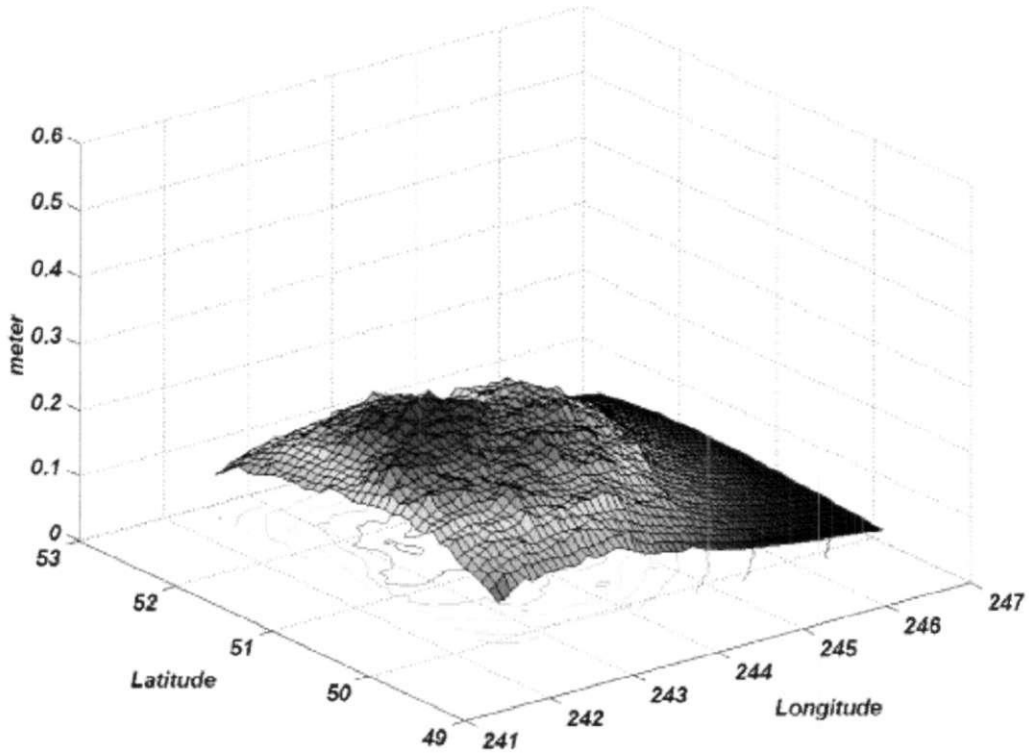


**Figure 4-1: Difference in the geoid contributions of (TC - CTC$^0$) using 15 and 30 arcsec DTMs (m)**

**Table 4-1: Terrain Effects on the geoid using different DTM resolutions (m)**

| Geoid differences | DTM resolution | Max | Min | Mean | Std | RMS |
|---|---|---|---|---|---|---|
| TC - CTC$^0$ | 15--30 | ***0.250*** | ***0.070*** | ***0.164*** | ***0.046*** | ***0.170*** |
| | 15--60 | ***0.608*** | ***0.171*** | ***0.400*** | ***0.114*** | ***0.416*** |
| DTE | 15--30 | ***0.244*** | ***0.068*** | ***0.159*** | ***0.045*** | ***0.166*** |
| | 15--60 | ***0.589*** | ***0.164*** | ***0.383*** | ***0.108*** | ***0.398*** |

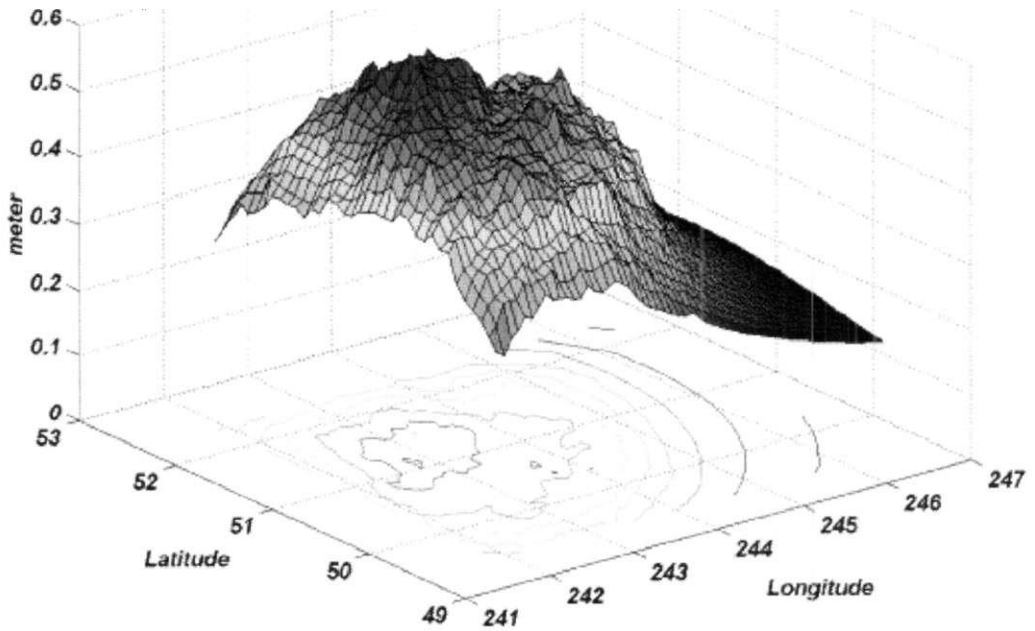


**Figure 4-2: Difference in the geoid contributions of (TC - CTC$^0$) using 15 and 60 arcsec DTMs (m)**

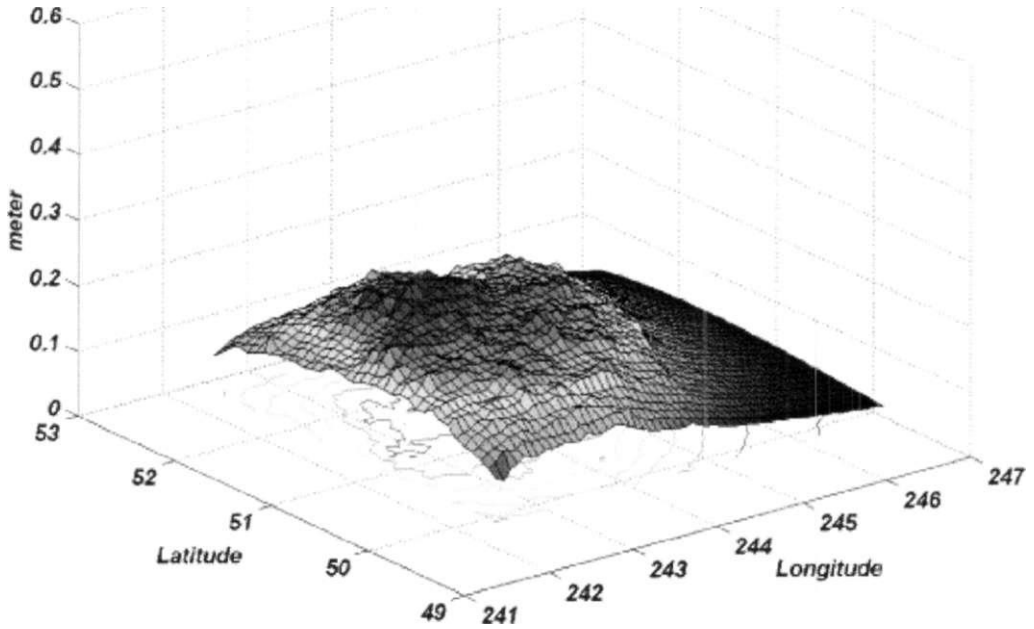


**Figure 4-3:Difference in the geoid contributions of the DTE using 15 and 30 arcsec DTMs (m)**

As seen from the results, the geoid is very sensitive to the DTM resolution used. Thus, here we stress again what was mentioned in the previous chapter, i.e., that the 15 arcsec DTM is better for geoid computation using ground data. In the following, a 15 arcsec DTM is used.

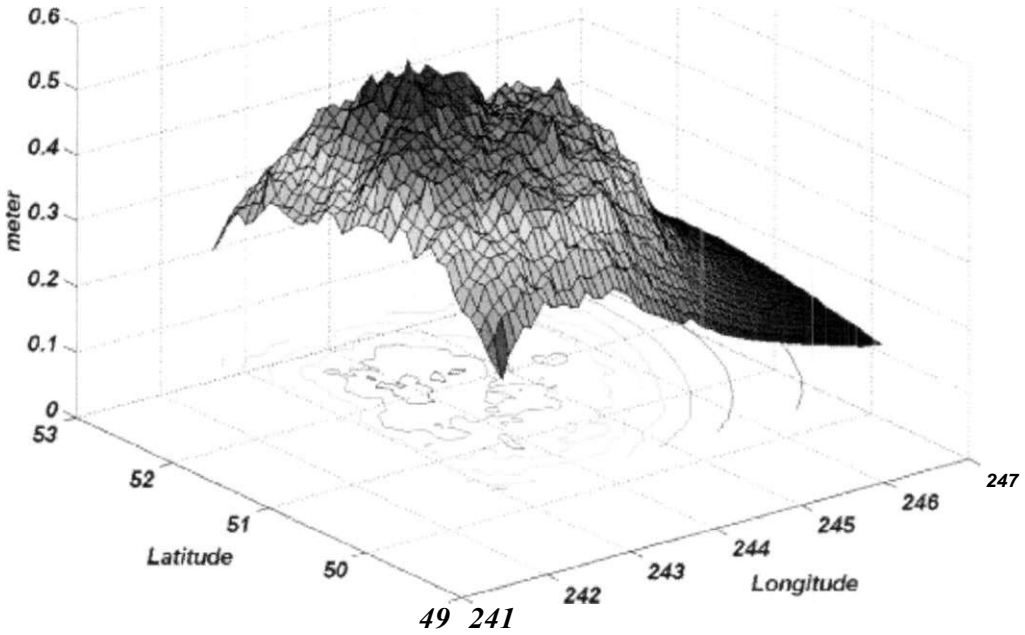


**Figure 4-4:Difference in the geoid contributions of the DTE using 15 and 60 arcsec DTMs (m)**

## 4.1.2 - Geoid modelling

In this section, computations of the geoid are carried out using gravity data obtained using the two methodologies; the first is that obtained from the D.C. (Fig. 3-14, Table 3-20), and the second is that obtained from the normal free-air gradient (Fig. 3-3, Table 3-2). The residual geoids, computed from Stokes' integral plus the GIE, are seen in Fig. 4-5 and 4-6 and their difference in Fig. 4-7; the statistics of these values are listed in Table 4-2. To obtain the final geoid, we have to add the contribution of the GM using Eq. 2.8.

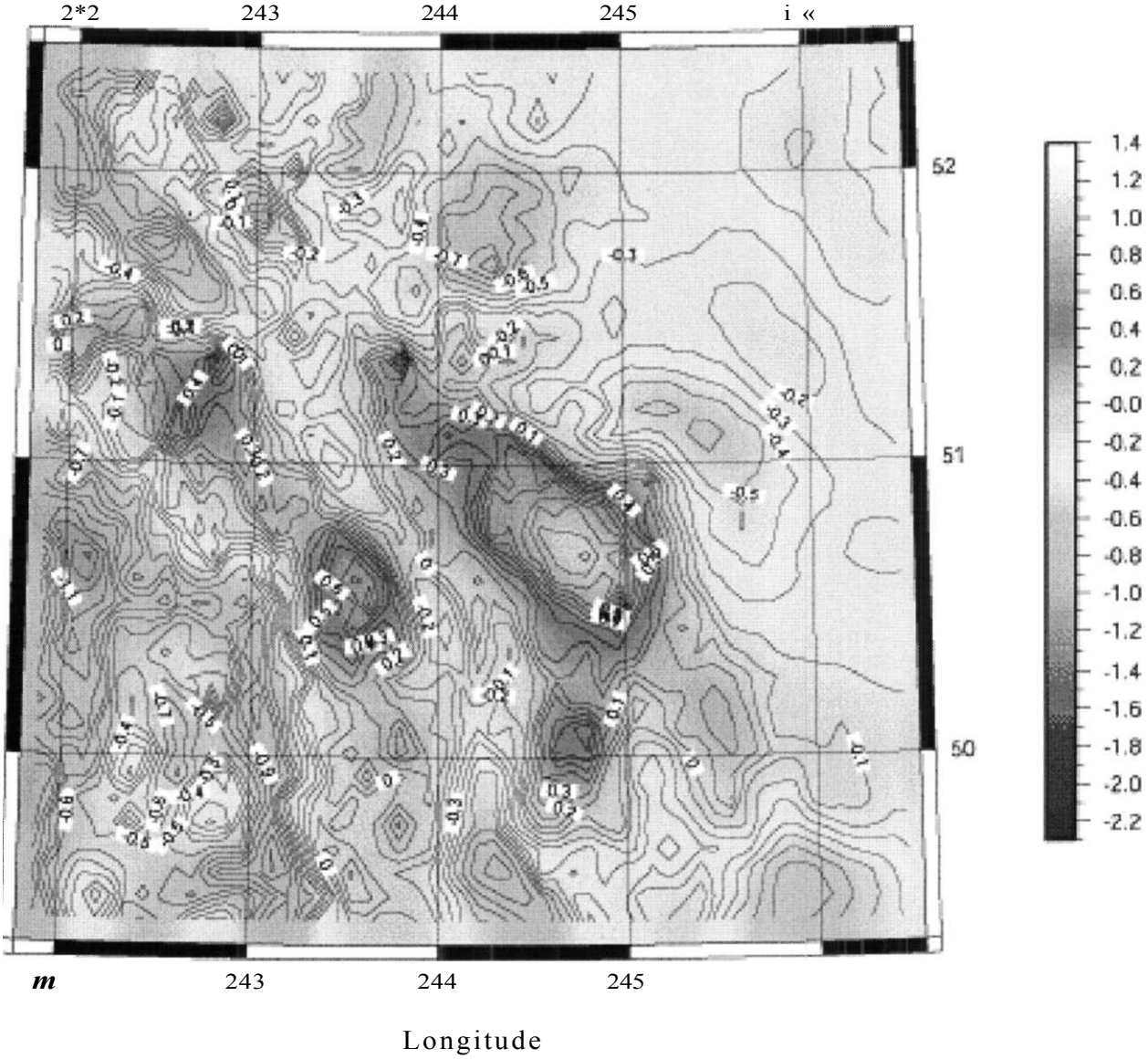


**Figure 4-5: Residual geoid computed from the 1st methodology (m)**

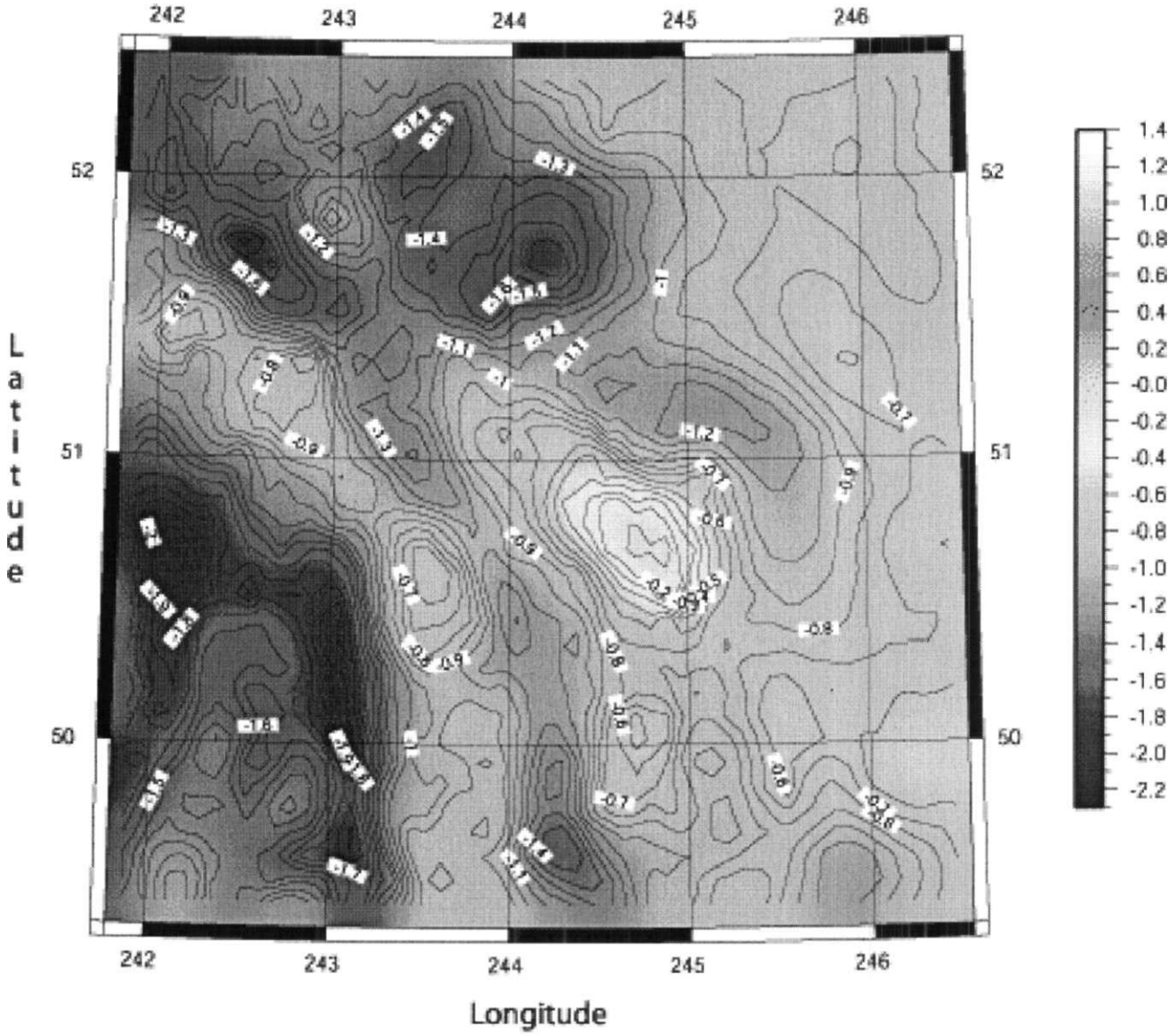


**Figure 4-6: Residual geoid computed from the 2nd methodology (m)**

From the values in Table 4-2 and their representation in Fig 4-7, it is noticed that the two methodologies give a different residual geoid with -82 cm bias between them and an RMS of 85 cm. This is considered a large difference. From Fig 4-7, it is seen that these large differences are correlated with the topography of the region, which is expected due to the two different methods used to downward continue the data to the reference sphere. It should be noted, too, that the geoid computed from the 1st methodology is higher than that computed from the 2nd methodology. It is expected that the magnification of the high frequency uncertainties (e.g., height uncertainties and DTM imperfection, errors in data) in the data, cause this difference in the 1st methodology due to the use of the inverse Poisson integral. The use of the 2nd Helmert condensation, as mentioned in the previous chapter, is also responsible for the differences, because of the rough field that is produced by this reduction (Heck, 2001).

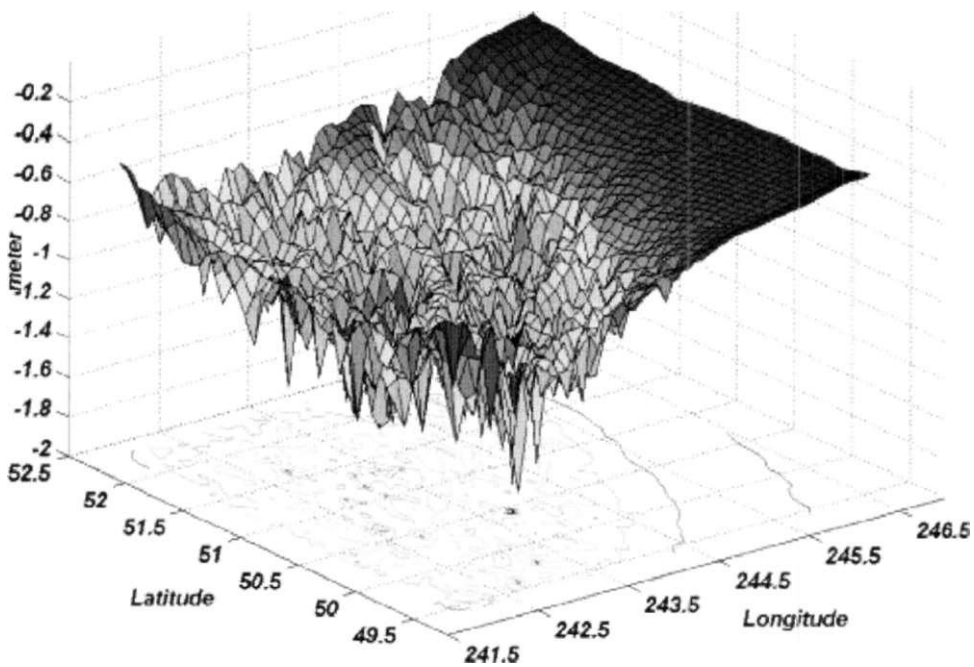


**Figure 4-7: Difference in geoids between the two methodologies (m)**

**Table 4-2: Statistics of the residual geoid from the two methodologies and their difference (m)**

| | Max | Min | Mean | Std | RMS |
|---|---|---|---|---|---|
| Res. Geoid, 1st method | *1.365* | *-1.426* | *-0.254* | *0.376* | *0.454* |
| Res. Geoid, 2nd method | *-0.002* | *-2.261* | *-1.070* | *0.360* | *1.128* |
| Difference | *-0.341* | *-1.864* | *-0.816* | *0.260* | *0.856* |

For an independent comparison between the two solutions, GPS/Levelling undulation benchmarks (BM) were used. Thirty-six Helmert orthometric heights, computed in 1995 by the Geodetic Survey Division in Canada, were used for this task; see Fig 4-8.

The two residual geoids were interpolated at the locations of the BMs and differences were formed after subtracting the 360 degree and order GM from the later. The statistics of the differences are listed in Table 4-3.

**Table 4-3: Statistics of the differences between the gravimetric and the control geoids at the BM (m)**

| | Max | Min | Mean | Std | RMS |
|---|---|---|---|---|---|
| 1st method-BM | *0.057* | *-1.731* | *-0.925* | *0.264* | *0.961* |
| 2nd method - BM | *0.704* | *-0.715* | *-0.314* | *0.351* | *0.467* |

**Table 4-4: Statistics of the differences between the gravimetric and the control geoids at the BM after the fit (m)**

| | Max | Min | Mean | Std | RMS |
|---|---|---|---|---|---|
| 1st method-BM | *0.464* | *-0.728* | *0.000* | *0.170* | *0.170* |
| 2nd method - BM | *0.173* | *-0.401* | *0.000* | *0.096* | *0.096* |

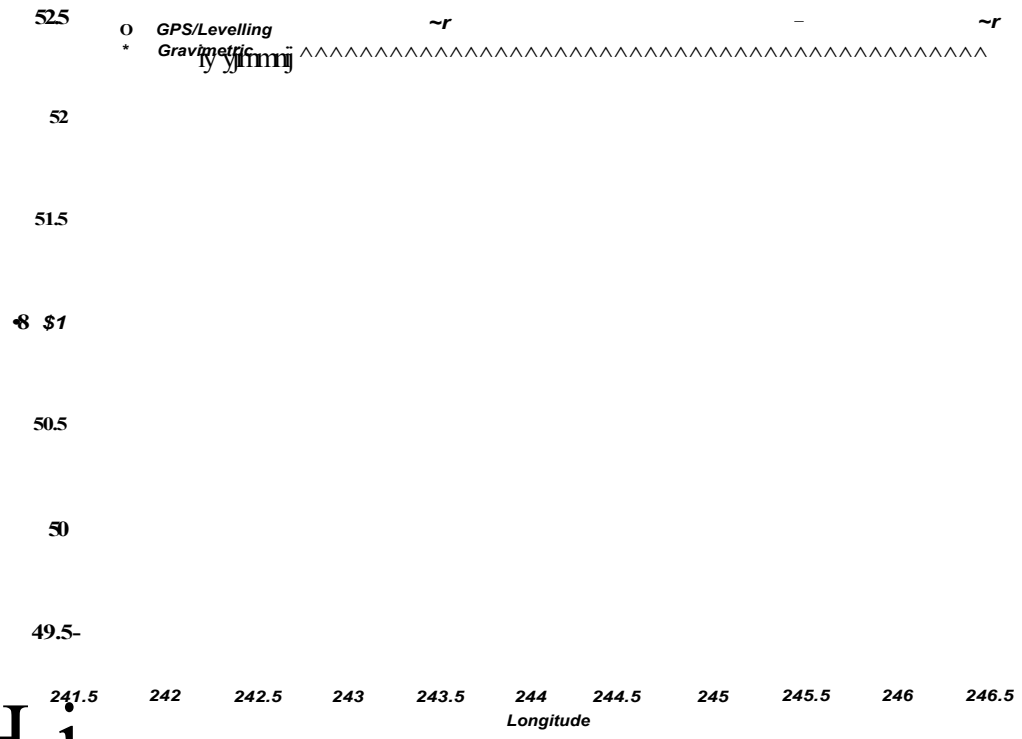


**Figure 4-8: Location of the GPS/Levelling points**

As was expected, the I^s methodology gives poorer agreement with the geoid at the BMs (RMS =96 cm). The 2^nd methodology gives an agreement of 47 cm RMS, which is still a considerable difference for a precise geoid determination. But it should be noted that the STD is smaller in the 1^st methodology, which means a large bias exists in the gravity anomalies, and in turn in the geoid when computed using this methodology.

After the four-parameter model fit (Eq. 2.37), on the other hand, the agreement of both methodologies improved significantly. The RMS goes down to 17 cm and 9 cm for the 1^st and 2^nd methodology, respectively.

The geoid determination using the airborne gravity data sets, analysed in Ch. 3, will be the focus of the following discussion.

## 4.2 - Geoid determined from airborne gravity data

As in the case of ground data, the airborne gravity data, after the appropriate reductions, will be input to Hotine's integral to give the geoid. In this section, the geoid will be evaluated using the two methodologies. Recall from the previous chapter that eight datasets were formed; four for each methodology.

Eight geoids, determined form the two methodologies, are evaluated and then compared to the ground solution. Since two ground solutions are available, the one coming from the 2nd methodology will be employed since it has a better fit to the BMs.

Now, it will be possible to investigate the following points:

1. Is filtering of the topographic effects essential from a practical point of view?
2. Which methodology gives a better fit to the reference geoid?
3. How different is the geoid determined from data filtered to different frequencies?
4. How good is the airborne geoid?

The first point will be investigated by studying the geoid determined from the two data sets ***data_60*** and ***datatc*** or ***datadte,*** depending on the methodology used. Recall that the ***datatc*** and ***data die*** were computed by adding the un-filtered TE after the gridding of the measured airborne gravity data. Comparing the geoid determined from the two methodologies with the reference geoid, gives the answer to the second point above.

Recall again that the following data sets were formed: ***data_30, data 60,*** and ***data_90.*** By determining the geoids from these data sets and inter-comparing them, a conclusion will be reached for the third point.

The fourth point will be answered after the comparison with the reference geoid.

### 4.2.1 - Airborne geoid from the 1st methodology

The four data sets created for the 1st methodology were the inputs to Hotine's integral. Figure 4-9 shows the four geoids.

**Table 4-5: Statistics of the differences between ground and airborne geoid using the 1st methodology (m)**

| Differences using | Max | Min | Mean | Std | RMS |
|---|---|---|---|---|---|
| ***dataSO*** | ***0.570*** | ***-0.332*** | ***0.119*** | ***0.165*** | ***0.218*** |
| ***data_60*** | ***0.616*** | ***-0.330*** | ***0.135*** | ***0.163*** | ***0.224*** |
| ***Data_90*** | ***0.642*** | ***-0.382*** | ***0.139*** | ***0.171*** | ***0.235*** |
| ***data dte*** | ***0.632*** | ***-0.331*** | ***0.136*** | ***0.164*** | ***0.227*** |

We also computed the geoid using ground data, derived from the 2nd methodology, on the same nodes of the grid. These two geoid types are now comparable. Figure 4-10 shows these differences, while Table 4-5 has their statistics. Discussions will follow in Sec. 4.2.3.

### 4.2.2 - Airborne geoid from the 2nd methodology

Here also, the four data sets created for the 2nd methodology were the inputs to Hotine's integral. Figure 4-11 shows the four geoids. The same reference geoid as above was used. Figure 4-12 shows these differences, while Table 4-6 has their statistics. Discussions will follow in Sec. 4.2.3.

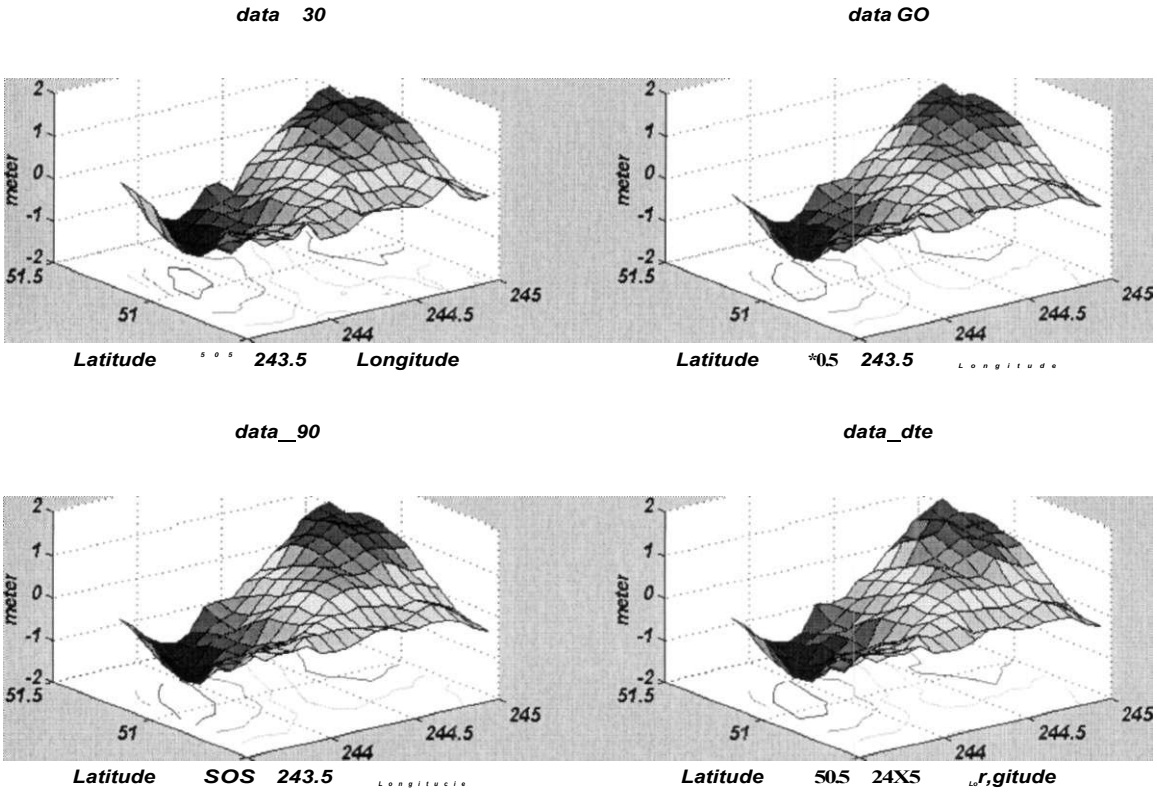


**Figure 4-9: The four residual geoids computed from the four data sets created using the 1st methodology (m)**

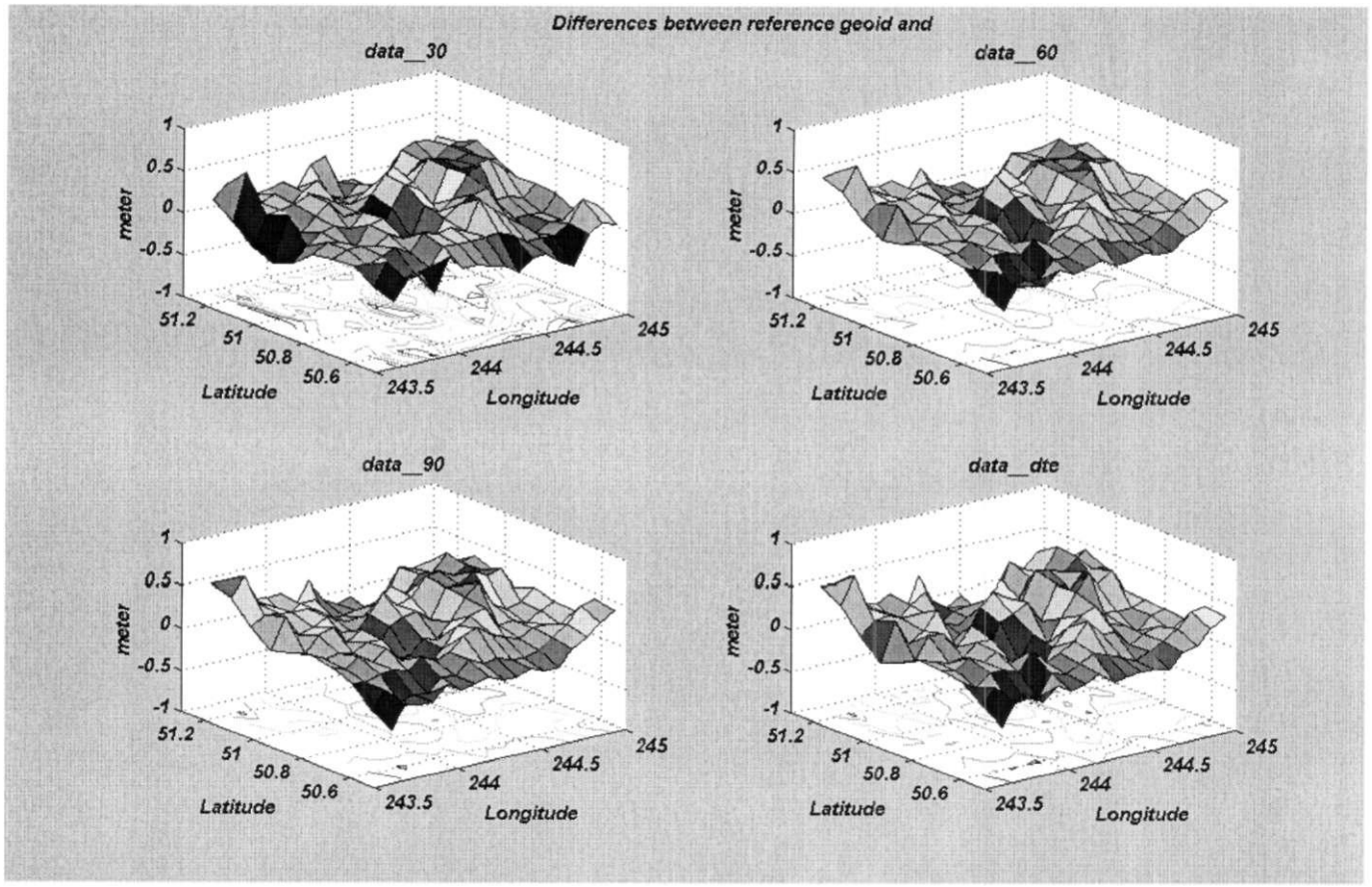


**Figure 4-10: Differences between the reference geoid and geoids computed from the 1st methodology (m)**

**Table 4-6: Statistics of the differences between ground and airborne geoid using the 2" methodology (m)**

| Differences using | Max | Min | Mean | Std | RMS |
|---|---|---|---|---|---|
| ***data_30*** | ***0.186*** | ***-0.222*** | ***0.006*** | ***0.064*** | ***0.064*** |
| ***data_60*** | ***0.216*** | ***-0.192*** | ***-0.001*** | ***0.052*** | ***0.052*** |
| ***Data 90*** | ***0.272*** | ***-0.220*** | ***-0.005*** | ***0.061*** | ***0.061*** |
| ***data dte*** | ***0.212*** | ***-0.201*** | ***-0.004*** | ***0.055*** | ***0.055*** |

### 4.2.3 - Discussion of geoid results from airborne gravity data

From the values in these tables (4-5 and 4-6), we can conclude that all three filtering frequencies, regardless of the methodology, give us similar geoids when using data on a 5' x 5' grid. This means that data sets fdtered to 1/30 Hz can give us the same geoid as data sets fdtered to 1/60 or 1/90 Hz, which have better agreement with the reference gravity field. In the case under study, having a flying speed of 100 m/sec, a high-resolution geoid of spacing 3 km can be achievable with a 5 cm RMS accuracy.

As for the fourth data set of each methodology, we conclude that filtering of the TE is not needed from the practical point of view when using data on a 5'x 5' grid. Rather, it is enough to reduce for the TE after gridding the measured gravity anomalies; a procedure that saves a lot of processing time and effort.

Regarding the methodology used, it is clear that the 2nd methodology gives better agreement with the reference geoid, where the RMS is around 5 cm; whereas that of the 1st methodology goes up to roughly 21 cm. This is due to the inverse Poisson integral that magnifies high frequencies in the data, which have high frequency characteristics. The same statement, drawn when ground data were used with the 2nd Helmert condensation method also applies here.

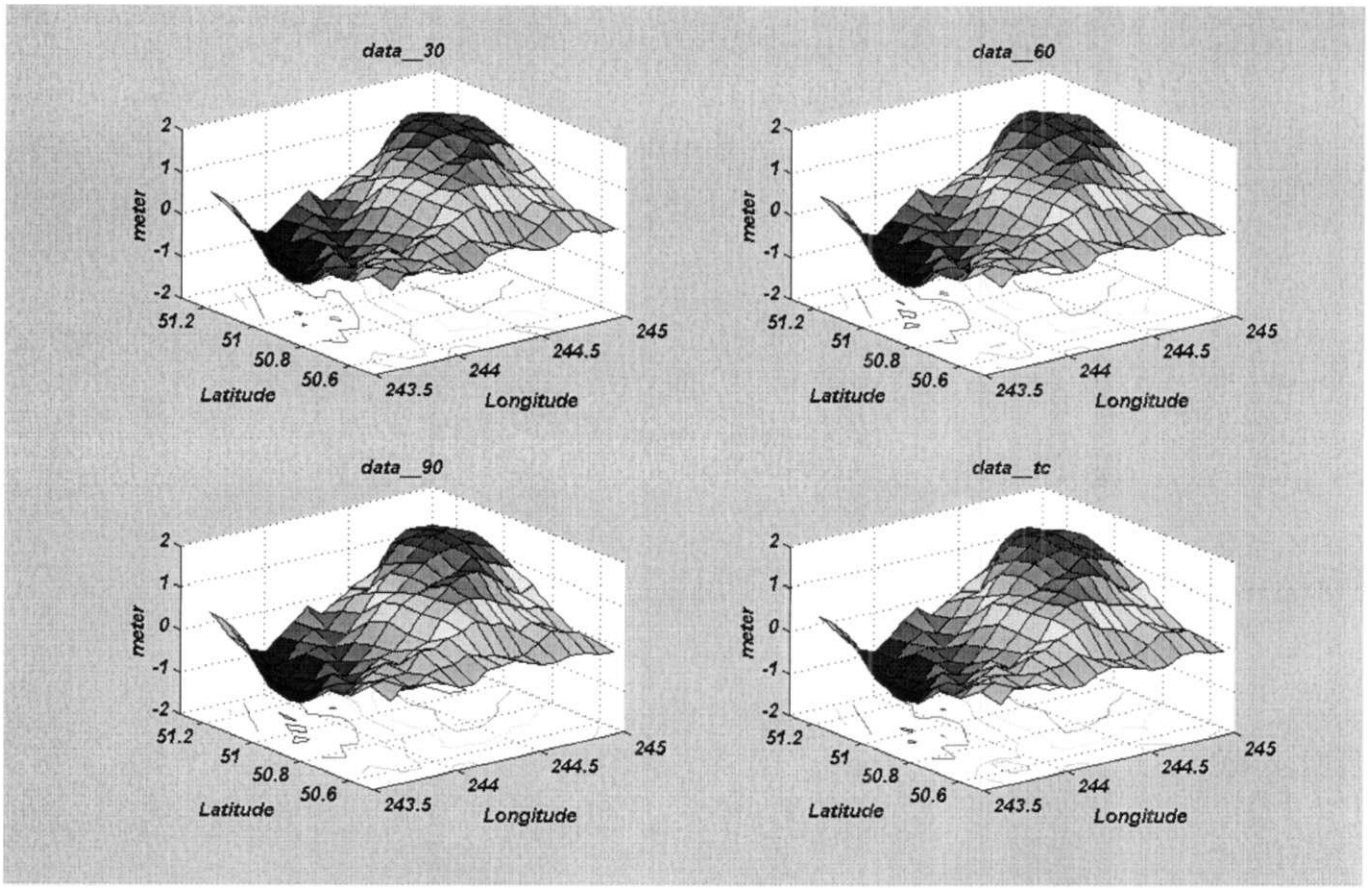


**Figure 4-11: The four residual geoids computed from the four data sets created using the 2 methodology (m)**

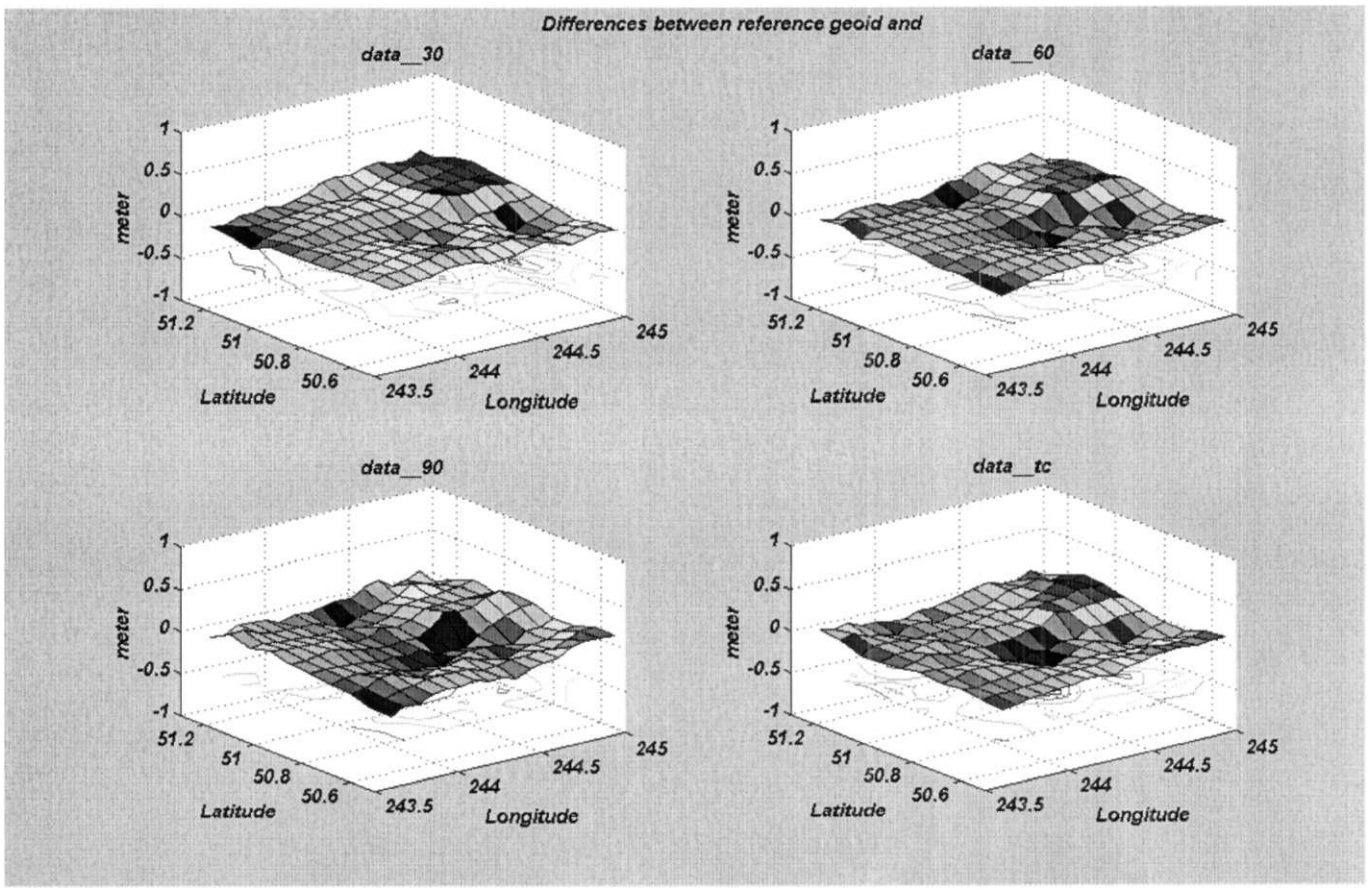


**Figure 4-12: Differences between the reference geoid and geoids computed from the 2" methodology (m)**

# Chapter 5

# Summary, Conclusions and Recommendations

## 5.1 - Summary

In this research, different practical and computational issues were investigated to determine the best possible geoid from airborne gravity data. These issues we redefined in the first chapter and they are: DTM resolution needed in airborne gravimetry to quantify the topography; the need of filtering the terrain effects; the difference in geoid determination methodology when using two different downward continuation methods; which airborne gravity data sets, filtered to different frequencies, can be used for geoid determination; and how good the airborne geoid is. Furthermore, the difference in downward continuation methods and different DTM resolutions were tested on ground gravity data.

Even though airborne gravimetry has been used for geoid determination for the last five years, the above topics were rarely visited. Hence, the importance of this research lies in its novelty in embracing these different issues that were only partially investigated before. Namely, these are the DTM resolution, filtering of TE, and comparisons between the two downward continuation methods.

To investigate the above points, an airborne gravity survey that took place in 1996 above the Canadian Rocky Mountains was used. Three DTM resolutions were used to test the sensitivity of gravity reductions on DTM resolution. The terrain effects were filtered and compared with their initial unfiltered values to examine the effect of filtering. The gravity

disturbances were brought to the reference sphere using two different downward continuation methods; one is the inverse Poisson integral and the other is the normal free-air gradient. After all these computations and comparisons, eight solutions of the same geoid were computed and inter-compared to answer the different questions defined in the Introduction. These eight solutions were also compared with the geoid determined from ground gravity data for validation.

As for the geoid determined from ground data, also three DTM resolutions were tested. The two methodologies to bring the gravity anomalies to the geoid were tested, too. The two geoid solutions computed were compared to undulations at existing GPS/Levelling BMs in that area and conclusions were drawn using the undulations at BMs as reference values.

## 5.2 - Conclusions

The answers to the questions stated in the Introduction will now be given, for both the airborne and ground data.

First, here are our conclusions regarding the five questions asked about the airborne gravimetry:

***1. What DTM resolution is needed in airborne gravimetry?***

A DTM resolution of 30 arcsec can provide the gravity effects of the topography with accuracy better than what the measuring system can offer. Differences in terrain effects computed from 15 and 30 arcsec DTMs are negligible. This indicates an insensitivity of the airborne gravity data to the high-frequency changes in the topography due to the large distance of these changes from the measuring instrument. A 60 arcsec DTM can safely be used in areas with moderate topography and where a high-accuracy geoid is not required.

***2. Is filtering of the topographic effects essential from the practical point of view?***

Although filtering of topographic effects is essential from the theoretical point of view and its effect is considerable on gravity, it is negligible in terms of the geoid, where this effect has an RMS of less than 1 cm for filtering frequencies of 1/30, 1/60, and 1/90 Hz.

***3. How different is the geoid determined from data filtered to different frequencies?***

While airborne data filtered to 1/30 Hz and 1/60 Hz give poorer agreement with the reference gravity filed compared with the data filtered to 1/90 Hz, geoids determined from all these data are of the same accuracy when a 5' x 5' grid is used.

***4. Which methodology gives a better fit to the reference geoid?***

The geoid determined from the 2nd methodology gave a better fit to the geoid computed from ground gravity data (a « 5 cm). It is believed that this is due to the magnification of the high frequency signals when the inverse Poisson integral is used in the 1st methodology (a « 22 cm), in addition to the roughness of the disturbances created by the 2nd Helmert condensation method and their use in the inverse Poisson integral.

***5. How good is the airborne geoid?***

It has been shown that an off-the-shelf inertial navigation system integrated with GPS can deliver a geoid accurate to about 5 cm (a) compared to a geoid computed from ground data on a 5'x5' grid. The same, if not better, accuracy can be achieved with 3x3 Km grid when airborne gravity data filtered to 1/30 Hz is used.

It should be noted here that when using gravity data on a denser than 5'x5' grid, the possibility of an unstable inverse Poisson solution exists.

As for the ground data, we can answer as follows:

1. ***How do the terrain effects computed from different Digital Elevation Model resolutions affect the geoid?***

The denser the DTM, the better the geoid is determined. In a mountainous region as the Rocky Mountains, a 30 arcsec DTM is by no means sufficient for determining a geoid accurate to the cm-level. Here, a 15 arcsec DTM was used and it is expected that a denser DTM will give better results.

2. ***Which methodology gives a best-fitting geoid to the GPS/levelling benchmarks, when using ground gravity data?***

The inverse Poisson integral creates problems due to the magnification of the high frequencies in the data, and due to the rough field it generates when Helmert's 2$^{nd}$ condensation is used, which, in turn, has a consequence on the geoid. The normal free-air gradient, although an approximation, gave a geoid that is closer to the GPS/levelling derived undulations than the geoid determined using the inverse Poisson integral for the D.C. The smaller STD in the 1$^{st}$ methodology indicates that a bias exists in the gravity data and it is propagated to the geoid, whose explanation is not clear.

All the above conclusions are valid for data/results on a 5'x5' grid.

## 5.3 - Recommendations

Although some ways of processing of the airborne gravity data to determine the geoid have been studied in this thesis, there still exist some other points that should be investigated and tested. These are listed below.

a) The 2$^{nd}$ Helmert condensation method was used in this thesis. This condensation method yields a rough gravity field. Helmert's 1$^{st}$ condensation method gives a

smoother field (Heck, 2001), which is highly recommended for downward continuation when the inverse Poisson integral is used. It is proposed that the 1st condensation method be tested and compared with the 2nd condensation method and the gradient solution.

b) Other downward continuation methods were investigated and tested, on both ground and airborne gravity data, in other studies. Investigations on the geoid determined using these methods have to be made.

c) Although the iterative method for the regularisation of the inverse Poisson integral is considered to be a good tool, it is important to test the impact of other regularisation methods on the geoid determination.

d) It was shown here that the geoid determined from airborne gravity data is within 5 cm RMS from the geoid determined from ground gravity data; this comparison was done on a 5'x5' grid. The airborne data filtered to 1/30 Hz give a resolution of 3 km; it is recommended to compute the geoid at this resolution and to try to use the different downward continuation methods to see if the same accuracy can be obtained. It is well known that the inverse Poisson integral stability depends on the ratio between the height of data and the grid resolution.

e) The conclusion on filtering the terrain effects was drawn on a 5'x5' grid. Is this conclusion valid when a denser grid is considered? This needs further investigation.

f) For ground data, a 15 arcsec DTM was recommended for use instead of 30 and 60 arcsec. A higher resolution is definitely needed in ground gravimetry. It is important to check whether denser DTM spacing is essential and to what resolution.

g) A through analysis of filtering and propagation of noise is essential. The investigation has to start from the measurement noise to reach the final product noise estimate passing through all processing.

h) It is highly recommended to use different datasets measured in different areas to confirm the conclusions drawn in this thesis and see if they can be considered universal.

# References


Andritsanos V. D. (2000): Optimal Combination of Heterogeneous and Satellite Data with the Use of Spectral Methods for Applications in Geodesy and Oceanography. Ph.D. Thesis. Department of Surveying and Geodesy. University of Thessaloniki (in Greek).

Andritsanos V. D., Sideris M. G, and Tziavos I. N. (2000): A Survey of Gravity Field Modelling Applications of the Input-Output System Theory (IOST). International Geoid Service. Bulletin N. 10. May 2000.

Barzaghi R., Fermi A., Tarantola S, and Sanso F. (1993): Spectral Techniques in Inverse Stokes and Over-Determined Problems. Surveys in Geophysics 14, 461-475.

Bayoud F. A. and M. G. Sideris (2001): Different Techniques for Optimally Combining Airborne with Ground Gravity Data. Presented at the EGS General Assembly, 2001.

Bendat J. S. and Piersol A. G. (1986): Random Data: Analysis and Measurement Procedures. Second edition. John Wiley and Sons, New York.

Bottom G. P. and Barzaghi R. (1993): Fast Collocation. Bull. Geod. 67:119-126.

Bouman J. (1998): Quality of Regularization Methods. DEOS Report no. 98.2

Bouman J., and Koop R. (1998): Stabilization of Global Gravity Field Solutions by Combining Satellite Gradiometry and Airborne Gravimetry. Presented at the IV Hotine-Marussi Symposium, Trento, Italy.

Bruton A. (2000): Improving the Accuracy and Resolution of SINS/DGPS Airborne Gravimetry. PhD Thesis, Dept. of Geomatics Engineering, University of Calgary, UCGE Report No. 20145, Calgary, Alberta.

Dragomir V., Ghitau M., Mihailescu M., Rotaru M. (1982): Theory of the Earth*s Shape. Elsevier.

Eren K. (1980): Spectral Analysis of GEOS3 Altimeter Data and Frequency Domain Collocation. Ohio State University, Department of Geodetic Sciences and Surveying. Report 297.

ESA, Reports for Missions Selection (1999): Gravity Field and Steady-State Ocean Circulation Mission, ESA SP-1233, The Netherlands.

Esan O. (2000): Spectral Analysis of Gravity Field Data and Errors in View of Sub-Decimetre Geoid Determination in Canada. MSc Thesis, Dept. of Geomatics Engineering, University of Calgary, UCGE Report No. 20137, Calgary, Alberta.

Fernandes M. J., Bastos L., Forsberg R., Olesen A., Leite F. (2000): Geoid Modelling in Coastal Regions Using Airborne and Satellite Data: Case Study in the Azeros. International association of Geodesy Symposia Vol. 121. Geodesy Beyond 2000 - The Challenges of the first decade.

Forsberg R., Kenyon S. (1995): Downward Continuation of Airborne Gravity Data. LAG Symposium G4. IUGG XXI General Assembly. Boulder. Colorado

Forsberg R., Solheim D. (2000): Geoid of the Nordic/Baltic Region from Surface /Airborne Gravimetry and GPS Draping. Presented at the GGG2000, Banff, Canada.

Glennie C. L. (1999): An Analysis of Airborne Gravity by Strapdown INS/GPS. PhD Thesis, Dept. of Geomatics Engineering, University of Calgary, UCGE Report No. 20125, Calgary, Alberta.

Glennie C. L. and Schwarz K. P. (1999): Airborne Gravity by Strapdown INS/GPS in a 100 km by 100 km Area of the Rocky Mountains. In: Proc. Of International Symposium on Kinematic Systems in Geodesy, Geomatics and Navigation (KIS97), Banff, Canada, June 3-6, pp. 619-624.

Haagmans R. E., de Min E., van Gelderen M. (1993): Fast Evaluation of Convolution Integrals on the Sphere Using the ID FFT, and a Comparison with Existing Methods for Stokes' Integral. Manuscr Geod 18:227-241.

Hammada Y. (1996): Airborne Gravity by GPS/INS, Comparison of Filtering Techniques. MSc Thesis, Dept. of Geomatics Engineering, University of Calgary, UCGE Report No. 20125, Calgary, Alberta.

Heck B. (2001): On the Use and Abuse of Helmert's Second Method of Condensation. Presented in the IAG 2001 Scientific Assembly 2 - 7 September 2001 - Budapest, Hungary.

Heiskanen, W. A., and Moritz, H. (1967): Physical Geodesy. W.H Freeman Company. San Francisco.

Hotine, M. (1969): Mathematical Geodesy. US. Department of Commerce, Washington, D.C. USA.

Kern M., Schwarz K. P. (2001): A Comparison of Direct and Indirect Numerical Methods for the Downward Continuation of Airborne Gravity Data. Presented in general Assembly of IAG 2002. Budapest, Hungary.

Lemoine F. G., Kenyon S. C, Factor J. K., Trimmer R. G., Pavlis N.K., Chinn D. S., Cox C. M., Klosko S. M., Luthcke S. B., Torrence M. H, Wang Y. M., Williamson. R. G., Pavlis. E. C, Rapp R. H, Olson. T. R. (1998) The Development of the Joint NASA GSFC and NEVIA Geopotential Model EGM96. NASA/TP-1998-206861.

Li J., Sideris M. G. (1997): Marine Gravity and Geoid Determination by Optimal Combination of Satellite Altimetry and Shipborne Gravimetry Data. Journal of Geodesy, 71:209-216.

Li Y. C. (1993): Optimised Spectral Geoid Determination. MSc Thesis, Dept. of Geomatics Engineering, University of Calgary, UCGE Report No. 20050, Calgary, Alberta.

Li Y. C. (2000): Airborne Gravimetry for Geoid Determination. PhD Thesis, Dept. of Geomatics Engineering, University of Calgary, UCGE Report No. 20141, Calgary, Alberta.

Martinec, Z. and Vanicek P. (1994a): Direct Topographical Effect of Helmert's Condensation for a Spherical Approximation of the Geoid. Manuscr. Geod. 19: 257-268.

Martinec, Z. and Vanicek P. (1994b): The Indirect Effect of Topography in Stokes-Helmert's Techniques for a Spherical Approximation of the Geoid. Manuscr. Geod. 19: 213-219.

Martinec, Z. (1998): Boundary Values Problems for Gravimetric Determination of Precise Geoid. Lecture notes in Earth sciences, 73, Springer.

Moritz H. (1980): Advanced Physical Geodesy. Herbert Wichmann Verlag, Karlsruhe. Abacus Press, Tunbridge Wells, Kent.

Moritz H. (1984): Geodetic Reference System 1980. Bull. Geod., 58: 388-398.

Nagy D. (1966): The Prism Method for Terrain Corrections Using Digital Computers. Pure Applied Geophysics. Vol. 63. pp 31-39.

Nagy D., Papp G., Benedek J. (2000): The Gravitational Potential and its Derivatives for the Prism. Journal of Geodesy, 74: 552-560.

Novak P. (2000): Evaluation of Gravity Data for the Stokes-Helmert Solution to the Geodetic Boundary-Value Problem. Ph.D. Thesis, Department of Geodesy and Geomatics Engineering, University of New Brunswick. Technical report NO. 207.

Novak P., Kern M., Schwarz K. P., Heck B. (2001): The Determination of the Geoid from Airborne Gravity Fata. Internal Report, Dept. of Geomatics Engineering, University of Calgary, UCGE Report No. 30013, Calgary, Alberta.

Omang O. C. D., Forsberg R. (2000): How to Handle Topography in Practical Geoid Determination: Three Examples. Journal of Geodesy, 74: 458-466.

Peng, M. (1996): Topographic Effects on the Gravity and Gradiometry by the 3D FFT and FHT Methods. UCGE Report # 20064. Dept of Geomatics Eng. Univ. of Calgary.

Rauhut A.C. (1992): Regularisation Methods for the Solution of the Inverse Stokes Problem. Ph.D. thesis. Dept. of Geomatics Engineering, University of Calgary, UCGE Report No. 20045, Calgary, Alberta.

Schwarz K. P. (1979): Geodetic Improperly Posed Problems and Their Regularization. Boll Geod E Scienze Affini, XXXVIII - N. 3.

Schwarz K. P., Li Y. C, Wei M. (1994): The Spectral Window of Airborne Gravimetry and Geoid Determination. Paper presented at the International Symposium on Kinematic Systems in Geodesy. Geomatics and Navigation, Dept of Geomatics Eng. Univ. of Calgary. Banff, Canada.

Schwarz K. P., Li Z. (1996a): An Introduction to Airborne Gravimetry and its Boundary Value Problems. Lectures Notes, JAG International Summer School. Como, Italy, May 26 - June 7.

Schwarz K. P., Li Y. C. (1996b): What Can Airborne Gravimetry Contribute to Geoid Determination? Journal of Geophysical Research, Vol. 101, NO. B8. P.P. 17873 - 17881.

Sideris M. G. (1984): Computation of Gravimetric Terrain Corrections Using Fast Fourier Transform Techniques. M.Sc. Thesis, Division of Surveying Engineering, University of Calgary, UCSE Report No. 20007, Calgary, Alberta.

Sideris M. G. (1987): Spectral Methods for the Numerical Solution of Molodensky's Problem. UCSE Rep. 20024, Dept. of Surveying Engineering. The University of Calgary, Calgary, Alberta.

Sideris, M. G. (1990): Rigorous Gravimetric Terrain Modelling Using Molodensky's Operator. Journal of Geodesy, 15: pp. 97-106.

Sideris M. G. and She B. B. (1992): A New High-Resolution Geoid for Canada and Part of the U.S. by the 1D-FFT Method. Bull Geod 69: 92-108

Sideris M. G. (1996): On the Use of Heterogeneous Noisy Data in Spectral Gravity Field Modelling Methods. Journal of Geodesy, 70: 470-479.

Sjoberg L. E. (1998): The Exterior Airy/Heiskanen Topographic-Isostatic Gravity Potential, Anomaly and Effect of Analytical Continuation in Stokes' Formula. Journal of Geodesy, 72: pp. 654-662.

Sjoberg L. E. and Nahavandchi H. (1999): On the Indirect Effect in Stokes-Helmert Method of Geoid Determination. Journal of Geodesy, 73: 87-93.

Sjoberg L. E. (2000): Topographical Effects by Stokes-Helmert Method of Geoid and Quasi-Geoid Determinations. Journal of Geodesy, 74: 255-268.

Sjoberg L. E. (2001): The Effect of Downward Continuation of Gravity Anomaly to Sea Level in Stokes' Formula. Journal of Geodesy, 74: 796-804.

Smith D. A., Robertson D. S., and Milbert D. G. (2001): Gravitational Attraction of Local Crustal Masses in Spherical Coordinates. Journal of Geodesy, 74: 783-795.

Stokes G. G. (1849): On the Variation of Gravity at the Surface of the Earth. Transactions of the Cambridge Philosophical Society, VIII, pp. 551-695.

Sun W., Vanicek P. (1996): On the Problems of Downward Continuation of the 5'x5' Mean Helmert's Gravity Disturbances. Journal of Geodesy, 72: 411-420.

Tikhonov A. N. (1963): Solution of Incorrectly Formulated Problems and Method of Regularization. Soviet Mathematics - Doklady., 4, pp 1034-1038.

Timmen L., Bastos L., Forsberg R., Gidskehaug A., Meyer U. (2000): Airborne Gravity Field Surveying for Oceanography, Geology and Geodesy - the Experience from AGMASCO. International association of Geodesy Symposia Vol. 121. Geodesy Beyond 2000 - The Challenges of the first decade.

Tscherning C. C. (1974): A FORTRAN TV Program for the Determination of the Anomalous Potential Using Step-Wise Least-Square Collocation. Ohio State University, Department of Geodetic Sciences and Surveying. Report 212.

Tsoulis D. (2001): A Comparison Between Airy/Heiskanen and Pratt/Hayford Isostatic Models for the Computation of Potential Harmonic Coefficients. Journal of Geodesy, 74: 637-643.

Tziavos I. N., Sideris M. G, Forsberg R., and Schwarz K. P. (1988): The Effect of the Terrain on Airborne Gravity and Gradiometry. JGR, Vol. 93 pp. 9173-9186.

Tziavos I. N., Sideris M. G, and Forsberg R. (1998): Combined Satellite Altimetry and Shipborne Gravimetry Data Processing. Marine Geodesy, 21:299-317.

Tziavos I. N. Forsberg R., and Sideris M. G. (1998): Marine Gravity Field Modelling Using Shipborne Gravity and Geodetic Missions Altimetry Data. Geomatics research Australasia, No. 69:1-18, November, 1998.

Vanicek P. and Martinec Z. (1994): The Stokes-Helmert Scheme for the Evaluation of a Precise Geoid. Manusc Geod 19:119-128.

Wenzel, G. (1999): Improved Gravity Field Modelling Using Ultra-High Degree Geopotential Models GPM98A, GPM98B and GPM98C. Prepared for Bulletin of International Geoid Service, Milan.